**University of Naples "Federico II"**

**Faculty of Engineering**

**Department of Materials and Production Engineering**

*PhD in Materials and Structures Engineering –XXIV Cycle*

# DESIGN AND PREPARATION OF 3D MULTIFUNCTIONAL SCAFFOLDS WITH ENHANCED AND TAILORED BIOMECHANICAL PROPERTIES

**Coordinator:**

*Prof. G. Mensitieri*

**Tutor:**

*Prof. A. Gloria*

*Prof. R. De Santis*

*Prof. L. Ambrosio*

**Author:**

*Teresa Russo*

*“Ah! Delle mie passate sciagure e della contentezza presente, come di tutto il bene e il male che mi sarà ancora serbato, sia benedetta la Provvidenza, della quale gli uomini e le cose, si voglia o non si voglia, sono mirabili stromenti [...] ch'ella sa adoprare a fini degni di sé”*

***Silvio Pellico**, Le mie prigioni*

*A chi ha saputo silenziosamente*
*supportarmi  in questo lungo cammino.*
*A chi mi ama incondizionatamente.*

# Contents

# ***PREFACE***

In the field of tissue engineering, polymeric and micro/nanocomposite substrates with suitable architectural features, mechanical, transport and surface properties are normally required according to specific applications.

In this context, the present research has been divided into two different steps evidencing some strategies to develop 3D multifunctional scaffolds with enhanced and tailored performances.

The first step highlights the possibility to extend a precisely controlled two-step procedure to immobilize RGD motifs on 3D rapid prototyped PCL scaffolds. In particular, the aim was to design 3D advanced scaffolds through 3D Fiber Deposition technique, that are able to guide cell functions, benefiting from an approach to control morphology, spatial distribution of surface treatment, as well as macro-, micro-, nano-mechanical performances. Nanoindentation and tensile measurements on the PCL fibers of 3D scaffolds have allowed to understand the effects of the surface modification via aminolysis. Furthermore, the efficacy of both functionalization and bioactivation was monitored by analytically quantifying functional groups and/or peptides at the interface. Cell adhesion studies verified the correct presentation of the peptide with enhanced cell attachment.

On the other hand, the second step of the research was mainly focused on the design of 3D PCL/biomimetic hydroxyapatite (HA) nanocomposite scaffolds for hard tissue regeneration. Accordingly, 3D fiber-deposited PCL/Mg,$CO_3$-substituted HA nanocomposite scaffolds were developed and the effects of the biomimetic HA nanoparticles on the biological and mechanical performances were suitably evaluated.

# Chapter I: Contents

# CHAPTER I
# General Introduction

## I.I Tissue Engineering

The loss or failure of an organ or tissue represents a frequent and devastating problem in health care. Thus, the need for substitutes to replace or repair tissues or organs problems is overwhelming.

For this reason, tissue engineering is becoming an important field of research. Tissue engineering is defined as a multidisciplinary field that integrates principles of engineering and life sciences to develop biological substitutes that restore, maintain or improve tissue function.[1-3] As easily understood, this approach involves a multidisciplinary knowledge gathered from the fields of engineering, biotechnology, life sciences, biology and, recently, from the appearance of micro- and nano-mechanical approaches for predicting the mechanical properties of natural tissues.[3-5]

Therefore, the main goal of tissue engineering and regenerative medicine strategies is to restore the function of damaged tissues by delivering a combination of cells, biological factors and a biomaterial scaffold on which these cells must adhere, organize and develop similarly to native tissue.[6]

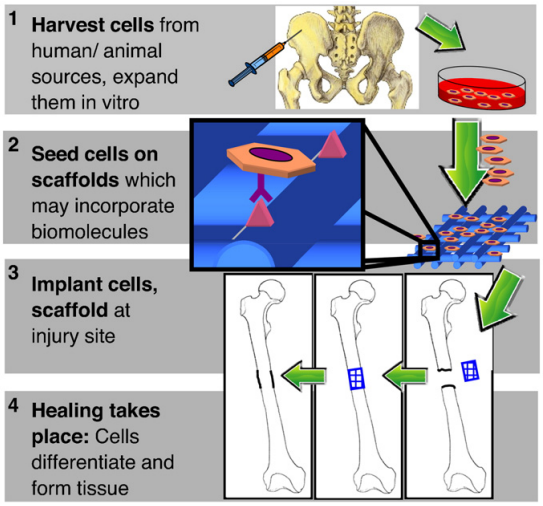


**Figure I.I: Tissue engineering paradigm.**

*In vivo*, cell fates are determined by a complex interaction of nano-scale physical and chemical signals. Therefore, scaffolds for tissue engineering often incorporate biosignals to create a controlled, bioinspired extracellular environment to direct tissue-specific cell responses. The intention is that, when presented with appropriate biological cues, cell receptors will bind to these signaling biomolecules and transmit the signals, at intracellular level, by activating signaling cascades. These cascades will modulate gene expression and determine important cell fate processes such as differentiation to ultimately regenerate functioning tissue. As nanotechnology can recapitulate the submicron-scale spatial orientation of extracellular signaling molecules, it may be a powerful tool for enhancing cell-biomaterial communication and inducing desired cell behaviors.

Signals from the extracellular microenvironment that may be incorporated into biomaterials fall into three major categories: (1) insoluble extracellular matrix (ECM) macromolecules, (2) diffusible/soluble molecules, and (3) cell–cell receptors (Figure I.II).[6]

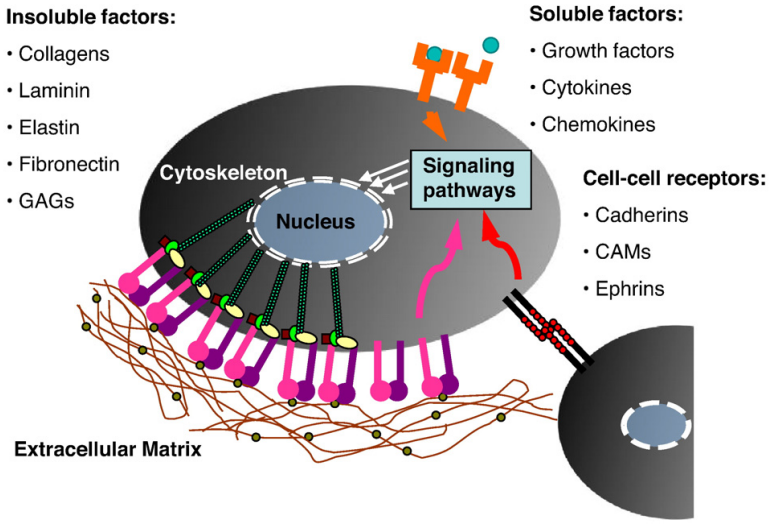


**Figure I.II: Bioactive signals found within the extracellular environment.**

## I.II Extracellular Matrix (ECM): structure and function *in vivo*

There is a great diversity of insoluble ECM molecules including structural proteins such as collagens, elastin and laminin, glycoproteins such as fibronectin and vitronectin, as well as glycosaminoglycans such as chondroitin sulfate.[7] *In vivo*, these

secreted ECM proteins form a meshwork of fibers or fibrils with ECM glycoproteins incorporated into them. The resulting matrix functions as both a structural and signaling scaffold to cells. ECM composition, immobilization and spatial arrangement vary for each tissue type. For example, bone ECM consists mostly of collagen I,[8] mineral and non-collagenous proteins such as osteocalcin, fibronectin and vitronectin.[9] However, cartilage ECM is predominantly composed of collagen II and aggrecans.[10] This tissue-specific difference in ECM composition may be instructive to tissue engineering because different ECM macromolecules regulate cell growth and differentiation by selectively stimulating different signaling pathways through ECM interactions with various cell receptors.[11]

Transmission of chemical and mechanical signals from the ECM is primarily mediated by integrins. Integrins are a family of cell-surface transmembrane receptors, each of which consists of α and β subunits. So far, 8 β and 18 α integrin subunits have been found. These integrin subunits associate to form 24 distinct αβ combinations, and each of these integrins has unique binding characteristics (Figure I.III).[12]

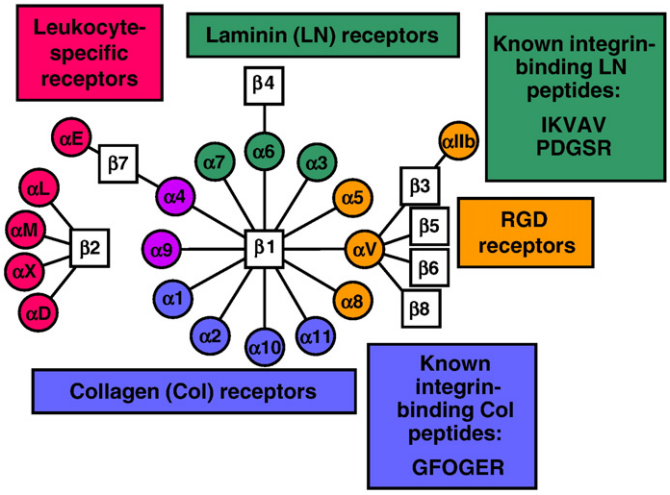


**Figure I.III: Integrin alpha and beta subunit combinations and binding specificity.[12]**

Most integrins bind to several types of ECM molecules and conversely, most ECM bind to more than one integrin. Integrins can also undergo bidirectional signaling. That is, when ECM binds to the extracellular domain of integrins, it activates intracellular signaling (outside-in). Conversely, intracellular signaling can affect the conformation of an integrin, which modulates its affinity to its ligand (inside-out).[13]

Both α and β integrin subunits pass through the cell membrane once and have large 700–1100 residue extracellular domains and small 30-50 residue cytoplasmic

domains. The extracellular domains of integrins serve to recognize and bind ECM. Upon ECM binding, integrins cluster and their cytoplasmic domains associate with both cytoskeletal and intracellular signal transduction molecules. The association of integrins with the cellular signaling network initiates downstream signaling cascades such as the protein kinase C, Rac, Rho and mitogen-activated protein kinase (MAPK) pathways. The coordinated clustering of ECM ligands, integrins and cytoskeletal components forms macromolecular aggregates known as focal adhesions on the inside and outside of the cell membrane.[14] These integrin–ECM interactions govern cell survival, growth, migration and differentiation[13,15,16] and are, therefore, useful targets of biomimetic tissue engineering strategies. Furthermore, because focal adhesions occur on submicron to nanometer size scales[17] and integrins are approximately 10 nm in diameter[18] and have 20 nm long extracellular domains,[19,20] integrin–ECM based biomaterial strategies are especially relevant applications for nanofabrication and nanopatterning technologies.

Although ECM macromolecules, such as collagens and fibronectin, have long protein backbones consisting of thousands of aminoacids, integrins recognize and bind to only a few short peptide sequences within the ECM molecules, triggering cell adhesion, signaling and spreading. In collagens I, II and III, cells bind to the Gly-Phe-Hyp-Gly-Glu-Arg (GFOGER) peptide sequence,[21,22] while in fibronectin, the Arg-Gly-Asp (RGD),[23] Pro-His-Ser-Arg-Asn (PHSRN),[24] Arg-Glu-Asp-Val (REDV),[25] and Lys-Asp-Val (LDV)[26] sequences are responsible for cell binding. Recognition sequences within laminin include RGD, as well as Ile-Lys-Val-Ala-Val (IKVAV),[27] Tyr-Ile-Gly-Ser-Arg (YIGSR)[28] and Pro-Asp-Ser-Gly-Arg (PDSGR)[29] (Figure I.III).

Integrin interactions with ECM peptide ligands trigger complex signaling pathways which regulate crucial cell behaviors such as proliferation and differentiation as well as tissue-level responses such as morphogenesis, homeostasis and regeneration.[12] Therefore, coatings of ECM macromolecules such as collagen and laminin or their recognition peptides such as RGD or IKVAV have been used to bio-functionalize surfaces or implants and drive tissue-specific cell responses. Although naturally derived ECM molecules have proved fairly successful in some applications[30] extracting and purifying matrix polymers in large scale is challenging, and animal-derived ECM may elicit an immune response. Furthermore, natural ECM biomaterials are difficult to modify, characterize and control. These limitations have driven the need for synthetic non-fouling materials functionalized with ECM-derived peptides[31]

which are easily synthesized, immobilized, may be presented at unnaturally high densities, and may be tailored in composition for each tissue-specific application. Although there are many ECM-derived cell-binding motifs, most bioadhesive tissue engineering strategies have been restricted to modifying materials with RGD, GFOGER, IKVAV and YIGSR and PHSRN. Most of these studies have focused on RGD due to its status as a universal and "promiscuous" adhesion peptide which is found in numerous ECM molecules and binds to multiple integrins (αvβ3, α5β1, αvβ1, α8β1, αvβ8, αvβ6, αvβ5 and αIIbβ3).[12]

In this regard, the current work, in the bargain, highlights the possibility to extend a precisely controlled two-step procedure to immobilize RGD motifs on 3D rapid prototyped PCL scaffolds, in order to promote cell adhesion and, subsequently, specific events at the cellular level. In particular, the aim of this research was to design 3D advanced scaffolds able to guide cell functions, benefiting from an approach to control morphology, spatial distribution of surface treatment, as well as macro-, micro-, nano-mechanical performances. On the other hand, the possibility to create nanocomposite scaffolds for repairing bone tissue defects is also showed. In particular, it is evidenced the effect of the inclusion of biomimetic hydroxyapatite nanoparticles on mechanical and biological performances of 3D rapid prototyped PCL scaffolds, also including the possibility to achieve a double layered scaffold, as will be shown below.

Accordingly, the following paragraphs will aim to clarify the approach and the goal of this research.

## I.III Scaffold Biomaterials: from inorganic materials and polymers to polymer-based composites

Natural, synthetic, semi-synthetic and hybrid materials have been widely proposed and tested as scaffolds for tissue regeneration.[2,32-41] Among synthetic and natural inorganic ceramic materials, hydroxyapatite (HA) and tricalcium phosphate have been considered as candidates for scaffold materials for bone tissue engineering.[2,42] Even though these ceramic materials resemble the natural inorganic component of bone and possess osteoconductive properties,[2,43] they are brittle and cannot properly match the mechanical properties of bone. Furthermore, ceramic scaffolds have also been found

to be unsuitable for the growth of soft tissues that are characterized by different cellular receptors and mechanical performances than hard tissues. Accordingly, synthetic and natural polymers may be considered an attractive alternative to the growth of most tissues.[2,38-44] Natural polymers used in tissue engineering include collagen, alginate, agarose, chitosan, fibrin and hyaluronic acid (or hyaluronan).[2,39-45] Unlike natural polymers, synthetic polymers are man-made polymers that may present several advantages as well as more flexibility and processability into different size and shapes.[45] The physical-chemical properties of such polymers can be easily modified, and the mechanical behavior and degradation can be suitably modulated by varying the chemical composition of the macromolecule. By incorporating functional groups and side chains, synthetic polymers can also be bioactivated with specific molecules. [45]

With regard to synthetic polymers, aliphatic polyesters such as polyglycolic acid (PGA), polylactic acid (PLA), their copolymers such as poly(lactic-*co*-glycolic acid) (PLGA) (also known as polylactide-*co*-glycolide), and polycaprolactone (PCL) are the most commonly used polymers for tissue engineering applications.[2,38,45-47] Products obtained from the degradation of these polymers can be removed by natural metabolic pathways.

As previously said, scaffolds were initially fabricated using either polymers or ceramics, however, polymeric scaffolds turned out to be too flexible, while the ceramic ones tended to be too brittle.[48,49] Consequently, over the past few years, composite materials consisting of polymers reinforced with inorganic ceramic fillers have attracted research interest in the field of tissue engineering[48,49] to reconstruct several types of tissues, such as bone, tendons or ligaments, meniscus and cartilage.

Compared to neat polymers, composites should present improved mechanical properties, better flexibility and structural integrity than brittle ceramic materials. This means that porous scaffolds with enhanced bioactivity and controlled reabsorption rates can be obtained by suitably combining polymers and ceramics.[49]

The term “composite material” generally refers to the combination, on a macroscopic scale, of two or more materials, that differ in composition or morphology, in order to obtain specific chemical, physical and mechanical properties. The advantage is that the resulting composite material may possess a combination of the best properties of their constituents, and often other interesting properties, which are not shown by the single constituents.[50,53] Hence, composite materials with polymeric matrices, that are

also defined as polymer-based composite materials, have emerged as suitable candidates for load bearing applications in several fields.

The polymeric matrix and its interaction with a reinforcing phase, that is in the form of continuous or discontinuous high stiffness fibers and particles, represents one of the major controlling factors in the properties of a composite. Since fiber-reinforced polymers show high strength and stiffness to weight ratios, they have gained research attention; little by little, the interest in applications for composites has also been extended to particulate polymer composites and, lately, to nanocomposites.[53] Different polymer-based composites have also been studied for biomedical applications. Specific advantages have been obtained in using polymer-based composite biomaterials that are also called "biocomposites".[53,54]

As can be easily understood, the concept of polymer-based composite material has been rapidly extended to the design of scaffolds for tissue engineering, the aim being to improve their functionality.

## I.IV Poly-ε-caprolactone

Poly-ε-caprolactone (PCL) is a biodegradable polyester with a low melting point of around 60°C and a glass transition temperature of about −60°C. PCL is obtained from ring opening polymerization of ε-caprolactone using a catalyst, such as stannous octanoate or different metal-based, enzymatic, and organic systems (Figure I.IV).[55,56] Polycaprolactone is commonly used in the manufacture of special polyurethanes, because it imparts good water, oil, solvent and chlorine resistance to the polyurethane produced. Furthermore, polycaprolactone is often used as an additive for resins, in order to improve their processability and their end use properties (e.g., impact resistance). Being compatible with a range of other materials, PCL can be mixed with starch to lower its cost and increase biodegradability or it can be added as a polymeric plasticizer to polyvinyl chloride (PVC).[57-59]

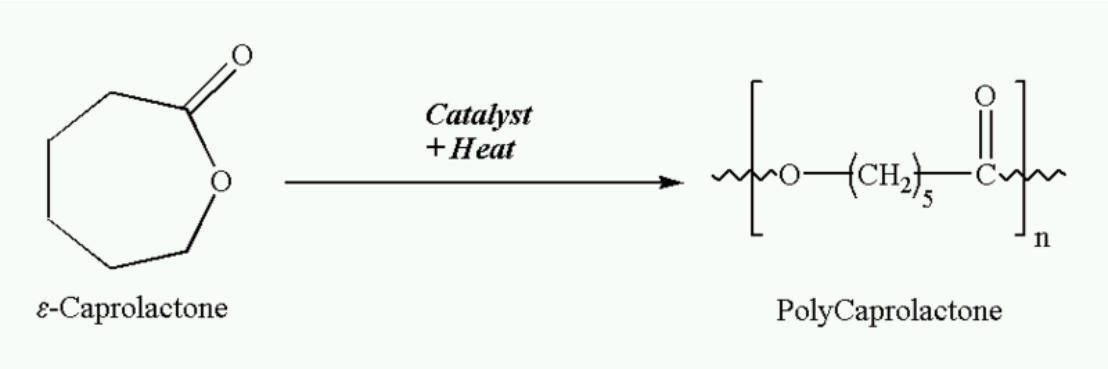


**Figure I.IV: Ring opening polymerization of ε-caprolactone to polycaprolactone.**

PCL has been used in different fields such as biomaterial for scaffolds in tissue engineering,[61,65–67] in long-term drug delivery systems[56,62,63] (in particular contraceptives delivery[60]), in microelectronics,[68] as adhesives,[64] and in packaging.[60] Its wide applicability and interesting properties (controlled degradability, miscibility with other polymers, biocompatibility and potential to be made from monomers derived from renewable sources) make PCL a very useful polymer if its properties can be controlled and it can be made inexpensively.

## *I.IV.I Chemical features*

From a chemical point of view, polycaprolactone represents a linear aliphatic polyester and it is characterized by the structural formula:

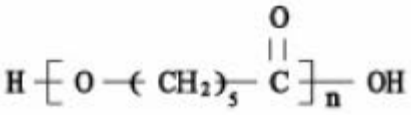

It is able to dissolve at room temperature in the presence of various solvents, such as dimethylacetamide (DMAC), benzene and chloroform, chosen according to the specific application.[72]

The most important feature of the PCL is its ability to degrade in physiological environment; in particular it is affected by degradation phenomena due to the ease of interaction that the aliphatic ester bonds along the backbone show with water molecules.

PCL biodegrades within several months to several years depending on the molecular weight, the degree of crystallinity of the polymer, and the conditions of

degradation.[60–68,70] Many microbes in nature are able to completely biodegrade PCL.[70] The amorphous phase is degraded firstly, resulting in an increase in the degree of crystallinity while the molecular weight remains constant.[61] Then, cleavage of ester bonds results in mass loss.[56,65] The polymer degrades by end chain scission at higher temperatures while it degrades by random chain scission at lower temperatures (Figure I.V).[64] PCL degradation is auto-catalyzed by the carboxylic acids liberated during hydrolysis[56] of the ester bond[73] but it can also be catalyzed by enzymes, resulting in faster decomposition.[63] While PCL can be enzymatically degraded in the environment, it cannot be degraded enzymatically in the body.[60]

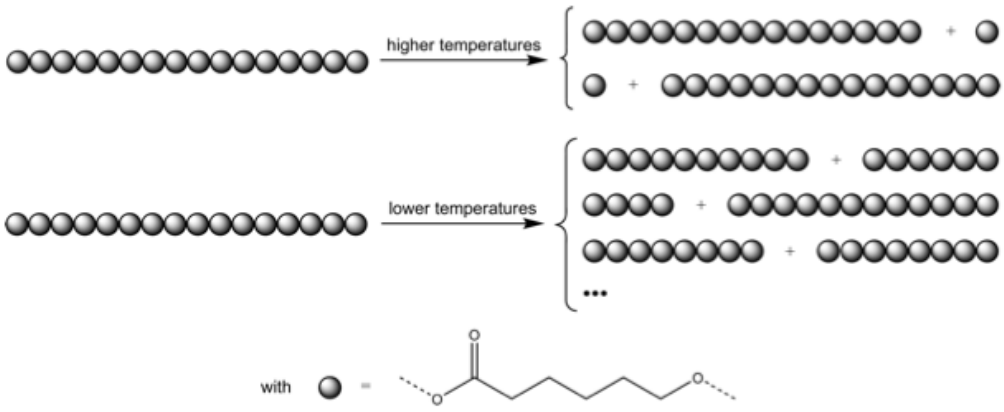


**Figure I.V: Cleavage of the polymeric chains during the degradation of PCL.[55]**

Many studies were made in order to better understand the degradation process of the PCL. For example, some studies have shown that free radicals produced by the reaction between the carboxylic group are much more reactive than oxygen radicals produced by reaction with oxydrile ($OH^-$) groups.[73] Other works aimed to study the evolution of physical and chemical properties during the degradation process.

Figure I.VI shows the trend of the molecular weight of the polymer in distilled water. It is clear that, due to the activation of hydrolysis, the breaking of bonds along the aliphatic macromolecules, which gradually become shorter, begins and this causes the loss of molecular weight, faster at first, and then most significant slower, until the complete degradation of the polymer.[73]

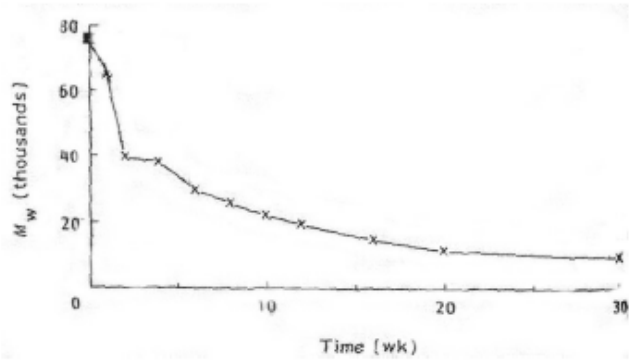


**Figure I.VI: PCL molecular weight versus time, after the introduction in distilled water.[74]**

Similarly, as the mechanism of degradation goes on, a percentage reduction in the amount of polymer occurs.[75]

The period of time where the degradation process take place is pretty long: in distilled water, it is of about 30 weeks, in agreement with the figure I.VI.[74]

Sun et al. (2008) highlighted that the *in vivo* degradation of PCL was observed for 3 years in rats. The distribution, absorption and excretion of PCL were traced in rats by radioactive labeling. PCL capsules with initial molecular weight ($M_w$) of 66000 g $mol^{-1}$ remained intact in shape during 2-year implantation. It broke into low molecular weight ($M_w$ 1⁄4 8000 g $mol^{-1}$) pieces at the end of 30 months. The molecular weight ($M_w$) of PCL decreased with time and followed a linear relationship between log $M_w$ and time (Figure I.VII).[69]

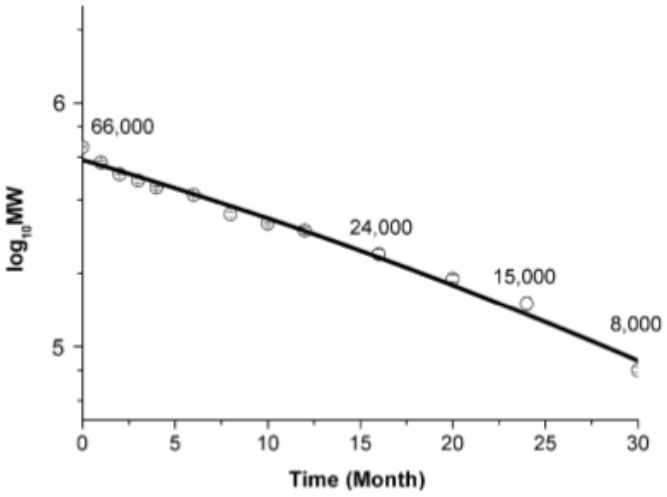


**Figure I.VII: Decrease in $M_w$ of PCL capsules, implanted in rats, with time. A linear relationship between the logarithm of $M_w$ and time was observed. [69]**

## *I.IV.II Physical features*

Polycaprolactone is a thermoplastic semi-crystalline polymer[76] characterized by high workability that enables the rapid modeling of the form that is more useful for the application. It is a very versatile polymer since it shows a high propensity to form compatible blends with a wide variety of polymers. In fact, it is easily co-polymerized with monomers such as ethylene oxide, cloroprene and methylmethacrylate, to achieve composites able to present, in addition to the widely documented biocompatibility, suitably mechanical properties.

The main limitation of the PCL lies in its mechanical properties (compressive strength of about 1.6 MPa[75] and tensile strength between 20.7 and 42.0 MPa[77]) that are lower if compared to those of hard tissue (i.e., cortical bone).

## *I.IV.III Biomedical applications*

PCL degrades by hydrolysis of its ester linkages in physiological conditions (such as in the human body) and has therefore received a great deal of attention for use as an implantable biomaterial. In particular, it is especially interesting for the preparation of long-term implantable devices, owing to its degradation which is even slower than that of polylactide.

PCL has been approved by the Food and Drug Administration (FDA) in specific applications used in the human body as (for example) a drug delivery device, suture (sold under the brand name Monocryl or generically), or adhesion barrier.

It is being investigated as a scaffold for tissue repair via tissue engineering,[61,65-67] and as a membrane for guided bone replacement (GBR)[78]. It has been used as the hydrophobic block of amphiphilic synthetic block copolymers used to form the vesicle membrane of polymersomes. A variety of drugs have been encapsulated within PCL beads for controlled release and targeted drug delivery.[56,62,63]

In odontology or dentistry (as composite named Resilon)[71], it is used in root canal filling. It performs like gutta-percha: it has the same handling properties and, for retreatment purposes, may be softened with heat, or dissolved with solvents like chloroform.[71] Similar to gutta-percha, there are master cones in all ISO sizes and accessory cones in different sizes available. The major difference between the

polycaprolactone-based root canal filling material (Resilon and Real Seal) and gutta-percha is that the PCL-based material is biodegradable but the gutta-percha is not degradable. There is lack of consensus in the expert dental community as to whether an absorbable root canal filling material, such as Resilon or Real Seal is desirable.[71]

## *I.IV.IV Hobbyist and Prototyping*

PCL also has many applications in the hobbyist market. Some brand names used in selling it to this market are Mold-Your-Own Grips, InstaMorph, Shapelock, Hand Moldable Plastic, and Friendly Plastic in the US, and Polymorph in the UK. It has physical properties of a very tough, nylon-like plastic that melts to a putty-like consistency at only 60°C.


**Figure I.VIII: Home-made bicycle light mounting, made from PCL.**

PCL's specific heat and conductivity are low enough that it is not hard to handle at this temperature. This makes it ideal for small-scale modeling, part fabrication, repair of plastic objects, and rapid prototyping where heat resistance is not needed. Though molten PCL readily sticks to many other plastics, if the surface is cooled, the stickiness can be minimized while still leaving the mass pliable.

## I.V Scaffolds for Tissue Engineering

The design of a scaffold able to guide tissue regeneration represents a promising challenge in the field of tissue engineering. The ideal scaffold should promote and control specific events at the cellular and tissue levels, as results of its unique chemical, biochemical and biophysical cues.[3,44] Consequently, a scaffold has to satisfy several requirements[2,3,67,79] that can be briefly summarized as follows.

It should be characterized by interconnecting pores of specific scale, and made using materials with controlled biodegradability or bioresorbability.

It should possess suitable mechanical properties to match the intended site of implantation and handling, as well as specific surface chemistry for promoting cell attachment, differentiation and proliferation.

In addition, the scaffold should not induce adverse reactions, and it should be easily manufactured into a variety of shapes and sizes.

Over the last two decades, the concept of cell guidance has also been progressively revised[32-54,67,72-77,79-85] since a new knowledge about the complex features of cell-material interaction has come to light. Thus, novel scaffold materials based on the cell guidance concept have been developed, benefiting from contemporary advances in the fields of molecular biology and materials science.[3,32]

Several polymeric and composite materials have been used to make three-dimensional (3D) porous scaffolds, using both conventional methods and more advanced manufacturing processes. [67,79,32-37,87-92]

Conventional techniques include solvent casting and particulate leaching, gas foaming, fiber meshes and fiber bonding, phase separation, melt molding, emulsion freeze drying, solution casting etc., whilst rapid prototyping is a common name for a group of techniques which can generate a physical model directly from a computer aided design (CAD) data and may act as a methodical interface between tissue and engineering.[91-95] Among Rapid Prototipyng techniques, 3D Printing, Stereolithography, Selective Laser Sintering (SLS), Fused Deposition Modeling (FDM), etc. are included. Differently from conventional processing techniques, rapid prototyping offers the possibility to strictly control pore geometry, size and interconnectivity, as well as the spatial distribution of pores within the structure. Among novel rapid prototyping techniques for scaffold fabrication, 3D Fiber

Deposition[2,34-37,94-96] has recently emerged as a method to manufacture well-defined and custom-made scaffolds for tissue regeneration, with 100% interconnected pores.
The main advantages of this CAD/CAM based technique consist in obtaining scaffolds with pores, which are interconnected per definition, as the structure can be built layer-by-layer alternatively depositing polymer fibers with a particular sequence of stacking.

## I.VI Rapid Prototyping (RP)

Materials of natural, synthetic, semi-synthetic and hybrid origins have been proposed and tested as scaffolds for tissue regeneration.[35,39,40]
Synthetic and natural inorganic ceramic materials, such as hydroxyapatite and tricalcium phosphate, have been considered as candidates for scaffold materials for bone tissue engineering.[42,91] These ceramics resemble the natural inorganic component of bone and possess osteoconductive properties.[43,91] The main drawback is that they are inherently brittle and cannot match the mechanical properties of bone. Moreover, ceramic scaffolds are not suitable for the growth of soft tissues since they are characterized by different cellular receptors and mechanical performances. Synthetic and natural polymers are an attractive alternative and versatile in their applications to the growth of most tissues.[46,47,99]
As for synthetic polymers, the previously mentioned aliphatic polyesters (PGA, PLLA, PLGA and PCL) are the most commonly used polymers for designing scaffolds. Products obtained from the degradation of these polymers (glycolic acid and lactic acid) are present in the human body and can be removed by natural metabolic pathways. On the other hand, naturally derived protein or carbohydrate polymers have been considered as scaffold materials for the growth of several tissue types.[46,94] By far the most popular natural polymer used for tissue engineering scaffolds is collagen.
Different techniques have been developed to fabricate 3D porous scaffolds, each characterized by its own advantages and limitations.
The introduction of RP technologies in the biomedical field has led to the division of scaffold fabrication techniques into two groups, defined as “conventional” and “novel” methods.[91,94] In particular, conventional methods are defined as processes to

obtain scaffolds that are characterized by continuous, uninterrupted pore structure, however, lacking any long-range channeling microarchitecture. Basically, these techniques include fiber meshes/fiber bonding, gas foaming, solvent casting/particulate leaching, phase separation, melt molding, freeze drying, solution casting, and emulsion freeze drying.[91,94]

The internal architecture of scaffolds, including pore size, pore shape and interconnectivity, are critical to their *in vivo* and mechanical performances, since it influences the degree and the path of tissue regeneration, and determines the mechanical properties of the scaffolds.[92-109] However, in many scaffold manufacturing techniques, the control of the internal architecture and interconnectivity is limited.[92-109] Conventional scaffold processing techniques are, in fact, incapable of precisely controlling pore size, pore geometry, spatial distribution of pores and construction of internal channels within the scaffold.[91,94] For example, scaffolds produced by solvent casting/particulate leaching cannot guarantee interconnection of pores because this is dependent on whether the adjacent salt particles are in contact. Furthermore, the interconnectivity provided by these techniques is strongly related to many processing variables, such as the rate of solvent evaporation and the 3D contact between the porogen particles.[89,92] Consequently, using conventional scaffold manufacturing methods to have precise control over the internal architecture and interconnectivity is very difficult. Moreover, scaffolds fabricated with conventional techniques can be shaped with custom-made molds.

Conversely, the technology transfer of solid freeform fabrication (SFF) to tissue engineering represents the key to produce customized scaffolds with reproducible internal morphology. This allows for a higher degree of architectural control, making structures to increase the mass transport of oxygen and nutrients throughout the scaffold.[91,94]

SFF is a collective term for a group of technologies that can manufacture objects in a layer-by-layer fashion from the 3D computer design of the object. SFF was initially developed for fabricating prototype engineering parts, thus the name “rapid prototyping” (RP) is also widely used.[79,89,91,92,94,109]

Since 1987, more than 20 SFF technologies have been developed and these technologies differentiate themselves mainly by the method by which the layers are laid down, solidified, and attached to the previous ones.[79,89,91,92,94,109]

Even though there are several commercial variants of SFF technology that differ significantly in the way they build up 3D models, they also present several common features, since all SFF technologies are characterized by three basic steps in their process: data input, data file preparation, and object building.[91-92,110-111] In particular, the general process involves producing a computer-generated model using computer-aided design (CAD) software. Successively, a CAD model is expressed as a series of cross-sectional layers, and the data are implemented by the SFF machine that creates the physical model. Some SFF technologies require an additional step of post-processing to remove either temporary supports or the excessive material trapped inside the void space in the built structure. Furthermore, if a second type of data source is data obtained from computed tomography (CT) or magnetic resonance imaging (MRI), medical scans can be used to create a customized CAD model and, consequently, a scaffold which should be characterized by the exact external shape required to correct the damaged tissue site.[91-92,110-111] Among these SFF technologies, many have been modified or developed towards the manufacturing of tissue engineering scaffolds, including 3D printing, fused deposition modeling, ink-jet printing, stereolithography, selective laser sintering and a few other extrusion-based technologies, such as 3D Bioplotting.[79,89,91,112-115]

3D printing incorporates a technology to eject a binder from a jet head that moves in accordance with the CAD cross-sectional data, onto a polymer powder surface. The binder dissolves and joins adjacent powder particles. The piston chamber is lowered and refilled with another layer of powder and the process repeated. The unbound powder acts to support overhanging or unconnected features and needs to be removed after component completion.[91,114]

Fused deposition modeling (FDM) uses a moving nozzle to extrude a fiber of polymeric material from which the physical model is built layer-by-layer. The model is lowered and the procedure repeated. Although the fiber must also produce external structures to support overhanging or unconnected features that need to be manually removed, the pore sizes in tissue engineering scaffolds are sufficiently small enough for the fiber strand to bridge across without additional support structures.[91,113,116-117]

In ink-jet printing the layout of the system consists of a build platform set on top of an elevator with a rolling cutter blade on one side of the platform and two print jets mounted on x, y rails. Two print materials are used, build materials and support materials. The build jet first lays down the design pattern by printing droplets onto the

platform. The support jet then prints support material around the printed pattern. After printing, the cutter blade comes over and cuts the build layer to a predetermined layer thickness, thereby controlling the accuracy in the z-direction. The build jet then prints build material for the next layer. The process repeats itself until the entire object is completed.[91-92,94]

As for stereolithography, the basic process involves selective polymerization of a liquid photocurable monomer by an ultraviolet laser beam. The UV beam is guided (x- and y-axis control) onto the liquid monomer surface, in accordance with the CAD cross-sectional data. After the first layer is built, the elevator holding the model is lowered into the vat so as to allow the liquid photopolymer to cover the surface. A "wiper arm" is then displaced over the liquid to flatten the surface. The procedure is repeated until the model is completed. This system requires support structures to be added to the model, to prevent any overhanging or unconnected features from falling to the bottom of the liquid-filled vat. After completion, the model is raised and any support structures are removed manually.[91-92,94,112,118]

In selective laser sintering (SLS), the build material of the system is either a polymer or a polymer-coated ceramic powder. The layout of the system consists of a build platform set on top of an elevator with a powder dispensing roller on one side of the platform and a $CO_2$ laser on the top of the machine. The powder bed on the platform is preheated to a temperature just below the glass transition temperature of the polymer to minimize the energy required in the subsequent fusing processing. In object building, the computer directs the $CO_2$ laser to a raster on the polymer or the polymer-coated ceramic powder bed causing the powder particles to fuse. After one layer is built, the platform moves downward to a specified distance to allow the powder dispensing roller to travel across the platform and coat the entire layer with fresh powder. The computer then directs the laser to a raster on the fresh powder to build the next layer. The process is repeated until the entire object is made. In building scaffold-like structures where multiple internal channels are present, there is loose, un-synthesized powder trapped inside the channels and it will require a post-processing step to remove the trapped powder.[91-94,119]

3D Bioplotting is an extrusion-based technology similar to FDM. This technology uses a pressurized nozzle to extrude the build material into the form of filaments which solidify onto the platform. The Bioplotter system, developed by researchers at the University of Freiburg, involves a moving extruder head (x-, y- and z-axis control)

and uses compressed air to force out a liquid or a paste-like plotting medium. The extruder head can be heated to the required temperature. The medium solidifies when it comes in contact with the substrate or previous layer.[33,86,91-94]

A comparison of the above-mentioned RP techniques on the basis of materials, advantages and disadvantages are summarized in Table I.I.[92-94]

| RP techniques | Materials | Advantages | Disadvantages |
|---|---|---|---|
| Stereolithography | Reactive resins | Good mechanical strength<br>Easy to remove support materials<br>Easy to achieve small features | Limited to reactive resins (mostly toxic)<br>Limited choice of photopolymerizable and biocompatible liquid polymer materials |
| 3D Printing | Ink + powder of bulk polymers, ceramics | No inherent toxic components<br>Fast processing<br>Low costs | Weak bonding between powder particles<br>Rough surface<br>Post-processing |
| Inkjet Printing | Wax or wax compounds | Excellent accuracy | Slow process<br>Material limited to low melting point wax |
| FDM/FDC | Some thermoplastic polymers/ceramics | Low costs | Elevated temperatures during process<br>Small range of bulk materials<br>Medium accuracy |
| Selective Laser Sintering | Metals, ceramics, bulk polymers, compounds | High accuracy<br>Good mechanical strength<br>Broad range of bulk materials | Elevated temperatures - local high energy input<br>Uncontrolled porosity<br>Trapped powder difficult to be removed |
| 3D Bioplotting | Swollen polymers (hydrogels), thermoplastic polymers, reactive resins, ceramics | Broad range of materials<br>Broad range of conditions<br>Incorporation of cells, protein and fillers | Slow processing<br>Low accuracy<br>Limited resolution<br>No standard condition-time consuming adjustment to new materials |

**Table I.I: Comparison of different rapid prototyping (RP) techniques on the basis of materials, advantages and disadvantages.[94,115]**

## I.VII 3D Fiber Deposition Technique

As previously described, RP techniques offer the possibility of directly fabricating scaffolds with different geometric structures and with different properties.

The scaffolds are built layer-by-layer through material deposition by CAD/CAM techniques, either as a molten thermoplastic material, as in the case of the fused deposition modeling technique, or as droplets together with a binding agent, as in the 3D printing technique.[33,89,91,116]

In 2000 a new RP technology based upon 3D dispensing of liquids and pastes in a liquid medium, also referred to as 3D plotting technology, was developed at the Freiburg Materials Research Center to produce objects with complex architectures according to computer design. Individual microstrands and microdroplets can be positioned combined with in situ bonding to produce architectures similar to non-woven materials.[33,86,115] The direction of the individual strands can be varied layer-by-layer. Therefore, it is possible to design scaffolds with interconnecting pores, thus

meeting the demands for cell attachment and cell growth. Among all of the RP techniques, 3D plotting and 3D Fiber Deposition[34,35] have been recently developed and used for tissue engineering purposes. In particular, 3D Fiber Deposition may be considered as a modified technique of 3D plotting for the extrusion of highly viscous polymers, and it is a fused deposition technique in which a molten polymer is extruded and then deposited through a servo-mechanically controlled syringe that applies pressure.[34,36,37] This process allows the realization of scaffolds with specific shape and size and 100% interconnectivity. Such scaffolds possess a defined structure and architecture, and can be built with a customized shape by CAD/CAM techniques.[33,86,115]

The key element of the 3D Fiber Deposition technique is a dispensing machine known as a Bioplotter, which was developed by Landers et al.[33,86,115] to fabricate scaffolds from hydrogels for soft tissue engineering (Figure I.IX). In particular, it consists of a dispenser, equipped with a heating jacket that is movable in three dimensions. The basic process involves dispensing of a flowable material stored into a cartridge through a thin needle by air-pressure control, and its subsequent hardening. The material can be dispensed in the presence of air or in a liquid. The advantage of dispensing in a liquid medium is that the buoyancy in the liquid prevents deformation in the dispensed but not the completely hardened structure.[115] Consequently, only highly viscous materials, such as polymer melts, can be processed in air. Hardening processes can be obtained through thermally induced solidification, solidification induced by a chemical reaction (e.g. a reactive component is added to the plotter material and a second one is added to the plotter medium), and solidification induced by precipitation. Among solidification processes, the thermally induced one includes solidification of melts and gelling of thermally reversible hydrogels, such as gelatin and agar.

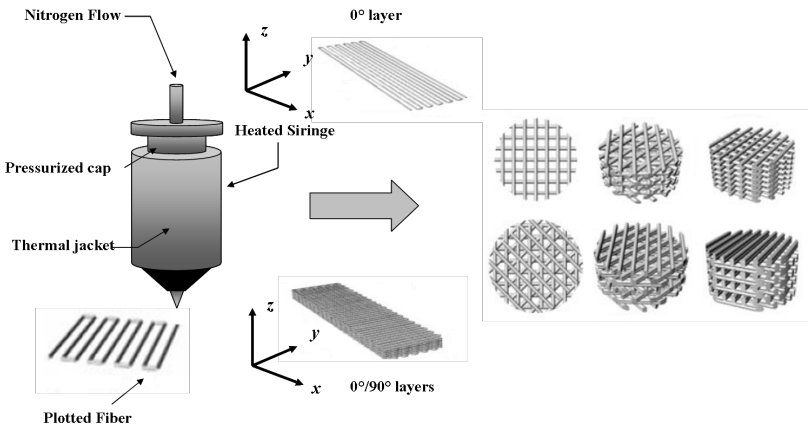


**Figure I.IX: Schematic representation of 3D Fiber Deposition process and different scaffold architectures.**[33,36,37]

The knowledge of the critical processing parameters is crucial to develop 3D fiber-deposited scaffolds. Briefly, if a molten polymer is assumed as a viscous Newtonian fluid and the Hagen-Poiseuille equation as valid,[34,120] the flow rate from the nozzle can be expressed according to:

$$Q = \frac{\pi \Delta P}{128 l \eta} \cdot d^4 \qquad (1)$$

The above described Hagen-Poiseuille equation (1) indicates that the flow rate (Q) is directly proportional to both the pressure gradient (ΔP) across the syringe and needle tip, and the needle diameter (d). Moreover, Q is inversely proportional to needle length (l) and polymer viscosity (η). A high Q value may result in over-deposition of the fiber, thus reducing porosity, whilst a low Q value reduces the fiber diameter, compromising the overall scaffold integrity.

A decrease in needle diameter reduces the flow rate, requiring considerably greater pressures to extrude fibers, and in the case of small needle diameters the pressures required to achieve a suitable flow rate can be greater than those usually used in practice, thus needing changes in viscosity.[34] Even though for small needle diameters polymer viscosity can be reduced through the addition of specific solvents or increasing the syringe temperature, the incomplete removal of solvents post-processing or polymer exposure to high temperatures can be detrimental to scaffold biocompatibility.[79,86] By exploiting the knowledge about the plotting process and the properties of the materials, 3D fiber-deposited scaffolds with desired properties may be obtained.

For the first time, Lander et al.[33,86,115] designed and characterized hydrogel scaffolds with a desired external shape and a well defined internal pore structure through 3D Bioplotting, also suggesting this technology as a bio-functional and cell compatible processing for hydrogels in the area of RP techniques. In particular, the versatile application potential of rapid prototyped agar scaffolds coated with a mixture of hyaluronic and alginic acid or with fibrin was demonstrated in cell culture using two cell types which were seeded on these hydrogel scaffolds, a human osteosarcoma cell line (CAL-72) and a mouse connective tissue fibroblast.

Woodfield et al.[34] presented and characterized the 3D Fiber Deposition technique for making 3D poly(ethylene glycol)-terephthalate-poly(butylene terephthalate) (PEGT/PBT) block co-polymer scaffolds with a 100% interconnecting pore network for articular cartilage tissue engineering. This technique allowed to design desired scaffold characteristics layer-by-layer by accurately controlling the deposition of molten co-polymer fiber from a pressure-driven syringe placed onto the mobile arm of a 3D plotter. Values of dynamic stiffness similar to those of native articular cartilage explants were obtained by suitably varying porosity, pore geometry and PEGT/PBT composition. It was demonstrated that these 3D fiber-deposited scaffolds seeded with bovine articular chondrocytes supported a homogeneous cell distribution and subsequent cartilage-like tissue formation following *in vitro* culture as well as subcutaneous implantation in nude mice. These results were highlighted by the presence of articular cartilage extracellular matrix constituents (glycosaminoglycans and type II collagen) throughout the interconnected pore structure. Interesting results were also achieved with respect to the attachment of expanded human articular chondrocytes.

Since nutrient limitation (e.g. oxygen) has been considered as a cause of the onset of chondrogenesis solely within the peripheral boundaries of larger constructs, the effect of the 3D fiber-deposited PEGT/PBT scaffold architecture on oxygen gradients in tissue engineered cartilaginous constructs was assessed by Malda et al.[35] through microelectrode measurements, and then compared to the results obtained from a compression-molded and particle-leached scaffold.

Even though it was not observed, an effect of scaffold architecture on oxygen gradients, cell distribution and matrix deposition was enhanced in 3D fiber-deposited scaffolds if compared to the compression-molded and particle-leached ones.[35] All of these results stressed the importance of a rationally designed scaffold for cartilage

tissue engineering applications, and suggested that organized structures, such as the 3D fiber-deposited scaffolds, with their less tortuous and more open structure may offer possibilities for the regulation of nutrient supply.[35]

In this context, Moroni et al.[33,36,37] designed, manufactured and characterized 3D fiber-deposited scaffolds processing poly(ethylene oxide terephthalate)-poly-(butylene terephthalate) (PEOT/PBT) block copolymers which belong to a class of materials known as thermoplastic elastomers, and possess mechanical properties depending on the PEOT/PBT weight ratio in block form and on the molecular weight of the initial poly(ethylene glycol) (PEG) blocks.

Several PEOT/PBT copolymer compositions were used to fabricate scaffolds with a Bioplotter device through heating polymer granules. Moreover, pores were varied in shape and size, by changing fiber diameter, spacing, sequence of stacking (i.e. pattern), and layer thickness. However, since pore geometry (and, hence, porosity) is defined by fiber diameter and spacing, and layer thickness, it is also strongly dependent on the deposition speed used during the process (Figure I.X).[36]

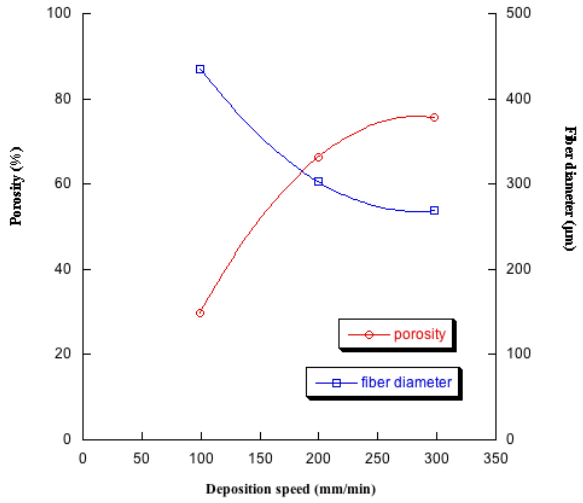


**Figure I.X: Effect of deposition speed on scaffold porosity and fiber diameter. Results obtained from 3D fiber-deposited PEOT/PBT scaffolds with specific composition and architecture.[36]**

Accordingly, in order to assess the influence of the pore geometry and architecture on the mechanical performances, 3D fiber-deposited PEOT/PBT scaffolds were characterized through dynamic-mechanical analysis (DMA).

In particular, with increasing porosity, DMA analysis showed a decrease of the elastic properties such as the storage modulus (E′) (Figure I.XI a)[37], whilst an increase of the

modulus was evaluated with decreasing the fiber spacing (Figure I.XI b).[37] Furthermore, it was also evidenced hat for PEOT/PBT scaffolds with the same composition and porosity but different architectures, E′ varied within a wide range of values (Figure I.XI c).[37]

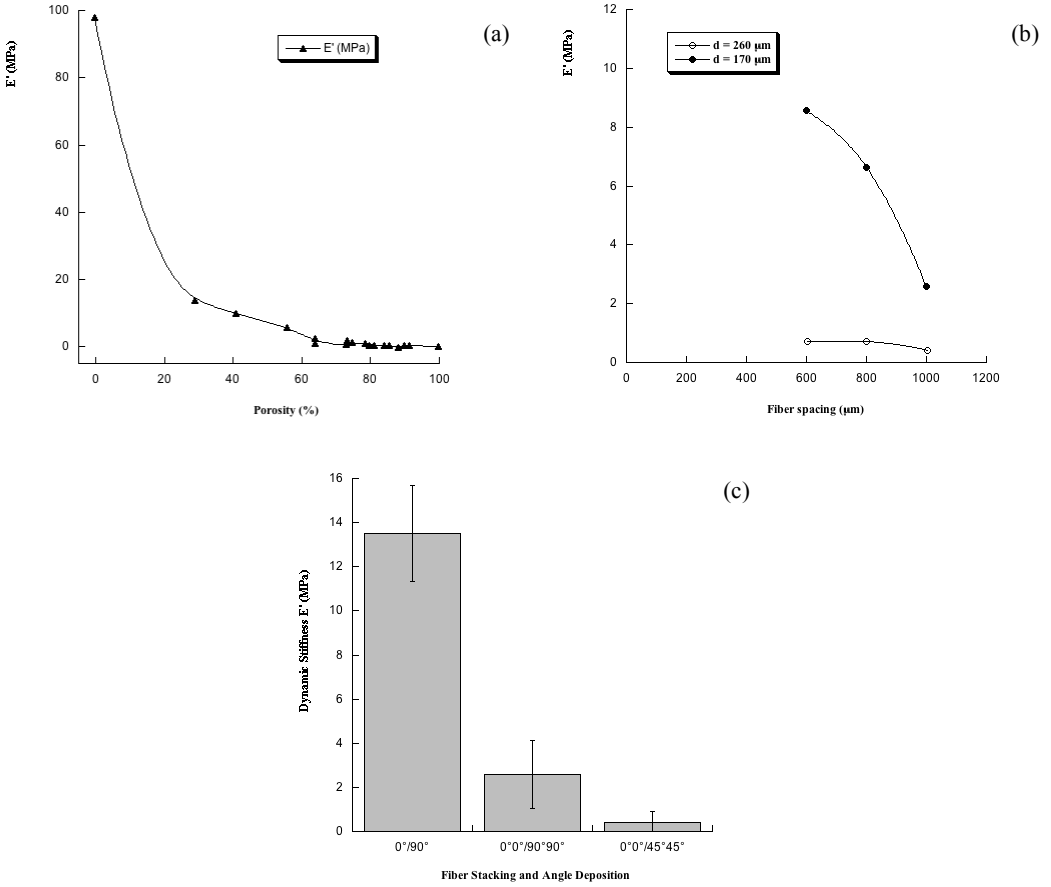


**Figure I.XI: a) Effect of porosity on the storage modulus E′ for 3D fiber-deposited PEOT/PBT scaffolds with specific composition; b) Effect of fiber spacing on the storage modulus E′ for 3D fiber-deposited PEOT/PBT scaffolds with specific composition and architecture, considering two different fiber diameters; c) Effect of architecture on the storage modulus E′ for 3D fiber-deposited PEOT/PBT scaffolds with same composition and porosity.[37]**

Another interesting approach was to make hollow fibers directly integrated in a 3D fiber-deposited structure, thus realizing scaffolds, which can be used in tissue engineering and controlled drug delivery applications as possible smart biomaterial devices.[93]

To realize hollow fibers with controllable hollow cavity diameter and shell thickness a rheological phenomenon, which is known as “viscous encapsulation” and often undesired in molten polymeric blends, was considered.[93]

Briefly, when two components of a polymer blend possess a significant difference in viscosity in the molten state fibers with a shell-core configuration can be extruded.

The polymer with lower viscosity tends to shift, when flowing through a narrow duct, such as the nozzle of an extruder (e.g. the needle used during the 3D Bioplotting process), towards the walls of the nozzle during extrusion. Due to the higher shear stresses at the walls this separation of the components produces a stratification or a ‘‘canalization’’ effect, thus providing fibers with a shell-core structure (Figure I.XII). By removing the polymer core by selective dissolution, hollow fibers can be obtained.[93]

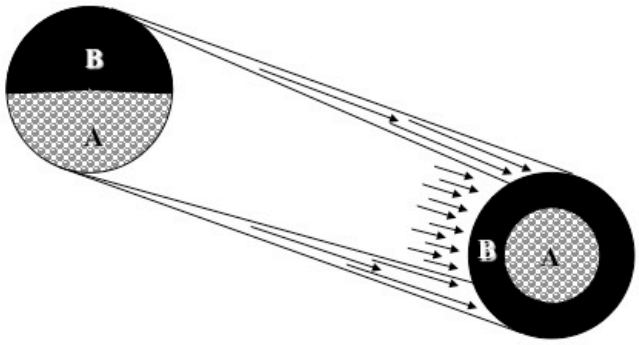


**Figure I.XII: Viscous encapsulation phenomenon: arrows indicate the encapsulation of the high viscosity polymer (A) by the low viscosity polymer (B), due to higher shear stress (longer arrows) at the nozzle walls.[93]**

Taking into consideration this phenomenon, Moroni et al.[93] manufactured and characterized PEOT/PBT scaffolds with hollow fibers through the direct deposition of the viscous encapsulated fibers in a CAD/CAM fashion and the subsequent selective core dissolution. In particular, PEOT/PBT scaffolds with hollow fibers were obtained by soaking 3D shell-core scaffolds in a specific solvent (i.e. acetone) for the poly(butylmethacrylate-methylmethacrylate) (P(BMA/MMA)) or for the PCL core polymers. Consequently, P(BMA/MMA) or PCL was selectively dissolved and only the PEOT/PBT well organized structure was left. However, it was found that viscous encapsulation occurred for specific values of melting index ratios when these polymers are extruded under proper rheological conditions of the 3D Fiber Deposition process used.[93]

Accordingly, by varying the polymers in the blend, the blend composition, and the extrusion needle diameter, the possibility to control the hollow cavity diameter and the shell thickness was also highlighted.

Benefiting from the same principle, biphasic 3D fiber-deposited scaffolds for cartilage tissue engineering with a shell-core fiber structure, in which the core polymer

provided appropriate mechanical properties and the shell polymer acted as a coating characterized by specific physicochemical surface properties, were designed and studied.[104] In this case, biphasic shell-core PEOT/PBT 3D scaffolds were manufactured from PEOT/PBT co-polymers with different compositions (hence, a different melting index), by exploiting viscous encapsulation and 3D Fiber Deposition technique. If compared to the core polymer, the shell polymer contained a higher molecular weight of the initial PEG segments used in the copolymerization and a higher weight percentage of the PEOT domains. Rapid prototyped scaffolds entirely produced with the shell or with the core polymers were also characterized and the results were compared with those of biphasic shell-core scaffolds. Even though for all of the investigated scaffolds comparable amounts of entrapped chondrocytes and of extracellular matrix formation were obtained, chondrocytes maintained their rounded shape and aggregated during the culture period on shell-core 3D fiber-deposited scaffolds, thus suggesting a proper cell differentiation into articular cartilage. Moreover, from a mechanical point of view, the biphasic shell-core scaffolds also evidenced an improved dynamic stiffness. All of these results suggested that the use of these biphasic shell-core 3D fiber-deposited scaffolds with appropriate mechanical and surface properties is a promising solution for cartilage tissue engineering.[121]

Furthermore, since cell seeding efficiency still remains a critical factor for optimal tissue regeneration, the possibility to combine the 3D Fiber Deposition technique with electrospinning was also demonstrated;[122] therefore, obtaining scaffolds where the periodical macrofibers typical of 3D fiber-deposited structures were integrated with the random electrospun ones. In these integrated structures, the 3D fiber-deposited scaffold acts as a structural support with adequate mechanical properties, whilst the electrospun network mainly works as a cell entrapment system.

An additional challenge in tissue engineering is that most tissues and organs are multiphasic in nature and contain multiple cell types. Consequently, an ideal scaffold should be capable of supporting multilineage cell types and few attempts have been made to engineer tissues consisting of different cell types.[38,123,124]

For these reasons, stabilized osteoblast-like cells (MG63) and normal endothelial cells (human umbilical vein endothelial cells, HUVEC) were co-seeded onto 3D fiber-deposited PCL scaffolds, and cultured by means of a rotary cell culture system in order to study their reciprocal cell interactions for enhanced bone tissue engineering.[38]

The proposed co-cultural endothelial and osteoblast-like cell model is based on the close mutual interaction of the two cell types, and this is sustained by histological evidence that osteoblasts and osteoprogenitor cells are always located adjacent to blood vessel endothelial cells.[38,125,126] Moreover, with regard to embryonic skeletal tissue osteogenesis and angiogenesis are temporally related.[38,127] All of these *in vivo* findings clearly highlight that these processes are mutually interdependent[38,128] and that endothelial cells may accelerate bone formation through angiogenesis as well as in bone remodeling.[38,129]

Since the maintenance, survival and growth of a 3D bio-construct is strongly related to a delicate balance between cell metabolism, nutrient transport and scaffold properties,[38,130,131] porous yet sufficiently stiff 3D structures with a suitable architecture were manufactured.

In particular, 3D fiber-deposited PCL scaffolds were fabricated with a Bioplotter device by extruding the molten polymer and alternatively depositing the fibers along the 0° and the 90° directions between two successive layers, thus obtaining a 0°/90° pattern.[38]

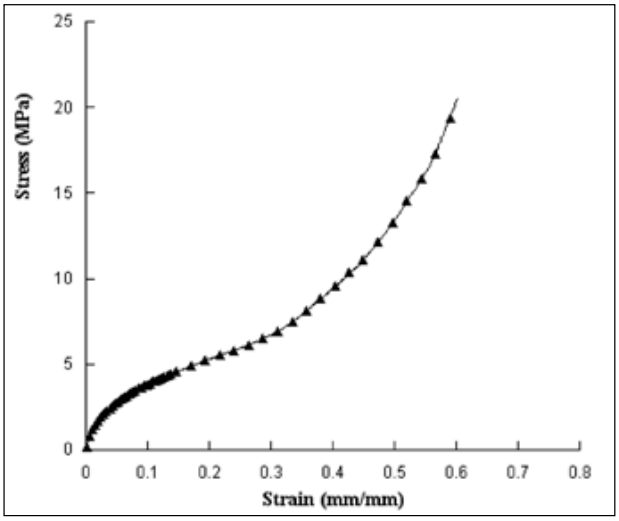


**Figure I.XIII: Typical stress-strain curve of a 3D fiber-deposited PCL scaffold with specific architecture, pore shape and size, tested in compression up to strain level of 60%.[2,38]**

As for the mechanical properties of these 3D PCL scaffolds, compression tests highlighted a modulus of 134.6 ± 8.5 MPa and a stress-strain curve (Figure I.XIII) similar to that of a flexible foam.[132]

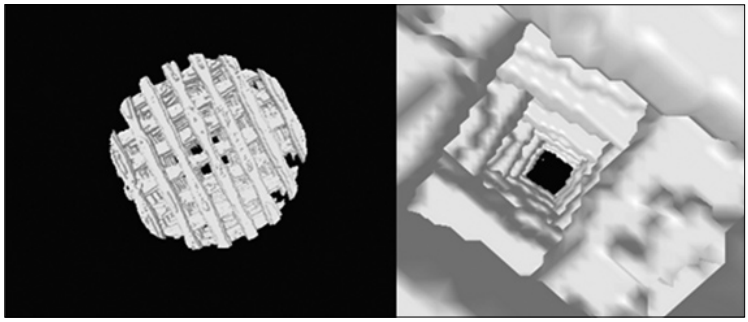

**Figure I.XIV: 3D reconstruction of a 3D fiber-deposited PCL scaffold obtained from Micro-CT analysis: a) top view, b) the inner structure highlighting the architecture and the pore interconnectivity.[38]**

After an initial relatively stiff mechanical response, there is a region with lower stiffness, finally followed by another stiff portion, similar to the densification region of flexible foams. However, unlike the typical behavior of flexible foam, the central part of the curve does not show a plateau.[38] Micro-CT and imaging analyses (Figure I.XIV) confirmed that the 3D fiber-deposited PCL scaffolds were characterized by a precise pore size and a repeatable microstructure, also showing sufficient consistency between real and theoretical values and an interconnectivity of 100%.[2,38]

In such a study on dynamic co-seeding onto 3D fiber-deposited PCL scaffolds, Kyriakidou et al.[38] underlined how osteoblasts increase proliferation of endothelial cells and endothelial cells amplify the growth of osteoblasts but decrease their differentiation. It was also suggested that dynamic seeding of osteoblasts and endothelial cells onto a 3D fiber-deposited polymeric scaffold was a useful approach to study the mechanisms of the interaction of endothelial and osteoblast cells, and to achieve a functional hybrid in which angiogenesis, furnished by neo-vascular organization of endothelial cells, may further support osteoblast growth.[2,38]

In light of what has been said, 3D Fiber Deposition is a powerful technique to design multifunctional and tailor-made scaffolds with suitable mechanical and surface properties, therefore, satisfying the need for tissue engineered porous structures with an organized and repeatable microarchitecture, which enables cells to assemble in an ordered matrix and allows adequate nutrient perfusion.

# References


1. R. Langer, J. P. Vacanti. *Tissue engineering***.** Science 1993; 260: 920-926.
2. A. Gloria, T. Russo, R. De Santis, L. Ambrosio. *3D fiber deposition technique to make multifunctional and tailor-made scaffolds for tissue engineering applications.* Journal of Applied Biomaterials and Biomechanics 2009; 7: 141-152.
3. A. Gloria, R. De Santis, L. Ambrosio. *Polymer-based composite scaffolds for tissue engineering*. Journal of Applied Biomaterials and Biomechanics 2010; 8: 57-67.
4. H. Y. Cheung, K. T. Lau, T. P. Lu, D. Hui. *Synthesis and characterization of PLLA–PLCA–PEG multiblock copolymers and their applications in modifying PLLA porous scaffolds*. Composite Part B Engineering 2007; 38: 291-300.
5. D. M. Ebenstein, L. A. Pruitt. *Nanoindentation of biological materials*. Nano Today 2006; 1: 26-33.
6. A. Shekaran, A. J. Garcia. *Nanoscale engineering of extracellular matrix-mimetic bioadhesive surfaces and implants for tissue engineering*. Biochemical Biophysical Acta 2011, 1810: 350–360.
7. B. Alberts, A.r Johnson, J. Lewis, M. Raff, K. Roberts, P. Walter. *Molecular Biology of the Cell* 4th ed, Garland Science, New York, 2002.
8. J. Rossert, B. de Crombrugghe, P.B. John, G.R. Lawrence, A.R. Gideon. *Type I Collagen: Structure, Synthesis, and Regulation*. In: *Principles of Bone Biology*, Second Edition, Academic Press, San Diego, 2002, pp. 189–210.
9. P.G. Robey, P.B. John, G.R. Lawrence, A.R. Gideon. *Bone Matrix Proteoglycans and Glycoproteins*. In: *Principles of Bone Biology*, Second Edition, Academic Press, San Diego, 2002, pp. 225–237.
10. H.Zhang, K.W.Marshall, H.Tang, D.M.Hwang, M.Lee, C.C.Liew. *Profiling genes expressed in human fetal cartilage using 13, 155 expressed sequence tags*. Osteoarthritis and Cartilage 2003; 11: 309–319.
11. A.E. Aplin, B. P. Hogan, J. Tomeu, R.L. Juliano. *Cell adhesion differentially regulates the nucleocytoplasmic distribution of active MAP kinases*. Journal of Cell Science 2002; 115: 2781–2790.

12. R.O. Hynes. *Integrins: bidirectional, allosteric signaling machines*. Cell 2002; 110: 673–687.
13. F. G. Giancotti, E. Ruoslahti. *Integrin signaling*. Science 1999; 285: 1028–1032.
14. V. Petit, J. P. Thiery. *Focaladhesions: structure and dynamics*. Biology of the Cell 2000; 92: 477–494.
15. S. Bourdoulous, G. Orend, D. A. MacKenna, R. Pasqualini, E. Ruoslahti, *Fibronectin matrix regulates activation of RHO and CDC42 GTPases and cell cycle progression*. The Journal of Cell Biology 1998; 143: 267–276.
16. C. S. Chen, M. Mrksich, S. Huang, G. M. Whitesides, D.E. Ingber. *Geometric control of cell life and death*. Science 1997; 276: 1425–1428.
17. K. Burridge, K. Fath, T. Kelly, G. Nuckolls, C. Turner. *Focal adhesions: transmembrane junctions between the extracellular matrix and the cytoskeleton*. Annual Review of Cell and Developmental Biology 1988; 4: 487–525.
18. R.O. Hynes, *Integrins: versatility, modulation, and signaling in cell adhesion*. Cell 1992; 69: 11–25.
19. N.A. Carrell, L.A. Fitzgerald, B. Steiner, H.P. Erickson, D.R. Phillips. *Structure of human platelet membrane glycoproteins IIb and IIIa as determined by electron microscopy*. The Journal of Biological Chemistry 1985; 260: 1743–1749.
20. M.V. Nermut, N.M. Green, P. Eason, S.S. Yamada, K.M. Yamada. *Electron microscopy and structural model of human fibronectin receptor*. The EMBO Journal 1988; 7: 4093–4099.
21. J. Emsley, C. G. Knight, R. W. Farndale, M. J. Barnes. *Structure of the integrin alpha2beta1-binding collagen peptide.* Journal of Molecular Biology 2004; 335: 1019–1028.
22. C. G. Knight, L. F. Morton, D. J. Onley, A. R. Peachey, A. J. Messent, P. A. Smethurst, D. S. Tuckwell, R. W. Farndale, M. J. Barnes. *Identification in collagen type I of an integrin alpha2 beta1-binding site containing an essential GER sequence*. The Journal of Biological Chemistry 1998; 273: 33287–33294.
23. D. J. Leahy, I. Aukhil, H. P. Erickson. *2.0 Å crystal structure of a four-domain segment of human fibronectin encompassing the RGD loop and synergy region*. Cell 1996; 84: 155–164.

24. S. Aota, M. Nomizu, K. M. Yamada. *The short aminoacid sequence Pro-His-Ser-Arg-Asn in human fibronectin enhances cell-adhesive function*. The Journal of Biological Chemistry 1994; 269: 24756–24761.
25. M. J. Humphries, S. K. Akiyama, A. Komoriya, K. Olden, K. M. Yamada, *Identification of an alternatively spliced site in human plasma fibronectin that mediates cell type-specific adhesion*. The Journal of Cell Biology 1986; 103: 2637–2647.
26. A. Komoriya, L. J. Green, M. Mervic, S. S. Yamada, K. M. Yamada, M. J. Humphries. *The minimal essential sequence for a major cell type-specific adhesion site (CS1) within the alternatively spliced type III connecting segment domain of fibronectin is leucine-aspartic acid-valine*. The Journal of Biological Chemistry 1991; 266: 15075–15079.
27. K. Tashiro, G. C. Sephel, B. Weeks, M. Sasaki, G. R. Martin, H. K. Kleinman, Y. Yamada. *A synthetic peptide containing the IKVAV sequence from the A chain of laminin mediates cell attachment, migration, and neurite outgrowth.* The Journal of Biological Chemistry 1989; 264: 16174–16182.
28. J. Graf, R. C. Ogle, F. A. Robey, M. Sasaki, G. R. Martin, Y. Yamada, H. K. Kleinman. *A pentapeptide from the laminin B1 chain mediates cell adhesion and binds the 67,000 laminin receptor*. Biochemistry 1987; 26: 6896–6900.
29. H. K. Kleinman, J. Graf, Y. Iwamoto, M. Sasaki, C. S. Schasteen, Y. Yamada, G. R. Martin, F. A. Robey. *Identification of a second active site in laminin for promotion of cell adhesion and migration and inhibition of in vivo melanoma lung colonization*. Archives of Biochemistry and Biophysics 1989; 272: 39–45.
30. S. F. Badylak, D. O. Freytes, T. W. Gilbert. *Extracellular matrix as a biological scaffold material: structure and function*. Acta Biomaterialia 2009; 5: 1–13.
31. K. Shakesheff, S. Cannizzaro, R. Langer. *Creating biomimetic micro-environments with synthetic polymer–peptide hybrid molecules*. Journal of Biomaterial Science-Polymer Edition 1998; 9: 507–518.
32. L.S. Nair, C.T. Laurencin. *Polymers as biomaterials for tissue engineering and controlled drug delivery*. Advances in Biochemical Engineering/Biotechnology, 2006; 102: 47-90.
33. L. Moroni, J.R. de Wijn, C.A. Van Blitterswijk. *Three-dimensional fiber-deposited PEOT/PBT copolymer scaffolds for tissue engineering: influence of porosity, molecular network mesh size and swelling in aqueous media on*

*dynamic mechanical properties*. Journal of Biomedical Material Research-Part A 2005; 75: 957-965.

34. T.B.F. Woodfield, J. Malda, J. de Wijn, F. Peters, J. Riesle, C.A. Van Blitterswijk. *Design of porous scaffolds for cartilage tissue engineering using a three-dimensional fiber-deposition technique*. Biomaterials 2004; 25: 4149-61.
35. J. Malda, T.B. Woodfield, F. van der Vloodt, C. Wilson, D.E. Martens, J. Tamper, C.A. van Blitterswijk, J. Riesle. *The effect of PEGT/PBT scaffold architecture on the composition of tissue engineered cartilage*. Biomaterials 2004; 26: 63-72.
36. L. Moroni, J.R. de Wijn, C.A. Van Blitterswijk. *3D fiber- deposited scaffolds for tissue engineering: influence of pores geometry and architecture on dynamic mechanical properties*. Biomaterials 2006; 27: 974-85.
37. L. Moroni, G. Poort, F. van Keulen, J. de Wijn, C.A. Van Blitterswijk. *Dynamic mechanical properties of 3D fiber-deposited PEOT/PBT scaffolds: an experimental and numerical analysis*. Journal of Biomedical Material Research 2006; 78A: 605-14.
38. K. Kyriakidou, G. Lucarini, A. Zizzi, E. Salvolini, M. Mattioli-Belmonte, F. Mollica, A. Gloria, L. Ambrosio. *Dynamic co-seeding of osteoblast and endothelial cells on 3D polycaprolactone scaffolds for enhanced bone tissue engineering*. Journal of Bioactive and Compatible Polymers 2008; 23: 227-43.
39. T. Hayashi. *Biodegradable polymers for biomedical uses*. Progress in Polymer Science 1994; 19: 663-702.
40. L.G. Griffith. *Polymeric biomaterials*. Acta Materialia 2000; 48: 263-277.
41. C. Giordano, D. Albani, A. Gloria, M. Tunesi, S. Batelli, T. Russo, G. Forloni, L. Ambrosio, A. Cigada. *Multidisciplinary perspectives for Alzheimer's and Parkinson's diseases: hydrogels for protein delivery and cell-based drug delivery as therapeutic strategies*. International Journal of Artificial Organs 2009; 32: 836-50.
42. K.J.L. Burg, S. Porter, J.F. Kellam. *Biomaterial developments for bone tissue engineering*. Biomaterials 2000; 21: 2347-59.
43. R.Z. Le Geros. *Properties of osteoconductive biomaterials: calcium phosphates*. Clinical Orthopaedics and Related Research 2002; 395: 81-98.

44. A.G. Mikos, G. Sarakinos , S.M. Leite, J.P. Vacanti, R. Langer. *Laminated three-dimensional biodegradable foams for use in tissue engineering*. Biomaterials 1993; 14: 323-30.
45. H.Y. Cheung, K.T. Lau, T.P. Lu, D. Hui. *A critical review on polymer-based bio-engineered materials for scaffold development*. Composite Part B Engineering, 2007; 38: 291-300.
46. F. Causa, P. A. Netti, L. Ambrosio. *A multi-functional scaffold for tissue regeneration: the need to engineer a tissue analogue*. Biomaterials 2007; 28: 5093-5099.
47. L.E. Freed, G. Vunjak-Novakovic, R.J. Biron, D.B. Eagles, D.C. Lesnoy, S.K. Barlow, R. Langer. *Biodegradable polymer scaffolds for tissue engineering*. Nature Biotechnology 1994; 12: 689-693.
48. J.E. Devin, M.A. Attawia, C.T. Laurencin. *Three-dimensional degradable porous polymer-ceramic matrices for use in bone repair*. Journal of Biomaterial Science-Polymer Edition 1996; 7: 661-669.
49. L.M. Mathieu, T.L. Mueller TL, P.E. Bourban, D.P. Pioletti, R. Müller, J.A.E. Manson. *Architecture and properties of anisotropic polymer composite scaffolds for bone tissue engineering*. Biomaterials 2006; 27: 905-16.
50. M.M. Schwartz. *Composite Materials Handbook*. 2nd ed. New York: McGraw-Hill; *1992.*
51. P.K. Mallick. *Composites Engineering Handbook*. New York: Marcel Dekker, Inc; 1997.
52. R.M. Jones. *Mechanics of Composite Materials*. 2nd ed. London: Taylor & Francis; 1999.
53. L. Nicolais, A. Gloria, L. Ambrosio. *The mechanics of biocomposites*. In: L. Ambrosio , ed. Biomedical composites. Cambridge, UK: Woodhead Publishing Limited, CRC Press; 2010: 411-40.
54. X.P. Ma, *Scaffolds for Tissue fabrication*, Materials Today 2004; 7: 30- 40.
55. M. Labet, W.Thielemans. *Synthesis of polycaprolactone: a review*. Chemical Society Review 2009; 38: 3484–3504.
56. V.R. Sinha, K. Bansal, R. Kaushik, R. Kumria, A. Trehan. *Poly-ε-caprolactone microspheres and nanospheres: an overview*. International Journal of Pharmaceutics 2004; 278: 1–23

57. I. Vroman, L. Tighzert. *Biodegradable Polymers*. *Materials* 2009; 2: 307-344.
58. M.F. Koenig, S.J. Huang. *Biodegradable blends and composites of polycaprolactone and starch derivatives*. Polymer 1995; 36: 1877-1882.
59. C. Bastioli, A. Cerutti, I. Guanella, G.C. Romano, M. Tosin. *Physical state and biodegradation behavior of starch-polycaprolactone systems*. Journal of Environmental Polymer Degr*adation* 1995; 3: 81-95.
60. Y. Ikada, H. Tsuji. *Biodegradable polyesters for medical and ecological applications.* Macromolecular Rapid Communications 2000; 21: 117–132.
61. C.X.F. Lam, S. H.Teoh, D.W. Hutmacher. *Comparison of. Degradation of PCL & PCL-TCP scaffolds in Alkaline Medium.* Polymer International 2007; 56: 718–728.
62. R. Chandra, R. Rustgi. *Biodegradable polymers*. Progress in Polymer Science 1998; 23: 1273–1335.
63. D.R. Chen, J.Z. Bei, S. G. Wang. *Polycaprolactone microparticles and their biodegradation*. Polymer Degradation and Stability 2000; 67: 455–459.
64. P. Joshi and G. Madras. *Degradation of polycaprolactone in supercritical fluids*. Polymer Degradation and Stability 2008; 93: 1901–1908
65. J. Peña, T. Corrales, I. Izquierdo-Barba, A.L. Doadrio, M. Vallet-Regì. *Long term degradation of poly(epsilon-caprolactone) films in biologically related fluids.* Polymer Degradation and Stability 2006; 91: 1424–1432.
66. M.J. Jenkins, K.L. Harrison, M.M.C.G. Silva, M.J. Whitaker, K.M. Shakesheff, S.M. Howdle. *Characterisation of microcellular foams produced from semi-crystalline PCL using supercritical carbon dioxide*. European Polymer Journal 2006; 42: 3145–3151.
67. D.W. Hutmacher, T. Schantz, I. Zein, K.W. Ng, S.H. Teoh, K.C. Tan. *Mechanical properties and cell culture response of polycaprolactone scaffolds designed and fabricated via fused deposition modeling.* Journal of Biomedical Material Research 2001; 55: 203-216.
68. J.L. Hedrick, T. Magbitang, E.F. Connor, T. Glauser, W. Volksen, C.J. Hawker, V.Y. Lee, R.D. Miller. *Application of Complex Macromolecular Architectures for Advanced Microelectronic Materials.* Chemistry-A European Journal 2002; 8: 3308–3319.

69. H. Sun, L. Mei, C. Song, X. Cui, P. Wang. *The in vivo degradation, absorption and excretion of PCL-based implant*. Biomaterials 2006; 27: 1735–1740.
70. R. A. Gross, B. Kalra. *Biodegradable Polymers for the Environment.* Science 2002; 297: 803–807.
71. M. Diesso. *Custom dental tray*. U.S. Patent N. US005112225A, 1992.
72. R. Langer*, Selected advances in drug delivery and tissue engineering*, Journal of Controlled Release 1999; 62: 7–11.
73. G.N. Bancroft, A.G. Mikos. *Fluid flow increases mineralized matrix deposition in 3D perfusion culture of marrow stromal osteoblasts in a dose- dependent manner*, Proceeding of the National Academy of Science of the United States of America 2002; 99: 12600–12605.
74. S.A.N. Ali, S.P. Zhong, P.J. Dhoerty, D.F. Williams. *Mechanism of polymer degradation in implantable devices*. Biomaterials 1993; 14: 1409-1418.
75. S. Ramakrishna, J. Mayer, E. Wintermantel, K.W. Leong. *Biomedical applications of polymer-composite materials: a review*. Composites Science and Technology 2001; 61: 1189-122.
76. I. Martin, D. Wendt, M. Heberer. *The role of bioreactors in tissue engineering*. Biotechnology 2004; 22: 80-86.
77. X. Yu, C.T. Laurencin. *Bioreactor-based bone tissue engineering*, PNAS August 2004; 101: 11203–11208.
78. Young-Ha Kim, Chong-Su Cho, Inn-Kyu Kang, Suk Young Kim and Oh Hyeong Kwon. *Characterization of Hydrophilized PCL Electrospun Sheet as an Efective Guided Bone Regeneration Membrane*. Key Engineering Materials 2007; 342/343: 293-296.
79. D.W. Hutmacher. *Scaffold design and fabrication technologies for engineering tissues state of the art and future perspectives.* Journal of Biomaterial Science - Polymer Edition 2001; 12: 107-124.
80. J.P. Vacanti, M.A. Morse, W.M. Saltzman, A.J. Domb, A. Perez-Atayde, R. Langer. *Selective cell transplantation using bioabsorbable artificial polymers as matrices.* Journal of Pediatric Surgery 1988; 23: 3-9.
81. K.R. Stone, W.G. Rodkey, R. Webber, L. Mckinney, J.R. Steadman. *Meniscal regeneration with copolymeric collagen scaffolds. In vitro and in vivo studies*

*evaluated clinically, histologically, and biochemically*. The American Journal of Sports Medicine 1992; 20: 104-111.

82. B.M. Wu, S.W. Borland, R.A. Giordano, L.G. Cima, E.M. Sachs, M.J. Cima. *Solid free-form fabrication of drug delivery devices*. Journal of Controlled Release 1996; 40: 77-87.
83. X.J. Yu, G.P. Dillon, R.B. Bellamkonda. *A laminin and nerve growth factor-laden three-dimensional scaffold for enhanced neurite extension.* Tissue Engineering 1999; 5: 291-304.
84. K.E. Healy, A. Rezania, R.A. Stile. *Designing biomaterials to direct biological responses.* Bioartificial Organs II: Technology, Medicine and Materials 1999; 875: 24-35.
85. M.C. Hacker, A.G. Mikos. *Trends in Tissue Engineering Research*. Tissue Engineering 2006; 12: 2049-2057.
86. R. Landers, R. Mulhaupt. *Desktop manufacturing of complex objects, prototypes and biomedical scaffolds by means of computer-assisted design combined with computer-guided 3D plotting of polymers and reactive oligomers*. Macromolecular Materials and Engineering 2000; 282: 17-21.
87. R. Landers, U. Hubner, R. Schmelzeisen, R. Mulhaupt. *Rapid prototyping of scaffolds derived from thermoreversible hydrogels and tailored for applications in tissue engineering*. Biomaterials 2002; 23: 4437-4447.
88. R. Landers, A. Pfister, U. Hubner, H. John, R. Schmelzeisen, R. Mulhaupt. *Fabrication of soft tissue engineering scaffolds by means of rapid prototyping techniques*. Journal of Material Science 2002; 37: 3107-3116.
89. S. Yang, K.F. Leong, Z. Du, C.K. Chua. *The design of scaffolds for use in tissue engineering. Part II. Rapid prototyping techniques*. Tissue Engineering 2002; 8: 1-11.
90. J.M. Taboas, R.D. Maddox, P.H. Krebsbach, S.J. Hollister. *Indirect solid free form fabrication of local and global porous, biomimetic and composite 3D polymeric-ceramic scaffolds*. Biomaterials 2003; 24: 181-194.
91. E. Sachlos, J.T. Czernuske. *Making tissue engineering scaffolds work. Review on the application of solid freeform fabrication technology to the production of tissue engineering scaffolds.* European Cells and Materials 2003; 5: 29-40.
92. T.M.G. Chu, in: P. X. Ma, J. Elisseeff, *Scaffolding in Tissue engineering*. Taylor and Francis: Northwest Florida 2006, pp. 139–153.

93. L. Moroni, R. Schotel, J. Sohier, J.R. de Wijn, C.A. Van Blitterswijk. *Polymer hollow-fiber three-dimensional matrices with controllable cavity and shell thickness*. Biomaterials 2006; 27: 5918-5926.
94. S.M. Peltola, F.P.W. Melchels, D.K. Grijpma, M. Kellomäki. *A review of rapid prototyping techniques for tissue engineering purposes.* Annals of Internal Medicine 2008; 40: 268-280.
95. D.W. Hutmacher. *Scaffolds in tissue engineering bone and cartilage*. Biomaterials 2000; 21: 2529-2543.
96. C.K. Chua, K.F. Leong, C.S. Lim, in: C.K. Chua, K.F. Leong, C.S. Lim, *Rapid prototyping–Principles and Applications*. World Scientific Pub Co: Singapore, 2003, pp. 25–33.
97. T. Hayashi. *Biodegradable polymers for biomedical uses*. Progress in Polymer Science 1994; 19: 663-702.
98. L.G. Griffith. *Polymeric biomaterials*. Acta Materialia 2000; 48: 263-77.
99. D.W. Hutmacher. *Scaffold design and fabrication technologies for engineering tissues - state of the art and future perspectives*. Journal of Biomaterial Science-Polymer Edition 2001; 12: 107-124.
100. B.S. Chang, C.K. Lee, K.S. Hong, H.J. Youn, H.S. Ruy, S.S. Chung, K.W. Park. *Osteo-conduction at porous hydroxyapatite with various pore configurations*. Biomaterials 2000; 21: 1291-1298.
101. Q.M. Jin, H. Takita, T. Kohgo, K. Atsumi, H. Itoh, Y. Kuboki. *Effects of geometry of hydroxyapatite as a cell substratum in BMP-induced ectopic bone formation*. Journal of Biomedical Material Research 2000; 51: 491-499.
102. L.M. Pineda, M. Büsing, R.P. Meinig, S. Gogolewski. *Bone regeneration with resorbable polymeric membranes. III. Effect of poly(L-lactide) membrane pore size on the bone healing process in large defects*. Journal of Biomedical Material Research 1996; 31: 385-394.
103. B.P. Robinson, J.O. Hollinger, E.H. Szachowicz, J. Brekke. *Calvarial bone repair with porous D,L-polylactide*. Archives of Otolaryngology-Head & Neck Surgery 1995; 112: 707-713.
104. S.L. Ishaug-Riley, G.M. Crane-Kruger, M.J. Yaszemski, A.G. Mikos. *Three-dimensional culture of rat calvarial osteoblasts in porous biodegradable polymers*. Biomaterials 1998; 19: 1405-1412.

105. K. Whang, K.E. Healy, D.R. Elenz, E.K. Nam, D.C. Tsai, C.H. Thomas, G.W. Nuber, F.H. Glorieux, R. Travers, S.M. Sprague. *Engineering bone regeneration with bioadsorbable scaffolds with novel microarchitecture*. Tissue Engineering 1999; 5: 35–51.

106. E. Saiz, L. Gremillard, G. Menendez, P. Miranda, K. Gryn, A.P. Tomsia. *Preparation of porous hydroxyapatite scaffolds prepared by stereolithography*. Material Science and Engineering-Part C 2007; 27: 546–550.

107. D. Liu. *Control of pore geometry on influencing the mechanical property of porous hydroxyapatite bioceramic*. Journal of Mater Science Letters 1996; 15: 419-421.

108. Schugens C, Grandfils C, Jerome R, P. Tessye, P. Delree, D. Martin, B. Malgrange, G. Moonen. *Preparation of a macroporous biodegradable polylactide implant for neuronal transplantation*. Journal of Biomedical Material Research 1995; 29: 1349-1362.

109. C.K. Chua, K.F. Leong, C.S. Lim. *Rapid prototyping process chain*. In: Chua CK, Leong KF, Lim CS, eds. *Rapid prototyping-Principles and Applications*. Singapore: World Scientific Pub Co, 2003; pp. 25-33.

110. R.P. Fedchenko, P.F. Jacobs. *Introduction*. In: Fedchenko RP, Jacobs PF, eds. *Stereolithography and other RP&M Technologies*. Dearborn, MI: Society of Manufacturing Engineers, 1996; 1-26.

111. P.F. Jacobs. *Special applications of RP&M*. In: Fedchenko RP, Jacobs PF, eds. *Stereolithography and other RP&M Technologies*. Dearborn, MI: Society of Manufacturing Engineers, 1996; 317-66.

112. C. Hull. *Method for production of three-dimensional objects by Stereolithography*. US Patent 4929402, 1990.

113. C.S. Scott. *Apparatus and method for creating three-dimensional objects*. US Patent 5121329, 1991.

114. J.F. Bredt, E. Sach, D. Brancazio, M. Cima, A. Curodeau, T. Fan. *Three dimensional printing system.* US Patent 5807437, 1998.

115. R. Landers, A.Pfister, U. Hubner, H. John, R. Schmelzeisen, R. Mulhaupt. *Fabrication of soft tissue engineering scaffolds by means of rapid prototyping techniques*. Journal of Material Science 2002; 37: 3107-3116.

116. D.W. Hutmacher, T. Schantz, I. Zein, K.W. Ng, S.H. Teoh, K.C. Tan. *Mechanical properties and cell cultural response of polycaprolactone scaffolds*

*designed and fabricated via fused deposition modelling*. Journal of Biomedical Material Research 2001; 55: 203-216.

117. I. Zein, D.W. Hutmacher, K.C. Tan, S.H. Teoh. *Fused deposition modeling of novel scaffold architectures for tissue engineering applications*. Biomaterials 2002; 23: 1169-1185.

118. C.K. Chua, K.F. Leong, C.S. Lim. *Liquid based rapid prototyping system*. In: Chua CK, Leong KF, Lim CS. *Rapid Prototyping-Principles and Applications*. Singapore: World Scientific Publishing Co, 2003; 35-110.

119. C.K. Chua, K.F. Leong, C.S. Lim. *Powder based rapid prototyping system*. In: Chua CK, Leong KF, Lim CS. *Rapid Prototyping-Principles and Applications*. Singapore: World Scientific Publishing Co, 2003; 173-236.

120. G. Vozzi, A. Previti, D. De Rossi, A. Ahuwalia. *Microsyringe-based deposition of two-dimensional polymer scaffolds with a well-defined geometry for application to tissue engineering*. Tissue Engineering 2002; 8: 1089-1098.

121. L. Moroni, J.A.A. Hendriks, R. Schotel, J.R. de Wijn, C.A. Van Blitterswijk. *Design of biphasic 3-dimensional fiber deposited scaffolds for cartilage tissue engineering applications*. Tissue Engineering 2007; 13: 361-371.

122. L. Moroni, R. Schotel, D. Hamann, J.R. de Wijn, C.A. Van Blitterswijk. *3D fiber-deposited electrospun integrated scaffold enhance cartilage tissue formation.* Advanced Functional Materials 2008; 18: 53-60.

123. W. Li, R. Tuli, X. Huang, P. Laquerriere, R.S. Tuan. *Multilineage differentiation of human mesenchymal stem cells in a three-dimensional nanofibrous scaffold*. Biomaterials 2005; 26: 5158-5166.

124. R.E. Unger, A. Sartoris, K. Peters, A. Motta, C. Migliaresi, M. Kunkel, U. Bulnheim, J. Rychly, C.J. Kirkpatrick. *Tissue-like self- assembly in cocultures of endothelial cells and osteoblasts and the formation of microcapillary-like structures on three-dimensional porous biomaterials*. Biomaterials 2007; 28: 3965-3976.

125. B. Decker, H. Bartles, S. Decker. *Relationships between endothelial cells, pericytes, and osteoblasts during bone formation in the sheep femur following implantation of tricalciumphosphate-ceramic*. Anatomical Record 1995; 242: 310-320.

126. F. Villars, L. Bordenave, R. Bareille, J. Amedee. *Effect of human endothelial cells on human bone marrow stromal cell phenotype: role of VEGF?* Journal of Cellular Biochemistry 2000; 79: 672-685.

127. J.L. Carrington, A.H. Reddi. *Parallels between development of embryonic and matrix-induced endochondral bone*. Bioassay 1991; 13: 403-408.

128. P. Collin-Osdoby. *Role of vascular endothelial cells in bone biology*. Journal of Cellular Biochemistry 1994; 55: 304-309.

129. D.S. Wang, M. Miura, H. Demura, K. Sato. *Anabolic effects of 1,25-dihydroxyvitamin D3 on osteoblasts are enhanced by vascular endothelial growth factor produced by osteoblasts and by growth factors produced by endothelial cells*. Endocrinology 1997; 138: 2953-2962.

130. E.A. Botchwey, M.A. Dupree, S.R. Pollack, E.M. Levine, C.T. Laurencin. *Tissue engineered bone: measurement of nutrient transport in three-dimensional matrices*. Journal of Biomedical Material Research-Part A 2003; 67: 357-367.

131. T.S. Karande, J.L. Ong, C.M. Agrawal. *Diffusion in musculoskeletal tissue engineering scaffolds: design issue related to porosity, permeability, architecture and nutrient mixing*. Annals of Biomedical Engineering 2004; 32: 1728-1743.

132. L.J. Gibson, M.F. Ashby. *Cellular Solids: Structure and Properties*. Cambridge, UK: Cambridge University Press, 1997.

# Chapter II: Contents

# CHAPTER II

# 3D Bioactive Poly(ε-caprolactone) Scaffolds

## II.I Preface: how to enhance cell recognition

Although many biodegradable synthetic polymers such as polyglycolic acid (PGA), poly(lactic acid) (PLA), poly(lactide-co-glycotide) (PLGA) and poly(caprolactone) (PCL) have been already used for making scaffolds to support the regeneration of several tissue-engineered organs,[1-66] the poor cytocompatibility of the synthetic polymers leads to the inefficiency of the scaffold in obtaining a friendly interface with living cells.

In biological tissues, cells are immersed in the extracellular matrix (ECM) that is a coacervate of glycosaminoglycans and proteins with various mechanical and signaling functions. In particular, fibroblast and osteoblast cells are known to express various integrins, each component having a large extracellular domain responsible for ligand binding, a transmembrane domain, and a short cytoplasmic domain responsible for interacting with the actin cytoskeleton.[67-68] Integrin heterodimers bind to specific aminoacid sequences, such as the arginine-glycine-aspartic acid (Arg-Gly-Asp or RGD) recognition motif that is largely present in many ECM proteins, including fibronectin, vitronectin, bone sialoprotein, and osteopontin.[69] Small synthetic peptides (a few hundred daltons) that contain aminoacid sequence RGD can thus mediate cell attachment as well as the large parental molecule (a hundred thousand dalton).

Consequently, in order to improve their cytocompatibility, modifications of the tissue engineering polymer-based materials are needed. In tissue engineering, cell adhesion to scaffold surface results a critical factor since adhesion occurs before other biological events such as cell spreading, migration and differentiation. In particular, cell adhesion is strongly related to the surface properties of biomaterials, and it is influenced by substratum surface properties, such as surface charge, wettability, roughness and topography. Most conventional materials do not meet the criteria for serving as tissue engineering scaffolds and, for this reason, many surface modification techniques have been developed to alter the surface properties of these materials.[70-78] Surface modification represents an effective approach to promote biological

interactions of a particular material for developing multifunctional scaffolds. Since surface modification only changes the outermost surface composition of a biomaterial, its bulk properties should not vary.

Many surface modification techniques such as γ-ray irradiation, plasma treatment, end-grafting, ozone oxidization, or *in situ* polymerization have been already considered to modify the materials surface properties, the aim being to improve the cytocompatibility of the polymeric materials without altering their bulk properties.

On the basis of this, biomimetic approaches have been developed to immobilize short peptides, such as RGD, onto synthetic or natural surfaces, to produce biofunctional materials able to promote and enhance cell attachment.[1,79] In particular, it has been found that a minimum RGD density of $1.0 \cdot 10^{-15}$ mol/cm$^2$, corresponding to a spacing of about 140 nm between peptide ligands, is sufficient to promote cell spreading, while a density of $1.0 \cdot 10^{-14}$ mol/cm$^2$ is needed to promote the formation of focal contacts.[4] However, such parameters strongly depend on peptide presentation and, in turn, from chemical and physical characteristics of the substrate. Moreover, spatial distribution and the aggregation of RGD peptides at the micro- and nano-scale significantly affect cell responses. For example, nano-scale clustering of RGD peptides can induce integrins to cluster, thus triggering complete cell signaling.[80,81]

Aminolysis, as shown in this work, may be considered an easy-to-perform chemical technique to engraft amino groups along polyesters chains, providing active sites through which other biomolecules such as collagen, gelatin, or RGD peptides can be further immobilized, obtaining cytocompatible surface on which cells can grow well, at the same time decreasing the surface hydrophobicity, neutralizing the acid generated during the scaffold degradation and reducing the inflammation around the implanted scaffold.[82]

## II.II Materials and Methods

### *II.II.I 3D Scaffold Design and Preparation*

The poly(ε-caprolactone) (PCL) pellets used in this study, ($M_w$ = 65000 g mol$^{-1}$) are a product of Sigma-Aldrich, St. Louis, MO.

3D block-shaped scaffolds characterized by a length ($l$) of 7.0 mm, a width ($w$) of 7.0 mm and a height ($h_0$) of 7.8 mm, were fabricated through 3D Fiber Deposition technique, using a Bioplotter dispensing machine (Envisiontec GmbH, Germany) equipped with a CAD/CAM system.

PCL pellets were initially placed in a stainless steel syringe and, then, heated at a temperature of 120°C through a cartridge unit placed on the mobile arm of the XYZ plotter. As PCL reached the molten phase, a nitrogen pressure of 8-8.5 bar was applied to the syringe through a cap. 3D models were loaded on the Bioplotter CAD/CAM system.

3D scaffolds were obtained by alternatively extruding and depositing the polymer fibers with different angle steps between two successive layers, making two different patterns: 0°/90° and 0°/45°/90°/135°. The nozzle used to extrude PCL fibers was a stainless steel needle characterized by an inner diameter of 400 μm. Each scaffold was characterized not only by the fiber diameter (depending on the needle diameter and/or the deposition speed), but also by the fiber spacing (strand distance, i.e. center-to-center distance) and layer thickness, which influence the overall pore size. The values of strand distance were set to 640 μm, while for the layer thickness was chosen 320 μm. A deposition speed of 50-55 mm/min was used.

## *II.II.II Micro-Computed Tomography*

A micro-computed tomography (Micro-CT) was performed through a SkyScan 1072 (Aartselaar, Belgium) system using a rotational step of 0.9° over an angle of 180°, in order to analyze the internal structure of the 3D scaffolds fabricated via rapid prototyping technique, pore shape and size. Cross-sections and 3D model of PCL scaffolds were reconstructed using Skyscan's software package and Image J software, that allowed to visualize and analyze the results from Micro-CT system scan. The pore network was visualized and the pore interconnectivity was studied.

## *II.II.III Surface modification of 3D fiber-deposited poly-ε-caprolactone scaffolds via aminolysis*

As PCL is a synthetic polymer, it does not possess molecular motifs for cell recognition.[83,84] To promote cell adhesion, its backbone has to be suitably modified by introducing functional groups for the following RGD conjugation.[85,86]

Most of modification methods may show many problems such as low level of functional groups, lack of control of peptide immobilized on PCL surface, and the eventual presence of uncontrolled degradation products.

In addition, the bioactive groups may not be covalently attached but only adsorbed onto the surface, thus leading to the possibility of being removed or exchanged upon introduction into *in vitro* culture or *in vivo* implantation.

On the other hand, it has been demonstrated that chemical methods can be successfully used for bioactivating polymer surfaces. Functional groups have been introduced on PCL via hydrolysis,[87,88] aminolysis,[87] plasma treatment,[73,89] or copolymerization.[74]

However, all the above mentioned studies clearly evidence a lack of control in the effective presentation of immobilized peptide toward cell, as well as in the characterization of surface properties after peptide conjugation. For this reason, it has been proposed[90] a systematic study of peptide ligand organization and spatial distribution on PCL surfaces, evaluating the effective peptide distribution and presentation able to activate specific cell functions (i.e., adhesion or differentiation).

PCL molecules are characterized by a great number of ester groups (-COO-), which can be hydrolyzed to carboxylic acid under alkaline condition. Moreover, the amino groups can be introduced onto the polyester surface through a reaction with diamine, providing that one amino group reacts with the -COO- group to form a covalent bond, -CONH-, while the other amino group is unreacted and free.[91] However, the hydroxyl-terminated chains will also be yielded on the polyester surface during this process. The decreasing of surface hydrophobicity, neutralization of the acid originated from the scaffold degradation, possibility to provide active sites through which other biomolecules, such as gelatine, collagen or arginine-glycine-aspartic acid (Arg-Gly-Asp or RGD) peptides can be immobilized, are the main advantages in tissue engineering that can be derived from the introduction of the amino groups.[91]

Moreover, it has already been demonstrated that aminolysis may be considered an easy-to-perform chemical technique to engraft amino groups along polyesters chains.[91]

In the case of PCL, amine groups were introduced onto film surfaces through treatment with a diamine, before attaching peptide sequences (i.e., RGD) using either glutaraldehyde, carbodiimide, or epoxy-amine chemistry.[91,92]

A two step-procedure has been used to immobilize peptides onto the polymer surface, involving a treatment with 1,6-hexanediamine followed by the use of 1-ethyl-3-(dimethylaminopropyl) carbodiimide[23], whilst Taniguchi et al. (2006) also modified PCL with poly(ethylene oxide) grafts before coupling with RGD containing peptides, thus obtaining an improvement in cellular responses.[92] Recent works have also highlighted the possibility to bioactivate 3D PCL scaffolds with RGD after aminolysis.[94,95]

In particular, in order to overcome the above mentioned problems (lack of control in the effective presentation of immobilized peptide toward cell, characterization of surface properties after peptide conjugation) the grafting of the synthetic peptide Gly-Arg-Gly-Asp-Tyr (GRGDY) which contains the RGD sequence of several adhesion molecules has been performed onto PCL sheets using a two-step procedure similar to those already reported in the literature,[22,23] involving a polymer aminolysis to graft primary amines on the film surface and a subsequent conjugation of the RGD motif. Unlike the other works, each step was precisely controlled through functional groups determination as well as chemical and physical parameter evaluation. Peptide surface density and distribution as well as penetration depth in the polymer substrate were deeply investigated through morphological and topological measurements. It was demonstrated that the conjugation of amine-terminated peptides by means of reductive amination after tether insertion may show a specific recognition of the solid signal to Mouse embryo fibroblasts (NIH3T3) integrin cell receptors highlighting a correct presentation of the peptide sequences.[91]

The possibility to extend this controlled two-step procedure to immobilize RGD motifs on 3D well-organized scaffolds, also taking into account the effect on their macro-mechanical behavior, could be a great challenge in tissue engineering.

Accordingly, a specific procedure was used to insert covalently amino groups onto the fiber surface of the designed 3D PCL scaffolds, using 1,6-hexanediamine (DEA).

Briefly, 3D fiber-deposited scaffolds were immersed at different times in 0.08 g/ml DEA/isopropanol (IPA) solution at 37°C. The aminolysis reaction was carried out in a custom-made reactor thermostatted in a water bath with adequate magnetic stirring for a suitable time, in batch mixer processing conditions. After the aminolysis treatment, solution was removed and the scaffolds were rinsed with deionized water at room temperature for 24 h. Successively, they were dried in vacuum desiccator and stored at room temperature for further modifications.

## *II.II.IV Determination of Engrafted Amines*

A ninhidryn-based procedure (Kaiser test, Aldrich) was employed to assess the amount of amino groups on the aminolyzed (PCL-$NH_2$) scaffolds. The samples were dissolved in kit solutions and heated at 100°C for 15 min. Afterwards, at room temperature methylenecloryde/ethanol solution was added to stabilize the blue compound and to bring in solution the polymer mixture. The absorbance was measured at 570 nm using an UV-vis spectrophotometer (Lambda 25, Perkin-Elmer). A calibration curve was obtained by 1,6-hexanediamine in methylenecloryde/ethanol solution.

## *II.II.V Peptide Conjugation*

Peptide sequences were covalently grafted peptides onto the surface in a two step way by using an epoxy crosslinker in mild aqueous condition. Firstly, the aminolyzed 3D scaffolds were treated with a 5% diethylene glycol diglycidyl ether (DGDGE) in a sodium carbonate solution (50 mM, pH 8.5), at room temperature gently shaking for 3h. Subsequently, the tether solution was rinsed out and the scaffolds were washed thoroughly with water. The conjugation step were performed adding 0.2 mg/ml of GRGDY (Inbios, Italy) in sodium carbonate solution (50 mM, pH=8.5), a scrambled sequence (GYDGR) was used as negative control for biological assessment. In both case, a Ethanolamine (2mM) aqueous solution was used to deactivate any unreacted oxyrane groups.

## *II.II.VI Determination of Conjugated Peptide*

The bicinchoninic acid (Micro-BCA) assay (Sigma-Aldrich) was used to quantify the peptide density directly onto the bioactivated surfaces above melting temperature of PCL samples.

Micro-BCA is a biochemical assay for determining the total level of peptide immobilized on solid support in a solution, using colorimetric techniques. This method combines the reduction of the $Cu^{2+}$ to $Cu^{1+}$ by peptide or protein in an alkaline medium with the highly sensitive and selective colorimetric detection of the $Cu^{1+}$ using a BCA containing reagent. The purple colored reaction product of this assay is relative to a chelation of two BCA molecules with one $Cu^{1+}$. This water-soluble compound exhibits a strong absorbance at 562 nm and is linearly proportional to the peptide concentration. The amount of peptide bound was determined with a standard curve for known quantity of the same peptide.

The number of peptide bonds and the presence of four aminoacids (cysteine, cystine, tryptophan and tyrosine) have been reported to be responsible for color formation in peptide samples when assayed with BCA.

The kit solutions were prepared as described by the supplier in a reduced volume (1 ml) and added to the sample. After heating the mixture at 37° for 2 h, the absorbance was read at 562 nm and compared with a calibration curve, obtained each time by using standard solution of GRGDY peptides curve in the range of concentration between 0.01 and 0.50 mM. Unmodified 3D PCL scaffolds were used as negative control.

## *II.II.VII Nanoindentation tests*

Nanoindentation tests were carried out on aminolyzed and not-aminolyzed PCL fibers, which were characterized by a diameter (D) of 340-360 μm and obtained through a Bioplotter Dispensing Machine.

All the tests were performed in a 1-5 mN load range, using a Nanotest Platform (Micromaterials, U.K.) with a diamond pyramid-shaped Berkovich-type indenter tip. Trapezoidal load functions, characterized by a loading-unloading rate of 300 μN/s and a peak-load hold period of 20 s, were imposed. Load-depth curves and hardness

values were evaluated. Hardness and reduced modulus were evaluated using the methods introduced by Oliver and Pharr (1992).

The interaction between the tip and the sample during the indentation process provides data that can be used to assess material properties such as Young's modulus or elastic modulus (E) and indentation hardness (H). As an example, it may be considered the load-depth curve shown in Fig. II.I.

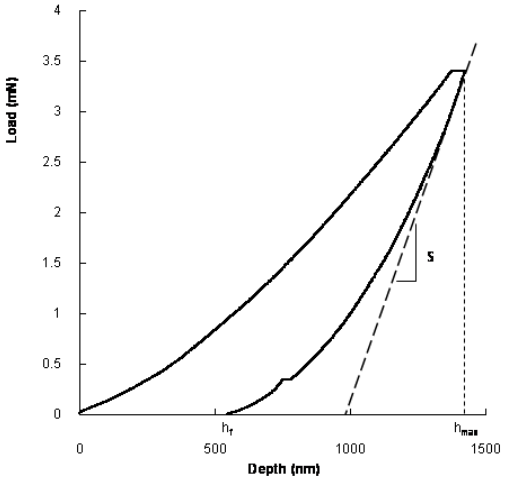


**Figure II.I: Typical load-depth curve obtained from nanoindentation tests, showing the loading-unloading process related to an applied trapezoidal load function.**

Taking into consideration the *compliance method*,[96,97] the hardness H and reduced modulus $E_r$ (the combined modulus of the tip and the sample) can be determined directly from analysis of load-displacement data using the relationships:

$$E_r = \frac{\sqrt{\pi}}{2}\frac{1}{\sqrt{A_c}}S$$

$$H = \frac{P_{max}}{A_c}$$

where S is the initial unloading stiffness (that means the slope of the unloading curve dP/dh, evaluated at the maximum load), $P_{max}$ is the maximum load, and $A_c$ is the projected contact area between the indenter tip and the sample at maximum load (and, hence, at maximum indentation depth $h_{max}$).

For an ideal Berkovich pyramid geometry, that is perfectly sharp with no defect at the tip, the relationship between the projected contact area and contact depth ($h_c$) is given by:[98,99]

$$A_c = 24.5h_c^2$$

The contact depth $h_c$ is considered as the actual value of the displacement, that mainly occurs, but not exclusively, in a plastic fashion.

If we consider that the material would show an elastic response at the beginning of the unloading phase, as in the case of a flat punch indenter, the difference ($h_{max}$-$h_c$) represents an evaluation of the instantaneous elastic recovery. To avoid the errors related to the flat punch assumption, that is normally used to evaluate the contact stiffness, Oliver and Pharr[96,97] suggested to introduce a correction factor (ε). Following this approach, the contact depth is evaluated by subtracting from the measured maximum indentation depth the downward elastic displacement of the indented surface through the following relationship:

$$h_c = h_{\max} - \varepsilon \frac{P_{\max}}{S}$$

where ε is a constant depending upon the tip geometry and results equal to 0.75 for a Berkovich tip.

However, the presence of tip imperfections requires appropriate calibrations to determine the area function $A_c(h_c)$ from indentations upon hard and plastic materials, also reducing the elastic and viscoelastic effects of the response. $A_c$ can be a polynomial function of the contact depth $h_c$ with coefficients obtained from a material of known elastic properties (i.e., fused silica, as in the present study) indented to different depths.[98] The reduced modulus ($E_r$) is related to the material Young's modulus by the relationship:[98,99]

$$\frac{1}{E_r} = \frac{(1-\nu_i^2)}{E_i} + \frac{(1-\nu_s^2)}{E_s}$$

where subscripts *i* and *s* refer to the tip and substrate materials, respectively, whilst ν is Poisson's ratio.

Once the indenter material properties (i.e., $E_i$ = 1141 GPa and $\nu_i$ = 0.07 for the diamond Berkovich tip used) and the Poisson's ratio of the material are known, the material Young's modulus ($E_s$) can be evaluated from the reduced modulus. However, the plane strain modulus $E' = E/(1 - \nu^2)$ is generally reported if the Poisson's ratio of the material is not known.[98,99]

Finally, an interesting consideration may be made regarding to the applied load function during the nanoindentation tests. It is well known that polymers exhibit time-dependent or viscoelastic behavior. Thus, the effect of viscoelasticity on indentation should be creep, or a sinking of the tip into the sample under a constant load. When creep behavior dominates the elastic response of the material, a "nose" can be observed on the indentation unloading curve.[98,100] In such a case, that means when the loading phase is followed by unloading without a hold at peak load, displacement increases slightly in the initial portion of the unloading process, since the creep rate of the material is initially higher than the imposed unloading rate. As consequence, the initial unloading region is characterized by a negative and changing slope, thus the modulus evaluation results impossible. To overcome this problem, a hold period at peak load should be incorporated in the applied load functions allowing the material to approach an equilibrium prior to unloading.[98] All of this suggests that trapezoidal load functions with appropriate hold periods have to be considered instead of triangular ones.

## *II.II.VIII Tensile tests*

Tensile tests were performed on unmodified PCL and PCL-$NH_2$ fibers according to the ASTM D3822 standard. All the tests were carried out using an INSTRON 5566 testing machine. The engineering stress (σ) was calculated as the force $F$ measured by the load cell divided by the fiber cross section ($A = \pi D^2/4$):

$$\sigma = \frac{F}{A}$$

whilst engineering strain (ε) was evaluated as the ratio between the fiber elongation $\Delta l$ and the initial fiber length $l_0$ (i.e. the initial grips separation):

$$\varepsilon = \frac{\Delta l}{l_0}$$

## *II.II.IX Compression tests*

Compression tests were performed on the 3D fiber-deposited scaffolds in the form of block-shaped specimen characterized by a length ($l$) of 7.0 mm, a width ($w$) of 7.0 mm and a height ($h_0$) of 7.8 mm. All the tests were carried out at a rate of 1 mm/min up to a strain value of 0.5 mm/mm, using an INSTRON 5566 testing machine. The stress was evaluated as the force $F$ measured by the load cell divided by the total area of the apparent cross section of the scaffold ($A_0 = l \cdot w$):

$$\sigma = \frac{F}{A_0}$$

while the strain $\varepsilon$ was defined as the ratio between the scaffold height variation $\Delta h$ and its initial height $h_0$:

$$\varepsilon = \frac{\Delta h}{h_0}$$

## *II.II.X Spatial Distribution of Surface Treatment*

Confocal Laser Scanning Microscopy (CLSM) was used to investigate the penetration depth of treatment by LSM 510 Zeiss confocal inverted microscope equipped with a Zeiss 20X/3 NA objective and an argon laser. Each stage of bioactivation (aminolysis and peptide covalent coupling) was followed conjugating the surface samples with two different fluorescent dyes. Firstly, the aminolysis treatment was analysed by coupling PCL-$NH_2$ surfaces with 0.1 mg/ml of Rhodamine B isothiocyanate (RBITC) in isopropanol (IPA) overnight at 4°C. Subsequently, surfaces were rinsed thoroughly with IPA and then with water for 24 h to remove any non covalent bound dye molecule.

In order to mimic the peptide route, Fluoresceinamine (FLUO) was linked to the epoxy-functionalized surfaces by first dissolving the dye in carbonate buffer at pH=8.5 in the same conditions used for peptide conjugation. Finally, samples were rinsed with buffer followed by copious amounts of distilled water to remove any non covalently linked molecules. The PCL fluorescent samples were then left to dry overnight in a vacuum desiccator before analysis. Unmodified PCL surfaces were

equally processed as control. Samples after RBITC or FLUO conjugation were respectively visualized using the characteristic wavelength of RBITC ($\lambda_{ex}$ = 543 nm; $\lambda_{em}$ = 572) and FLUO ($\lambda_{ex}$ = 496 nm; $\lambda_{em}$= 518 nm).

To compare the results, CLSM settings, in particular, laser power, pinhole aperture, detector gain and amplifier offset were kept constant for both kinds of observations. The penetration depth of treatment was visualized by z-stack acquisitions through the fiber by starting from the outer part. Intensity profiles of fluorescent dyes as function of penetration depth were obtained along a line drawn in the radius direction (here indicated as z-direction).

## *II.II.XI Cell Adhesion Study*

Mouse embryo fibroblasts NIH3T3 were maintained at 37°C and 5% $CO_2$ in Dulbecco's modified Eagle medium (DMEM) supplemented with 10% fetal bovine serum (FBS, BioWhittaker, Walkersville, MD), 2 mM L-glutamine (Sigma, St. Louis, MO), 1000 U/l penicillin (Sigma, St. Louis, MO) and 100 mg/l streptomycin (Sigma, St. Louis, MO). In particular, PCL, PCL-$NH_2$, PCL-DGDGE-GYDGR and PCL-DGDGE-GRGDY 3D scaffolds were sterilized with antibiotics and pre-incubated in serum-free medium for 16-18 h. After the incubation, 5 x $10^4$ cells were seeded on all the different kinds of 3D scaffolds and grown in DMEM w/o FBS to avoid unspecific cell adhesion depending on serum protein adsorption.

Scanning Electron Microscopy (SEM) analyses were performed by a Leica 420 microscope in order to evaluate cell adhesion and shape. At 24 h after cell seeding, the 3D fiber-deposited scaffolds were rinsed with PBS and fixed with 2.5% glutaraldehyde (pH= 7.4) (Sigma-Aldrich, Italy) for 2h at room temperature. The cell-scaffold constructs were dehydrated in graded ethanol concentrations (from 50% to 100% v/v in ethanol), air-dried, gold sputtered and analyzed by SEM. Four different kinds of 3D scaffolds were studied: PCL, PCL-$NH_2$, PCL-DGDGE-GYDGR and PCL-DGDGE-GRGDY.

Furthermore, the several cell-scaffold constructs were also analyzed (PCL, PCL-$NH_2$, PCL-DGDGE-GYDGR and PCL-DGDGE-GRGDY) through Confocal Laser Scanning Microscopy (CLSM). They were fixed with 4% paraformaldeyde for 20 min at room temperature, after 24 h from cell seeding, rinsed twice with PBS buffer and

incubated with PBS-BSA 0.5% to block unspecific binding. Actin microfilaments were stained with phalloidin-tetramethylrhodamine B isothiocyanate (Sigma-Aldrich). Phalloidin was diluted in PBS-BSA 0.5% and incubated for 30 min at room temperature. The images were acquired by using a helium-neon excitation laser at the wavelength of 543 nm and a 20x objective.

## II.III Results and Discussion

### *II.III.I Micro-Computed Tomography*

Micro-computed tomography (Micro-CT), that is an attractive single and nondestructive method to study the characteristics of scaffolds, has firstly allowed to highlight the morphological and architectural features of the 3D fiber-deposited PCL structures. This analysis has confirmed that well-organized PCL scaffolds have been obtained, showing precise pore size and shape, as well as a repeatable microstructure (Figure II.II).

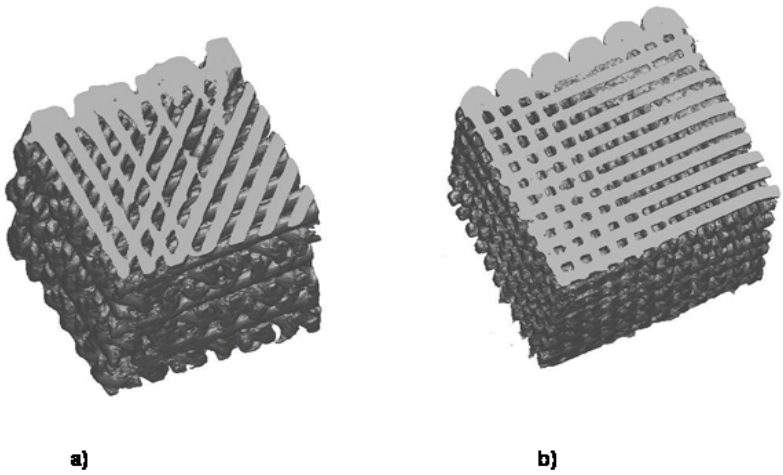


**Figure II.II: 3D reconstructions obtained from Micro-CT analysis on PCL fiber-deposited scaffolds with 0°/45°/90°/135° (a) and 0°/90° (b) lay down patterns.**

In particular, imaging analyses have evidenced a sufficient consistency between real and theoretical values, showing a mean fiber diameter of 340-360 μm and a center-to-center fiber distance of about 640-660 μm between two fibers in a common layer, as expected on the basis of the process/instrument parameters employed during the fabrication (i.e., needle inner diameter, deposition speed, fiber spacing, etc.). Scaffold

interconnectivity, which is normally defined as 100% x volume of interconnected pores/volume sum of interconnected and closed pores, has been also evaluated and found to be equal to 100%.

## *II.III.II Determination of Engrafted Amines and Conjugated Peptide*

It has already been demonstrated that aminolysis may be considered an easy-to-perform chemical technique to engraft amino groups along polyesters chains.[79] By treating these 3D well-organized PCL scaffolds with a 1,6-hexandiamine in an aprotic solvent at a 37°C, an high density of amino groups were rapidly obtained onto the PCL fiber surface of the structure. The reaction starts by a nucleophilic attack onto the ester by an amino group at one end of diamine leading to the formation of an amide and leaving at the other end a free amino group emerging the PCL fiber surface. The functionalization pathway of the PCL scaffolds, that means the functionalization of the fiber surface of the porous structure, is reported in Figure II.III. In addition to the new bond formation along the polymer surface, from the rupture of ester group were produced hydroxyl groups that could remain attached onto fiber surface or leached out during the washes.

As summarized in Figure II.III, the scaffold surface bioactivation was then performed by covalently grafting the GRGDY peptide via a homobifunctional cross-linker. Diethylene glycol diglycidyl ether (DGDGE) is an epoxy crosslinker, water soluble that reacts quite well with amine in mild condition.

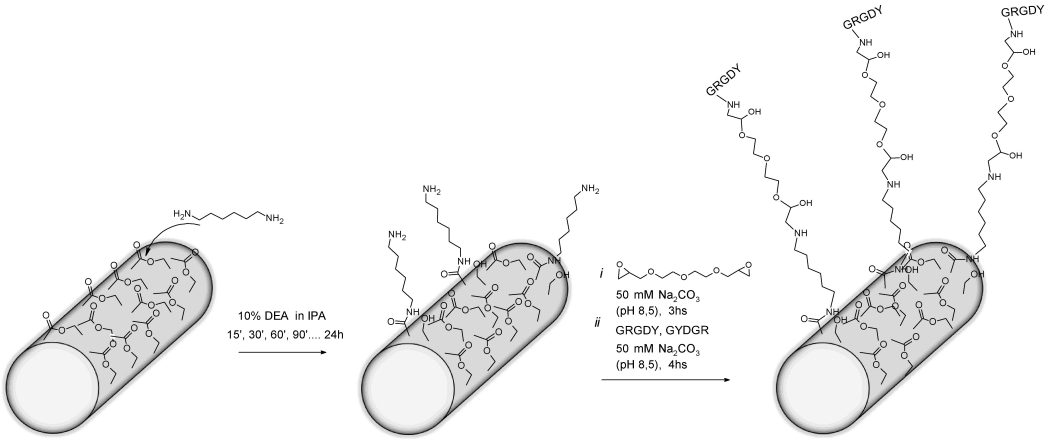


**Figure II.III: Scheme of the two-step procedure used to immobilize GRGDY peptides on PCL fibers of the 3D scaffolds. DEA and IPA indicate 1,6-hexanediamine and isopropanol, respectively. The chemical structure of DGDGE is also reported.**

After aminolysis, an analytical determination of amino groups engrafted onto the surface of PCL fibers constituting the well-organized scaffold was performed by a slight modification procedure based on Kaiser test.[79,101,102]

With regard to the evolution of aminolysis treatment of the 3D scaffolds, a high amino-density of 161.3 ± 15.3 nmol/cm$^2$ was reached after 30 min of aminolysis, and, then, a decrease of surface amines was observed over the time (Figure II.IV).

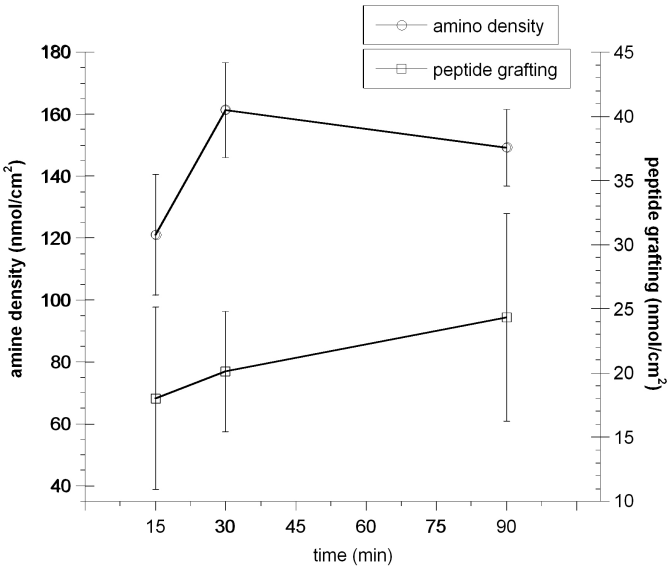


**Figure II.IV: Amine and peptide grafted density as function of time. Data are graphically reported as mean value, and bars represent the standard deviation.**

The amount of peptides immobilized on PCL fibers of the scaffolds was then evaluated using a one-pot colorimetric assay based on the BCA-Cu$^{+1}$ purple color complex. This assay is widely employed to assess proteins both in solution and on adsorbing solid substrates in a very reproducible way and with high sensitivity (picomolar scale).

The number of peptide bonds and the presence of four aminoacids (cysteine, cystine, tryptophan and tyrosine) have been reported to be responsible for color formation in peptide sample when assayed with BCA. Studies with tri- and tetra-peptides suggest that the extent of color formation is due to the presence of several functional groups.[82] The advantages in using BCA method include a compatibility with ionic and non ionic detergents, a stable working reagent and a tolerance to the presence of compounds that could interfere. As described by Tyllianakis et al.[103], this method can be used to determine the total solid supports functionalized with cysteine and tyrosine,

it requires only one incubation step and allows to determine the amount of the functional groups. The quantification of the different groups should be calculated from a standard curve of an appropriate substance.

In the current study, a one-step colorimetric method has been reported to quantify the surface concentration of GRGDY peptides covalently bound on the fibers of the 3D PCL scaffolds. The quantification was carried out by a standard curve using a known-concentration of 1,6-hexanediamine.

The results obtained from micro-BCA assay have highlighted that the tyrosine present in our peptide provides significantly different amount of color formation at 37 °C, thus suggesting a partial reaction of the BCA reagent with tyrosine. Moreover, the BCA reagent requires at least a tri-peptide in order to oxidize the peptide backbone. The concentration of peptides covalently coupled to the PCL has been calculated by taking into account the surface area of sample rather than nominal surface area. A nominal peptide density of 20.13 ± 4.68 nmol/cm$^2$ has been achieved (Figure II.V).

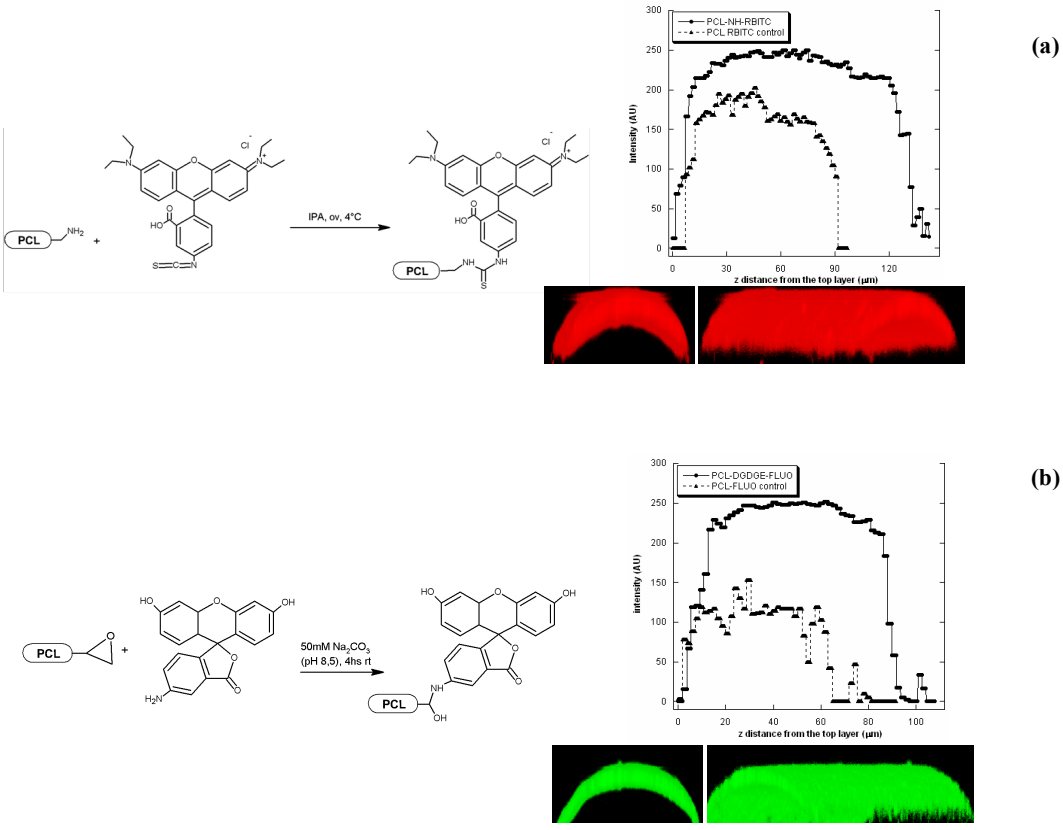


**Figure II.V: Intensity profiles of fluorescent molecules in the depth during the two-step conjugation procedure – (a) CLSM intensity profile as a function of depth in the z-direction of a PCL-NH-RBITC fiber; (b) CLSM intensity profile as a function of depth in the z-direction of a PCL-DGDGE-FLUO fiber.**

To analyze the spatial distribution and penetration depth during each step of bioactivation, Confocal Laser Scanning Microscopy (CLSM) was employed. For this reason, two different dyes were coupled: rhodamine B isothiocyanate activated (RBITC) to label free amino groups after aminolysis treatment, whereas in a second step, fluoresceinamine (FLUO) was conjugated to the epoxy-activated PCL surface to mimic the peptide behavior studying its distribution on the scaffold fiber surface.
Accordingly, Figure II.V clearly shows the intensity profile of the fiber cross-section along the radius (here indicated as z-direction), evidencing a penetration depth more than 140 μm for the aminolysis treatment. With regard to the Fluoresceinamine bound surfaces, the total penetration depth of the treatment was about 80 μm, thus providing an important information on the potential peptide penetration depth.

## *II.III.III Nanoindentation tests*

In the literature, many works have already shown how several surface modifications and RGD immobilization may improve the wettability and/or the biological performances of PCL scaffolds.
For example, Zhang et al. (2009) have previously extended a simple method to immobilize RGD peptide on 2D PCL films to the case of 3D well-organized scaffolds, investigating the human bone marrow stromal cells (hMSCs) behavior[84]. Their modification strategy allowed to obtain a successful Arg-Gly-Asp-Cys (RGDC) immobilization on 3D rapid prototyped PCL scaffolds via aminolysis and a heterobifunctional crosslinker sulfosuccinimidyl 4-(N-maleimidomethyl) cyclohexane-1-carboxylate (sulfo-SMCC). Zhang et al. (2009) have widely studied hMSCs attachment, cellular distribution, signal transduction and survival on their RGD-modified PCL scaffolds, demonstrating that the modification elicits specific cellular responses and improves the final cell–biomaterial interaction.[104]
However, it is worth noting that none of the above mentioned studies has assessed the effect of the surface modification on the mechanical behavior of the 3D rapid prototyped scaffolds.
Consequently, trying to fill this gap present in the literature, nanoindentation, tensile and compression tests were carried out with the aim to highlight the effect of

aminolysis on the surface and bulk material properties, as well as on the macro-mechanical performances of the 3D fiber-deposited PCL scaffolds.

Advanced materials as well as biological tissues show hierarchical structures with particular features down to the nanometer or micrometer scale. For this reason, a technique that can probe mechanical properties at these scales has to be considered. In this context, nanoindentation is emerging as a valuable mechanical testing technique for biomaterials. Hardness and microhardness testing (e.g. Vickers and Knoop indentation) [5,85] have been already considered to investigate the mechanical properties of hard tissues such as teeth and bones.[105-108] However, nanoindentation enhances the spatial, force, and displacement resolutions of these traditional techniques, thus providing a powerful tool to study tissues and biomaterials with submicron resolution. Nanoindentation is also useful for measuring mechanical properties of microstructural features within bulk samples, characterizing the properties of individual constituents within composite or heterogeneous samples, or mapping mechanical properties across a sample surface. Because of its small probe size, nanoindentation can be used to measure local material properties in small, thin, and heterogeneous samples. Nanoindentation, that is an instrumented or depth-sensing indentation, involves the application of a controlled load to the surface inducing local surface deformation. Load and displacement are monitored during the loading and unloading phases. Thus, properties such as hardness and reduced modulus are calculated from the unloading curves using well-established equations. Considering its typical working force range and displacement range (1 μN-500 mN and 1 nm-20 μm, respectively) nanoindentation technique surely bridges the gap between Atomic Force Microscopy (AFM) and macro-scale mechanical testing.

Accordingly, in the present study, nanoindentation measurements on PCL fibers have displayed differences in terms of load-depth curves and, hence, of hardness values. Both aminolyzed (PCL-$NH_2$) and unmodified (PCL) fibers have evidenced hardness (H) values which generally decrease as load increases from 1 to 5 mN. In particular, measurements on unmodified PCL fibers have evidenced hardness values ranging from 0.50 to 0.27 GPa in the load range investigated. These values result greater than those obtained for PCL fibers which were modified via aminolysis (0.1 - 0.03 GPa) (Figure II.VI a). This suggests that after aminolysis the fiber surface becomes softer. Consistently with hardness values, the reduced modulus ($E_r$) of unmodified PCL

fibers (4.2 – 1.2 GPa) results higher than those obtained from the PCL-$NH_2$ ones (1 - 0.3 GPa) (Figure II.VI b).

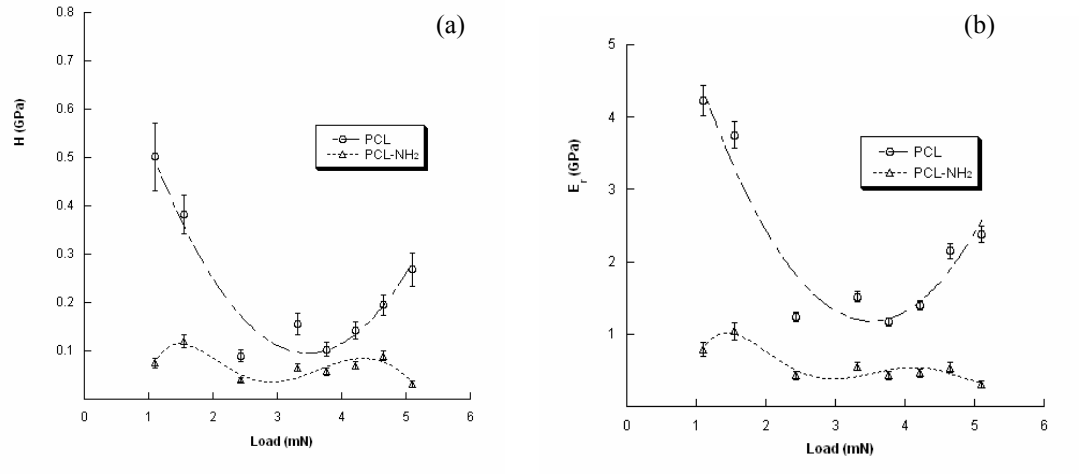


**Figure II.VI: Results obtained from nanoindentation tests on PCL and PCL-$NH_2$ fibers: hardness (a) and reduced modulus (b) as function of the applied load (1-5 mN). Data are graphically reported as mean value, and bars represent the standard deviation. The dashed lines are just a guide for the eye.**

The reduced modulus may be considered a combined modulus obtained from nanoindentation tests as it is related to the Young's moduli of both tip and sample, and to the their Poisson's ratios. The tip properties are usually known, thus the Young's modulus of a material can be evaluated from the reduced modulus if the Poisson's ratio of the sample material is known.

## *II.III.IV Tensile tests*

Tensile tests have shown a ductile behavior for both PCL-$NH_2$ and unmodified PCL fibers. In particular, the stress-strain curves obtained show an initial linear region, then a little decrease in the slope occurs up to a local maximum stress value, followed by a decrease of the tensile stress. Then, a plateau-like region is evident, and finally a new increase of stress until the failure is generally reached. During testing the propagation of multiple necks were also observed along the aminolyzed fibers in comparison with the unmodified ones, as can be also evidenced by the fluctuating stress values after the first local maximum of the stress-strain curve (Figure II.VII).

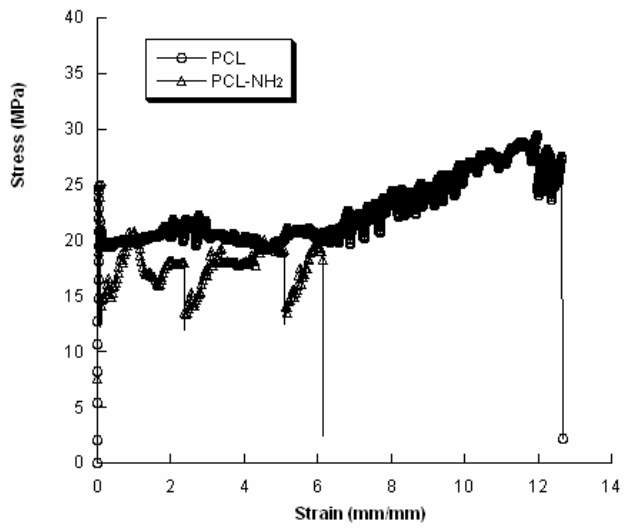


**Figure II.VII: Typical stress-strain curves obtained from tensile tests on PCL and PCL-$NH_2$ fibers.**

Furthermore, even though the surface treatment strongly reduces the maximum strain, it seems to provide no differences in terms of modulus (E) and yield stress ($\sigma_y$) (Table II.I).

| **Fibers** | **E (MPa)** | **$\sigma_y$ (MPa)** | **$\varepsilon_{max}$ (mm/mm)** |
|---|---|---|---|
| PCL | 570.5 ± 50.1 | 25.0 ± 3.5 | 12.7 ± 1.1 |
| PCL-$NH_2$ | 550.0 ± 48.6 | 24.2 ± 3.7 | 6.5 ± 0.5 |

**Table II.I: Results from tensile tests performed on PCL and PCL-$NH_2$ microfibers: tensile modulus (E), yield stress ($\sigma_y$) and maximum strain ($\varepsilon_{max}$), reported as mean value ± standard deviation.**

## *II.III.V Compression tests*

Considering that both nanoindentation and tensile measurements have allowed to evidence the effect of the modification via aminolysis on the surface and bulk properties, compression tests were carried out to analyze the effect on the macro-mechanical performance of the 3D fiber-deposited scaffolds.

Unlike nanoindentation and tensile measurements on PCL fibers, compression tests have evidenced that the aminolyzed 3D fiber-deposited scaffolds show stress-strain curves similar to those obtained for the unmodified ones. For both PCL-$NH_2$ and PCL

scaffolds, compressive stress-strain curves may be divided into three different regions: after an initial relatively stiff mechanical response, there is a region with lower stiffness, finally followed by another stiff portion, similar to the densification region of flexible foams (Figure II.VIII).

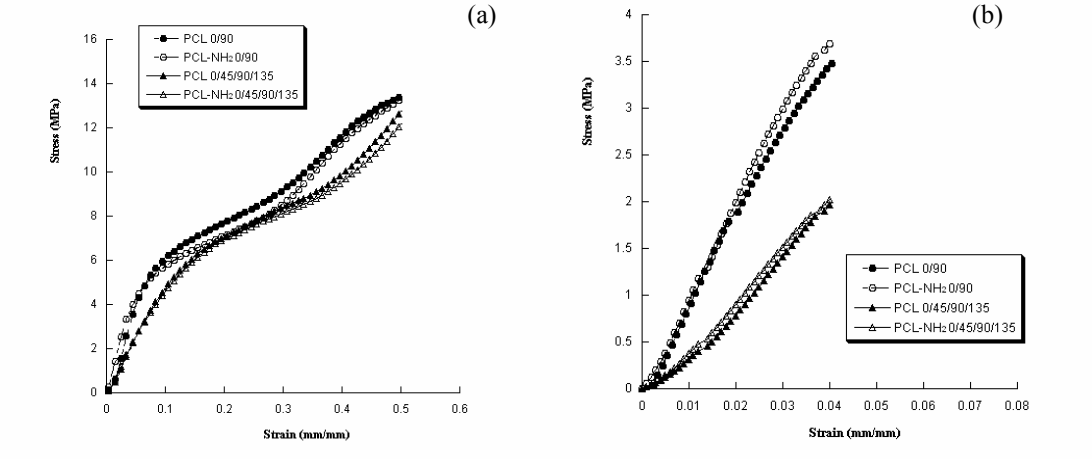


**Figure II.VIII: Effect of lay-down pattern and surface modification via aminolysis on the mechanical properties of 3D rapid prototyped scaffolds. (a) Typical stress-strain curves for PCL scaffolds characterized by two different lay-down patterns (0°/90° and 0°/45°/90°/135°), before (PCL) and after aminolysis (PCL-$NH_2$). (b) Stress-strain curves reported up to a strain level of 0.04 mm/mm, in order to better highlight the different initial stiffness of the 3D morphologically-controlled structures.**

However, differently from the typical behavior of a flexible foam, the central zone is not a plateau, i.e. does not have zero slope but just a lower one if compared with the other two portions of the stress-strain curve. This behavior is also consistent with that already reported for 3D fiber-deposited PCL scaffolds.[1,36]

The compressive modulus (E) has been evaluated as the slope of the initial linear region of the stress-strain curve.

As expected, the architecture, that means the specific lay-down pattern used (0°/90° or 0°/45°/90°/135°), also influences the mechanical behavior of the 3D PCL scaffolds in compression.

To emphasize the effect of architecture and surface modification and on the compressive mechanical performances of the 3D fiber-deposited scaffolds, values of compressive modulus and maximum stress have been reported as mean value ± standard deviation, for the two different lay-down patterns (0°/90° and 0°/45°/90°/135°), also before and after aminolysis (Table II.II).

| Lay-Down Pattern | Compressive Modulus E (MPa) | | Maximum Stress σ (MPa) | |
|---|---|---|---|---|
| | PCL | PCL-$NH_2$ | PCL | PCL-$NH_2$ |
| 0°/45°/90°/135° | 63.0 ± 4.7 | 61.1 ± 5.1 | 12.3 ± 1.1 | 12.0 ± 1.3 |
| 0°/90° | 89.1 ± 6.9 | 87.9 ± 8.1 | 13.5 ± 1.3 | 13.2 ± 1.5 |

**Table II.II: Effect of lay-down pattern and surface modification via aminolysis on the mechanical properties of 3D rapid prototyped scaffolds. Compressive modulus and maximum stress reported as mean value ± standard deviation, for PCL scaffolds characterized by two different lay-down patterns (0°/90° and 0°/45°/90°/135°), before (PCL) and after aminolysis (PCL-$NH_2$).**

The lay-down pattern strongly influences the mechanical behavior of the 3D fiber-deposited PCL scaffolds, especially in terms of initial stiffness. As reported in Table II.II, before the surface modification via aminolysis, PCL scaffolds characterized by a 0°/90° pattern exhibit compressive modulus (89.1 ± 6.9 MPa) which is greater than that obtained for a 0°/45°/90°/135° pattern (63.0 ± 4.7 MPa). At a strain value of 50%, a maximum stress of 13.5 ± 1.3 MPa and 12.3 ± 1.1 MPa has been evaluated for 0°/90° and 0°/45°/90°/135° patterns, respectively.

Furthermore, the surface treatment via aminolysis does not negatively affect the macro-mechanical behavior of the 3D fiber-deposited scaffolds, as evaluated through compression tests. For example, after aminolysis, PCL scaffolds characterized by a 0°/90° pattern have shown values of compressive modulus (87.9 ± 8.1 MPa) that are similar to those achieved before the surface treatment (89.1 ± 6.9 MPa), as well as a maximum stress of 13.2 ± 1.2 MPa compared to a value of 13.5 ± 1.3 MPa obtained for the corresponding not-aminolyzed structures.

Analogue observations might be made for the 3D fiber-deposited PCL scaffolds with a 0°/45°/90°/135° pattern, taking into account the results numerically reported in terms of modulus and maximum stress, before and after the surface treatment via aminolysis (Table II.II).

## *II.III.VI Cell Adhesion Study*

All the steps carried out till this point can be briefly summarized as follows: a) design and fabrication of "morphologically-controlled" scaffolds through 3D Fiber

Deposition technique; b) optimization of the one-step surface treatment, especially through the precise quantification of amino-groups and the analysis of the penetration depth; c) RGD peptides quantification; d) mechanical characterization performed to assess the effect of the functionalization on the surface and bulk PCL properties, as well as on the macro-mechanical compression performances of the structures. However, even though the above mentioned steps are crucial, the knowledge of cell-material interactions results to be a key element in designing 3D advanced multifunctional scaffolds with suitable morphology and properties, that are able to guide cell adhesion. For this reason, as a final step of this research, to analyze the bioactivation of 3D fiber-deposited scaffolds at the cell-material interface, their interaction with fibroblast cells was studied through Scanning Electron Microscopy (SEM) and Confocal Laser Scanning Microscopy (CLSM).

SEM analyses have highlighted that NIH3T3 cells already adhere on the PCL fiber of the 3D scaffolds after 24 h from seeding, showing a morphology that drastically changes on the different samples (Figure II.IX).

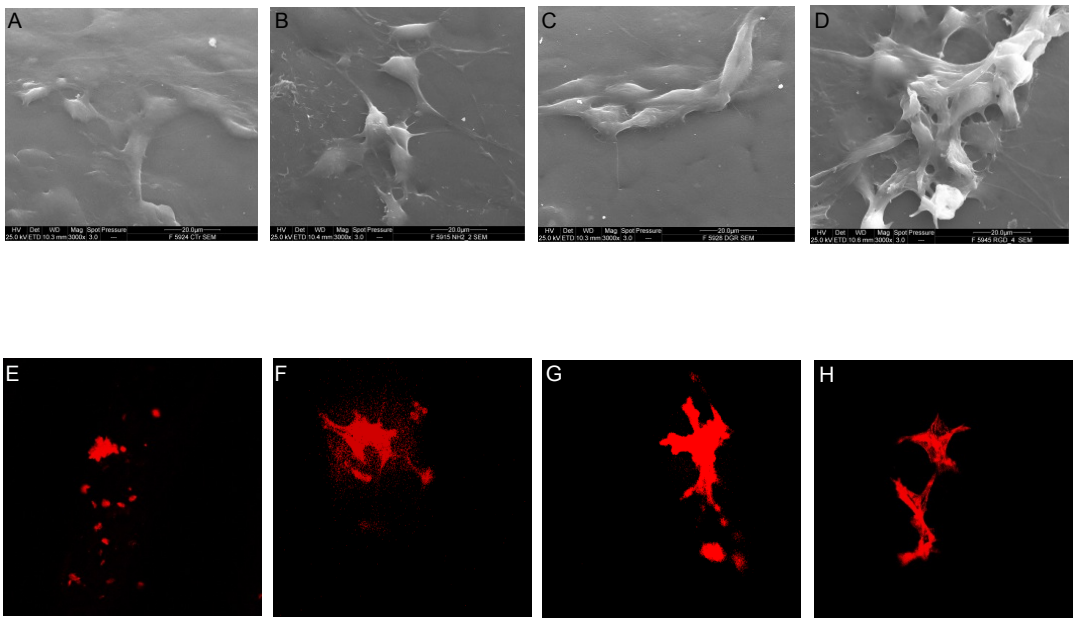


**Figure II.IX: Cell adhesion study after 24 h from cell seeding: SEM micrographs (A PCL; B PCL-$NH_2$; C PCL-DGDGE-GYDGR; D PCL-DGDGE-GRGDY), bar 20 µm; confocal laser scanning microscope images of phalloidin staining of microfilaments (E PCL; F PCL-$NH_2$; G PCL-DGDGE-GYDGR; and H PCL-DGDGE-GRGDY).**

In particular, with regard to unmodified PCL, PCL-$NH_2$, and PCL-DGDGE-GYDGR scaffolds, cells did not show an appropriate shape, indicating a poor adhesion to the

substrate (respectively Figure II.IX A-E, B-F, and C-G). Conversely, as for PCL bioactivated with RGD peptide, cells correctly adhered and were well spread on the fiber surface, evidencing a good interaction with the material (Figure II.IX D,H).
Moreover, at higher magnification, the formation of *filopodia* was observed. The effect of PCL functionalization in enhancing cell adhesion was further confirmed by actin cytoskeleton staining. This qualitative analysis indicated that cells better adhered on RGD bioactivated scaffolds, as demonstrated by the presence of stress fibers, compared to cells seeded on unmodified PCL, PCL-$NH_2$, and PCL-DGDGE-GYDGR surfaces, where there is no evidence of a complete cytoskeleton organization.
After 48 h from cell seeding, the effect of RGD peptide immobilization on cell adhesion results more evident as evidenced by Figure II.X, where it is worth noting the presence of cells that tend to fill the space between the fibers of 3D scaffolds.

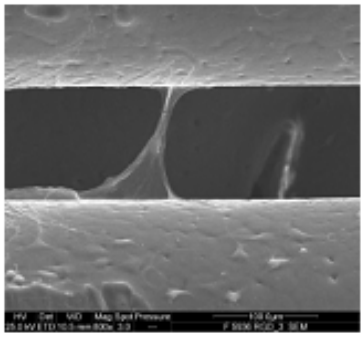

**Figure II.X: Cell adhesion study after 48 h from cell seeding - SEM micrographs (PCL-DGDGE-GRGDY), bar 50 µm.**

## II.IV Conclusions

The ligand presentation at the cell-material interface results crucial in cell recognition of bioactive ligands immobilized onto polymeric substrates. Consequently, RGD motifs are being widely considered to design biomimetic surfaces that could trigger a specific function in cell behavior at the cell-material interface. In particular, cell adhesion should be suitably enhanced and tailored since it represents the basic feature in the cell-material interaction. Previous works have already evidenced that aminolysis represents an easy route to introduce primary amines with high yield that can be easily optimized. In this work, the precisely controlled two-step procedure proposed by Causa et al. (2010) for 2D PCL films was successfully extended to

immobilize RGD motifs on 3D rapid prototyped scaffolds, thus designing 3D advanced multifunctional scaffolds able to guide cell functions. The determination of amines and peptides effectively engrafted on the fiber surface of 3D scaffolds, as well as the treatment penetration depth was suitably assessed and discussed. Nanoindentation and tensile measurements carried out on PCL fibers allowed to underline the effect of the functionalization on the surface and bulk properties. More importantly, the surface modification did not negatively affect the macro-mechanical behavior of the 3D rapid prototyped scaffolds as evaluated through compression tests. On the other hand, results from cell adhesion study evidenced that the conjugation of amine-terminated peptides through reductive amination after tether insertion enhanced NIH3T3 cell adhesion and spreading. This means that a specific recognition of the solid signal (i.e., a correct presentation of the peptide sequences) to NIH3T3 integrin cell receptors was presented.

Accordingly, the present study could be considered as an approach to control scaffold morphology, spatial distribution of surface treatment as well as macro-, micro-, nano-mechanical performances, for guiding cell adhesion or promoting specific cell-material interactions as eventually in the case of different peptide sequences or structure.

I would like to thank dr. E. Battista and dr. R. Della Moglie from Center for Advanced Biomaterials for Health Care (ABC) of the Italian Institute of Technology (IIT@CRIB), Naples (Italy) and prof. F. Causa from Department of Materials and Production Engineering (DIMP), Interdisciplinary Research Center on Biomaterials (CRIB) and Italian Institute of Technology (IIT@CRIB), Naples (Italy), for their support and collaboration in the functionalization and bioactivation of polymeric and nanocomposite scaffolds.

# References


1. A. Gloria, R. De Santis, L. Ambrosio. *Polymer-based composite scaffolds for tissue engineering*. Journal of Applied Biomaterials and Biomechanics 2010; 8: 57-67.
2. H. Y. Cheung, K. T. Lau, T. P. Lu, D. Hui. *Synthesis and characterization of PLLA–PLCA–PEG multiblock copolymers and their applications in modifying PLLA porous scaffolds*. Composite Part B Engineering 2007; 38: 291-300.
3. D. M. Ebenstein, L. A. Pruitt. *Nanoindentation of biological materials*. Nano Today 2006; 1: 26-33.
4. A. Shekaran, A. J. Garcia. *Nanoscale engineering of extracellular matrix-mimetic bioadhesive surfaces and implants for tissue engineering*. Biochemical Biophysical Acta 2011, 1810: 350–360.
5. B. Alberts, A.r Johnson, J. Lewis, M. Raff, K. Roberts, P. Walter. *Molecular Biology of the Cell* 4th ed, Garland Science, New York, 2002.
6. J. Rossert, B. de Crombrugghe, P.B. John, G.R. Lawrence, A.R. Gideon. *Type I Collagen: Structure, Synthesis, and Regulation*. In: *Principles of Bone Biology*, Second Edition, Academic Press, San Diego, 2002, pp. 189–210.
7. P.G. Robey, P.B. John, G.R. Lawrence, A.R. Gideon. *Bone Matrix Proteoglycans and Glycoproteins*. In: *Principles of Bone Biology*, Second Edition, Academic Press, San Diego, 2002, pp. 225–237.
8. H.Zhang, K.W.Marshall, H.Tang, D.M.Hwang, M.Lee, C.C.Liew. *Profiling genes expressed in human fetal cartilage using 13, 155 expressed sequence tags*. Osteoarthritis and Cartilage 2003; 11: 309–319.
9. A.E. Aplin, B. P. Hogan, J. Tomeu, R.L. Juliano. *Cell adhesion differentially regulates the nucleocytoplasmic distribution of active MAP kinases*. Journal of Cell Science 2002; 115: 2781–2790.
10. R.O. Hynes. *Integrins: bidirectional, allosteric signaling machines*. Cell 2002; 110: 673–687.
11. F. G. Giancotti, E. Ruoslahti. *Integrin signaling*. Science 1999; 285: 1028–1032.

12. V. Petit, J. P. Thiery. *Focaladhesions: structure and dynamics*. Biology of the Cell 2000; 92: 477–494.
13. S. Bourdoulous, G. Orend, D. A. MacKenna, R. Pasqualini, E. Ruoslahti, *Fibronectin matrix regulates activation of RHO and CDC42 GTPases and cell cycle progression*. The Journal of Cell Biology 1998; 143: 267–276.
14. C. S. Chen, M. Mrksich, S. Huang, G. M. Whitesides, D.E. Ingber. *Geometric control of cell life and death*. Science 1997; 276: 1425–1428.
15. K. Burridge, K. Fath, T. Kelly, G. Nuckolls, C. Turner. *Focal adhesions: transmembrane junctions between the extracellular matrix and the cytoskeleton*. Annual Review of Cell and Developmental Biology 1988; 4: 487–525.
16. R.O. Hynes, *Integrins: versatility, modulation, and signaling in cell adhesion*. Cell 1992; 69: 11–25.
17. N.A. Carrell, L.A. Fitzgerald, B. Steiner, H.P. Erickson, D.R. Phillips. *Structure of human platelet membrane glycoproteins IIb and IIIa as determined by electron microscopy*. The Journal of Biological Chemistry 1985; 260: 1743–1749.
18. M.V. Nermut, N.M. Green, P. Eason, S.S. Yamada, K.M. Yamada. *Electron microscopy and structural model of human fibronectin receptor*. The EMBO Journal 1988; 7: 4093–4099.
19. J. Emsley, C. G. Knight, R. W. Farndale, M. J. Barnes. *Structure of the integrin alpha2beta1-binding collagen peptide.* Journal of Molecular Biology 2004; 335: 1019–1028.
20. C. G. Knight, L. F. Morton, D. J. Onley, A. R. Peachey, A. J. Messent, P. A. Smethurst, D. S. Tuckwell, R. W. Farndale, M. J. Barnes. *Identification in collagen type I of an integrin alpha2 beta1-binding site containing an essential GER sequence*. The Journal of Biological Chemistry 1998; 273: 33287–33294.
21. D. J. Leahy, I. Aukhil, H. P. Erickson. *2.0 Å crystal structure of a four-domain segment of human fibronectin encompassing the RGD loop and synergy region*. Cell 1996; 84: 155–164.
22. S. Aota, M. Nomizu, K. M. Yamada. *The short aminoacid sequence Pro-His-Ser-Arg-Asn in human fibronectin enhances cell-adhesive function*. The Journal of Biological Chemistry 1994; 269: 24756–24761.

23. M. J. Humphries, S. K. Akiyama, A. Komoriya, K. Olden, K. M. Yamada, *Identification of an alternatively spliced site in human plasma fibronectin that mediates cell type-specific adhesion*. The Journal of Cell Biology 1986; 103: 2637–2647.
24. A. Komoriya, L. J. Green, M. Mervic, S. S. Yamada, K. M. Yamada, M. J. Humphries. *The minimal essential sequence for a major cell type-specific adhesion site (CS1) within the alternatively spliced type III connecting segment domain of fibronectin is leucine-aspartic acid-valine*. The Journal of Biological Chemistry 1991; 266: 15075–15079.
25. K. Tashiro, G. C. Sephel, B. Weeks, M. Sasaki, G. R. Martin, H. K. Kleinman, Y. Yamada. *A synthetic peptide containing the IKVAV sequence from the A chain of laminin mediates cell attachment, migration, and neurite outgrowth.* The Journal of Biological Chemistry 1989; 264: 16174–16182.
26. J. Graf, R. C. Ogle, F. A. Robey, M. Sasaki, G. R. Martin, Y. Yamada, H. K. Kleinman. *A pentapeptide from the laminin B1 chain mediates cell adhesion and binds the 67,000 laminin receptor*. Biochemistry 1987; 26: 6896–6900.
27. H. K. Kleinman, J. Graf, Y. Iwamoto, M. Sasaki, C. S. Schasteen, Y. Yamada, G. R. Martin, F. A. Robey. *Identification of a second active site in laminin for promotion of cell adhesion and migration and inhibition of in vivo melanoma lung colonization*. Archives of Biochemistry and Biophysics 1989; 272: 39–45.
28. S. F. Badylak, D. O. Freytes, T. W. Gilbert. *Extracellular matrix as a biological scaffold material: structure and function*. Acta Biomaterialia 2009; 5: 1–13.
29. K. Shakesheff, S. Cannizzaro, R. Langer. *Creating biomimetic micro-environments with synthetic polymer–peptide hybrid molecules*. Journal of Biomaterial Science-Polymer Edition 1998; 9: 507–518.
30. L.S. Nair, C.T. Laurencin. *Polymers as biomaterials for tissue engineering and controlled drug delivery*. Advances in Biochemical Engineering/Biotechnology, 2006; 102: 47-90.
31. L. Moroni, J.R. de Wijn, C.A. Van Blitterswijk. *Three-dimensional fiber-deposited PEOT/PBT copolymer scaffolds for tissue engineering: influence*

*of porosity, molecular network mesh size and swelling in aqueous media on dynamic mechanical properties*. Journal of Biomedical Material Research-Part A 2005; 75: 957-965.

32. T.B.F. Woodfield, J. Malda, J. de Wijn, F. Peters, J. Riesle, C.A. Van Blitterswijk. *Design of porous scaffolds for cartilage tissue engineering using a three-dimensional fiber-deposition technique*. Biomaterials 2004; 25: 4149-61.
33. J. Malda, T.B. Woodfield, F. van der Vloodt, C. Wilson, D.E. Martens, J. Tamper, C.A. van Blitterswijk, J. Riesle. *The effect of PEGT/PBT scaffold architecture on the composition of tissue engineered cartilage*. Biomaterials 2004; 26: 63-72.
34. L. Moroni, J.R. de Wijn, C.A. Van Blitterswijk. *3D fiber- deposited scaffolds for tissue engineering: influence of pores geometry and architecture on dynamic mechanical properties*. Biomaterials 2006; 27: 974-85.
35. L. Moroni, G. Poort, F. van Keulen, J. de Wijn, C.A. Van Blitterswijk. *Dynamic mechanical properties of 3D fiber-deposited PEOT/PBT scaffolds: an experimental and numerical analysis*. Journal of Biomedical Material Research 2006; 78A: 605-14.
36. K. Kyriakidou, G. Lucarini, A. Zizzi, E. Salvolini, M. Mattioli-Belmonte, F. Mollica, A. Gloria, L. Ambrosio. *Dynamic co-seeding of osteoblast and endothelial cells on 3D polycaprolactone scaffolds for enhanced bone tissue engineering*. Journal of Bioactive and Compatible Polymers 2008; 23: 227-43.
37. T. Hayashi. *Biodegradable polymers for biomedical uses*. Progress in Polymer Science 1994; 19: 663-702.
38. L.G. Griffith. *Polymeric biomaterials*. Acta Materialia 2000; 48: 263-277.
39. C. Giordano, D. Albani, A. Gloria, M. Tunesi, S. Batelli, T. Russo, G. Forloni, L. Ambrosio, A. Cigada. *Multidisciplinary perspectives for Alzheimer's and Parkinson's diseases: hydrogels for protein delivery and cell-based drug delivery as therapeutic strategies*. International Journal of Artificial Organs 2009; 32: 836-50.
40. K.J.L. Burg, S. Porter, J.F. Kellam. *Biomaterial developments for bone tissue engineering*. Biomaterials 2000; 21: 2347-59.

41. R.Z. Le Geros. *Properties of osteoconductive biomaterials: calcium phosphates*. Clinical Orthopaedics and Related Research 2002; 395: 81-98.
42. A.G. Mikos, G. Sarakinos , S.M. Leite, J.P. Vacanti, R. Langer. *Laminated three-dimensional biodegradable foams for use in tissue engineering*. Biomaterials 1993; 14: 323-30.
43. H.Y. Cheung, K.T. Lau, T.P. Lu, D. Hui. *A critical review on polymer-based bio-engineered materials for scaffold development*. Composite Part B Engineering, 2007; 38: 291-300.
44. F. Causa, P. A. Netti, L. Ambrosio. *A multi-functional scaffold for tissue regeneration: the need to engineer a tissue analogue*. Biomaterials 2007; 28: 5093-5099.
45. L.E. Freed, G. Vunjak-Novakovic, R.J. Biron, D.B. Eagles, D.C. Lesnoy, S.K. Barlow, R. Langer. *Biodegradable polymer scaffolds for tissue engineering*. Nature Biotechnology 1994; 12: 689-693.
46. J.E. Devin, M.A. Attawia, C.T. Laurencin. *Three-dimensional degradable porous polymer-ceramic matrices for use in bone repair*. Journal of Biomaterial Science-Polymer Edition 1996; 7: 661-669.
47. L.M. Mathieu, T.L. Mueller TL, P.E. Bourban, D.P. Pioletti, R. Müller, J.A.E. Manson. *Architecture and properties of anisotropic polymer composite scaffolds for bone tissue engineering*. Biomaterials 2006; 27: 905-16.
48. M.M. Schwartz. *Composite Materials Handbook*. 2nd edition New York: McGraw-Hill; *1992*.
49. P.K. Mallick. *Composites Engineering Handbook*. New York: Marcel Dekker, Inc; 1997.
50. R.M. Jones. *Mechanics of Composite Materials*. 2nd edition London: Taylor & Francis; 1999.
51. L. Nicolais, A. Gloria, L. Ambrosio. *The mechanics of biocomposites*. In: L. Ambrosio, ed. *Biomedical composites*. Cambridge, UK: Woodhead Publishing Limited, CRC Press; 2010: 411-40.
52. X.P. Ma, *Scaffolds for Tissue fabrication*, Materials Today 2004; 7: 30- 40.
53. R. Langer, *Selected advances in drug delivery and tissue engineering*, Journal of Controlled Release 1999; 62: 7–11.
54. G.N. Bancroft, A.G. Mikos. *Fluid flow increases mineralized matrix*

*deposition in 3D perfusion culture of marrow stromal osteoblasts in a dose- dependent manner*, Proceeding of the National Academy of Science of the United States of America 2002; 99: 12600–12605.

55. S.A.N. Ali, S.P. Zhong, P.J. Dhoerty, D.F. Williams. *Mechanism of polymer degradation in implantable devices*. Biomaterials 1993; 14: 1409-1418.
56. S. Ramakrishna, J. Mayer, E. Wintermantel, K.W. Leong. *Biomedical applications of polymer-composite materials: a review*. Composites Science and Technology 2001; 61: 1189-122.
57. I. Martin, D. Wendt, M. Heberer. *The role of bioreactors in tissue engineering*. Biotechnology 2004; 22: 80-86.
58. X. Yu, C.T. Laurencin. *Bioreactor-based bone tissue engineering*, PNAS August 2004; 101: 11203–11208.
59. D.W. Hutmacher. *Scaffold design and fabrication technologies for engineering tissues state of the art and future perspectives.* Journal of Biomaterial Science -Polymer Edition 2001; 12: 107-124.
60. D.W. Hutmacher, T. Schantz, I. Zein, K.W. Ng, S.H. Teoh, K.C. Tan. *Mechanical properties and cell culture response of polycaprolactone scaffolds designed and fabricated via fused deposition modeling.* Journal of Biomedical Material Research 2001; 55: 203-216.
61. J.P. Vacanti, M.A. Morse, W.M. Saltzman, A.J. Domb, A. Perez-Atayde, R. Langer. *Selective cell transplantation using bioabsorbable artificial polymers as matrices.* Journal of Pediatric Surgery 1988; 23: 3-9.
62. K.R. Stone, W.G. Rodkey, R. Webber, L. Mckinney, J.R. Steadman. *Meniscal regeneration with copolymeric collagen scaffolds. In vitro and in vivo studies evaluated clinically, histologically, and biochemically*. The American Journal of Sports Medicine 1992; 20: 104-111.
63. B.M. Wu, S.W. Borland, R.A. Giordano, L.G. Cima, E.M. Sachs, M.J. Cima. *Solid free-form fabrication of drug delivery devices*. Journal of Controlled Release 1996; 40: 77-87.
64. X.J. Yu, G.P. Dillon, R.B. Bellamkonda. *A laminin and nerve growth factor-laden three-dimensional scaffold for enhanced neurite extension.* Tissue Engineering 1999; 5: 291-304.

65. K.E. Healy, A. Rezania, R.A. Stile. *Designing biomaterials to direct biological responses.* Bioartificial Organs II: Technology, Medicine and Materials 1999; 875: 24-35.
66. M.C. Hacker, A.G. Mikos. *Trends in Tissue Engineering Research*. Tissue Engineering 2006; 12: 2049-2057.
67. A. Shekaran, A.J. Garcia. *Nanoscale engineering of extracellular matrix-mimetic bioadhesive surfaces and implants for tissue engineering.* Biochimica et BIophysica Acta 2011; 1810: 350-360.
68. U. Hersel, C. Dahmen, H. Kessler. *RGD modified polymers: biomaterials for stimulated cell adhesion and beyond. RGD modified polymers: biomaterials for stimulated cell adhesion and beyond.* Biomaterials 2003; 20: 4385-4415.
69. A.J. Garcia, C.D. Reyes. *Bio-adhesive surfaces to promote osteoblast differentiation and bone formation.* J. Dent Res 2005; 84: 407-413.
70. A. McConachie, D. Newman, M. Tucci, A. Puckett, A. Tsao, J. Hughes, H. Benghuzzi. *The effect on bioadhesive polymers either freely in solution or covalently attached to a support on human macrophages.* Biomedical Science Instrumentation 1999, 35, 45-50.
71. K. Cai, K. Yao, Y. Cui, Z. Yang, X. Li, H. Xie, T. Qing, L. Gao. *Influence of different surface modification treatments on poly(d,l-lactic acid) with silk fibroin and their effects on the culture of osteoblast in vitro*. Biomaterials 2002, 23, 1603-1611.
72. J. Yang, J. Bei, S. Wang. *Enhanced cell affinity of Poly (D, L-lactide) by combining plasma treatment with collagen anchorage.* Biomaterials 2002; 23: 2607-2614.
73. P. K. Chu, J. Y. Chen, L. P. Wang, N. Huang. *Plasma-surface modification of biomaterials.* Material Science and Engineering 2002; R 36: 143-206.
74. Y. Zhu, K. S. Chian, M. B. Chan-Park, P. S. Mhaisalkara, B. D. Ratner. *Protein bonding on biodegradable poly(L-lactide-co-caprolactone) membrane for esophageal tissue engineering.* Biomaterials 2006; 27: 68-78.
75. M. Gabriel, G. P. Van Nieuw Amerongen, V. W. M. Van Hinsbergh, A. V. Van Nieuw Amerongen, A. Zentner. *Direct grafting of RGD-motif-*

*containing peptide on the surface of polycapolactone films*. Journal of Biomaterial Science-Polymer Edition 2006; 17: 567-577.

76. L. Y. Santiago, R. W. Nowak, J. P. Rubin, K. G. Marra. *Peptide-surface modification of poly(caprolactone) with laminin-derived sequences for adipose-derived stem cell applications.* Biomaterials 2006; 27: 2962-2969.
77. I. Taniguchi, W.A. Kuhlman, A.M. Mayes, L.G. Griffith. *Functional modification of biodegradable polyesters through a chemoselective approach: application to biomaterial surfaces.* Polymer International 2006, 55, 1385-1397.
78. P.D. Dalton, T. Woodfield, D.W. Hutmacher. Snapshot: Polymer scaffolds for tissue engineering. Biomaterials 2009; 30: 701-702.
79. R. Langer, J.P. Vacanti. *Tissue engineering*. Science 1993; 260: 920-926.
80. D.M. Ebenstein, L.A. Pruitt. *Nanoindentation of biological materials.* Nano Today 2006; 1: 26-33.
81. M.T. Raimondi, M. Moretti, M. Cioffi, C. Giordano, F.K. Laganà, R. Pietrabissa. *The effect of hydrodynamic shear on 3D engineered chondrocyte systems subject to direct perfusion*. Biorheology 2006; 43: 215-222.
82. C. Giordano, F. Causa, G. Candiani. *Gene therapy: The state of the art and future directions.* Journal of Applied Biomaterials and Biomechanics 2006, 4, 73-79.
83. A. Cigada. *Biomaterials, tissue engineering, gene therapy*. Journal of Applied Biomaterials and Biomechanics 2008, 6, 127-131.
84. P. D. Dalton, T. Woodfield, D. W. Hutmacher, Biomaterials 2009, 30, 701.
85. H. Zhang, C. Y. Lin, S. J. Hollister, Biomaterials 2009, 30, 4063.
86. C. Giordano, F. Causa, F. Bianco, G. Perale, P. A. Netti, L. Ambrosio, A. Cigada, Int. J. Artif. Organs 2008, 31, 1017.
87. R. Landers, U. Hubner, R. Schmelzeisen, R. Mulhaupt. *Rapid prototyping of scaffolds derived from thermoreversible hydrogels and tailored for applications in tissue engineering*. Biomaterials 2002; 23: 4437-4447.
88. G. Perale, G. Pertici, C. Giordano, F. Daniele, M. Masi, S. Maccagnan. *Nondegradative microextrusion of resorbable polyesters for pharmaceutical and biomedical applications: the cases of poly-lactic acid*

*and poly-caprolactone.* Journal of Applied Polymer Science 2008; 108: 1591-1595.

89. J. Yang, J. Bei, S. Wang. *Enhanced cell affinity of poly (,-Lactide) by combining plasma treatment with collagen anchorage.* Biomaterials 2002, 23, 2607-2614.
90. F. Causa, E. Battista, R. Della Moglie, D. Guarnieri, M. Iannone, P.A. Netti. *Surface investigation on biomimetic materials to control cell adhesion: the case of RGD conjugation on PCL.* Langmuir. 2010; 26: 9875-9884.
91. T.M.G. Chu, in: P. X. Ma, J. Elisseeff, *Scaffolding in Tissue engineering*. Taylor and Francis: Northwest Florida 2006, pp. 139–153.
92. L.G. Griffith. *Polymeric biomaterials*. Acta Materialia 2000; 48: 263-277.
93. R.Z. LeGeros. *Properties of osteoconductive biomaterials: calcium phosphates*. Clinical Orthopaedics and Related Research 2002; 395: 81-98.
94. A.G. Mikos, G. Sarakinos, S.M. Leite, J.P. Vacanti, R. Langer. *Laminated three-dimensional biodegradable foams for use in tissue engineering*. Biomaterials 1993; 14: 323-330.
95. L.E. Freed, G. Vunjak-Novakovic, R.J. Biron, D.B. Eagles, D.C. Lesnoy, S.K. Barlow, R. Langer. *Biodegradable polymer scaffolds for tissue engineering*. Biotechnology 1994; 12: 689-693.
96. W.C. Oliver, G.M. Pharr. *An improved technique for determining hardness and elastic modulus using load and displacement sensing indentation experiments*. Journal of Material Research 1992; 7: 1564-1583.
97. W.C. Oliver, G.M. Pharr. *Measurement of hardness and elastic modulus by instrumented indentation: Advances in understanding and refinements to methodology.* Journal of Material Research 2004; 19: 3-20.
98. B.J. Briscoe, L. Fiori, E. Pelillo. *Nano-indentation of polymeric surfaces.* Journal of Physics D, Applied Physics 1998; 31: 2395-2405.
99. Y. Hu, L. Shen, H. Yang, M. Wang, T. Liu, T. Liang, J. Zhang. *Nanoindentation Studies on Nylon 11/Clay Nanocomposites.* Polymer Testing 2006; 25: 492-497.
100. C. Klapperich, K. Komvopoulos, L. Pruitt. *Nanomechanical Properties of Polymers Determined From Nanoindentation Experiments.* Journal of Tribology – Trans. ASME 2001; 123: 624-631.

101. E. Kaiser, R. L. Colescott, C. D. Bossinger, P. I. Cook. *Color test for detection of free terminal amino groups in the solid-phase synthesis of peptides.* Analytical Biochemistry 1970; 34: 595-598.

102. V.K. Sarin, S.B. Kent, J.P. Tam, R.B. Merrifield. *Quantitative monitoring of solid-phase peptide synthesis by the ninhydrin reaction.* Analytical Biochemistry 1981; 117: 147-157.

103. E.P. Tyllianakis, S.E. Kakabakos, G.P. Evangelatos, D.S. Ithakissios. *Direct colorimetric determination of solid-supported functional groups and ligands using bicinchoninic acid.* Analytical Biochemistry 1994; 219: 335-340.

104. H. Zhang, C. Y. Lin, S. J. Hollister. *The interaction between bone marrow stromal cells and RGD-modified three-dimensional porous polycaprolactone scaffolds.* Biomaterials 2009; 30: 4063-4069.

105. J.H. Kinney, S.J. Marshall, G.W. Marshall. *The mechanical properties of human dentin: a critical review and re-evaluation of the dental literature*. Critical Reviews in Oral Biology and Medicine 2003; 14: 13-29.

106. N.E. Waters. *Some mechanical and physical properties of teeth.* Symposia of the Society for Experimental Biology 1980; 34: 99-135.

107. P.E. Riches, N.M. Everitt, D.S. McNally. *Knoop microhardness anisotropy of the ovine radius.* Journal of Biomechanics 2000; 33: 1551-1557.

108. J. K. Weaver. *The microscopic hardness of bone*. Journal of Bone Joint Surgery 1966; A48: 273-288.

# Chapter III: Contents

# CHAPTER III
# 3D PCL/Mg,$CO_3$-substituted hydroxyapatite nanocomposite scaffolds

## III.I Preface

Recently, much attention has been driven toward the synthesis of new substituting biomaterials mimicking natural bone, as an alternative to autograft and allograft. In particular, several studies have focused on the development of new biomimetic non-stoichiometric apatites as a result of a better understanding of the functional role of the active groups contained in natural bone tissue. These new substituting biomaterials must necessarily have a higher rate of biodegradability and bioactivity compared to stoichiometric hydroxyapatite. [1]

A controlled bioreabsorbability together with the comprehension of the mechanisms that, in physiological conditions regulates the solubility, represent a key element in the development of these new biomaterials. The cristallinity grade of powders and the addition of doping groups replacing those presents in the apatite network, although it will result in improved similarity to that of natural bone tissue, influence the solubility of these new biomaterials in physiological conditions.[1]

Even though for a long time the inorganic phase of bones and teeth has been represented and idealized as stoichiometric hydroxyapatite [HA: $Ca_{10}(PO_4)_6(OH)_2$],[1-13] biological apatites are poorly crystalline and contain anionic and cationic substitutions in the sites of hydroxyapatite crystal structure, thus resulting far from the typical stoichiometric HA.[14]

For this reason, during the past years, research has been focused on the synthesis of non-stoichiometric hydroxyapatite that is hydroxyapatite containing specific substituting ions, at both the cationic and anionic reticular sites. Among the substituents of the calcium ion ($Ca^{2+}$), $Mg^{2+}$ is of great interest, as it plays a crucial role in the new bone tissue formation. In particular, it has been shown that the amount of magnesium present in the bone tissue is variable during the calcification process and decreases as the mineralization progress continues. Qualitative alterations of bone

matrix are linked to the role of Mg: it has been demonstrated that a deficiency in Mg leads to the cessation of bone growth, reduction of osteoblast and osteoclast activities, osteopenia and, hence, bone fragility.[2-11]

Several studies on the chemical synthesis and characterization of partially Mg-substituted apatite have shown that the presence of Mg ion seems to accelerate the nucleation kinetics of hydroxyapatite, to inhibit its crystallization, producing a synthetic apatite characterized by a lower level of crystallinity, making it morphologically more similar to natural apatite (i.e., Figure III.I shows the crystalline structure of the stoichiometric hydroxyapatite).[7-9,11,14,16]

Although the synthetic "Mg-doped" hydroxyapatite results more soluble and absorbable than "non-doped" hydroxyapatite, there is a limit to the introduction of Mg ion into the apatite network without altering the reticular structure. As an example, the formation of tricalcium magnesium phosphate rather than hydroxyapatite was favored if the molar ratio Mg/Ca in solution was above 0.3.[2-13]

On the other hand, the substitution of the Ca ion with the Mg one can be increased by simultaneously incorporating carbonate ions into the apatite structure, as the carbonate ion is also found in the structure of natural apatite. The carbonate ion ($CO_3^{2-}$) can partially substitute the $OH^-$ ion (site A) and/or the $PO_4^{3-}$ ion (site B). Both the total carbonate content (in the range of 3-8 weight percent) and the relative quantities of type A and type B carbonation (A/B in the range of 0.7-0.9) found in biological carbonate depend on the age of the individual.[7-9,11,14,16]

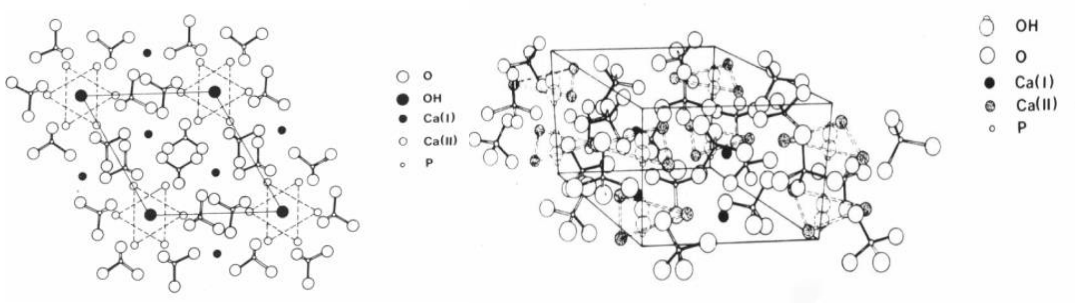


**Figure III.I: Projection of the constituting ions of the hydroxyapatite on the basal plane (left) and Hexagonal structure of hydroxyapatite (right).**

Synthetic carbonation should preferably take place at site B, giving a reduction of the crystallinity and an increase of the solubility of the apatite phase. Moreover, type A carbonation is characterized by a lesser affinity of the apatite for the osteoblast cells,

thus resulting in a lesser cellular adhesion and a decreased production of collagen compared to non-substituted HA.

Accordingly, the synthesis of Mg carbonate hydroxyapatite (MCHA) results important to develop synthetic materials that mimic the inorganic phase of bone tissue both with respect to its composition and to its morphology.

To date, synthetic hydroxyapatites present problems (slow bioabsorption and insufficient activation of the osteoblasts) related to the fact that they are stoichiometrically pure, while natural apatites contain such doping ions as carbonate and magnesium. It seems that carbonate-doped hydroxyapatites are absorbed better by the osteoclasts, probably for an improved solubility caused by the substitution of phosphate with carbonate. On the other hand, a faster osteointegration for apatites doped with magnesium is probably due to the stimulating effect of magnesium both on the growth of the osteoblasts and on the secretion of matrix proteins.

Moreover, it is important that the magnesium is not simply superficially absorbed but also inserted into the crystalline matrix, in order to avoid its massive and swift release.

As reported in literature, several works on the synthesis of Mg- and Mg,$CO_3$-substituted hydroxyapatite[6,8-9,12,17-23] are simply based on the immersion of HA or carbonated HA in magnesium nitrate solution.[6,8,12,18-20]

The Mg,$CO_3$ biological-like substituted hydroxyapatite considered in the present work has been synthesized by the Institute of Science and Technology for Ceramics (ISTEC), National Research Council (CNR) – Faenza (Italy), using magnesium chloride ($MgCl_2$, which is otherwise a constituent of the synthetic body fluid) as reagent, starting from the classical neutralization route involving calcium oxide and ortophosphoric acid.

This synthesis allows to avoid additions of ammonia during the process to control and maintain high the value of the pH, contrarily to the synthesis based on calcium nitrate and ammonium hydrogen phosphate, making the whole synthesis easier and more suitable for industrialization. $MgCl_2$ was already used in the synthesis of Mg-doped calcium deficient apatite starting from a mixture of calcium hydrogen phosphate and tetra-calcium phosphate powders[5]: thus, the interaction among the reactants is not comparable to that involved in the synthesis process below described and it is well known that the physico-chemical properties of the synthetic HA are strongly influenced also by the precursors used.

# III.II Materials and Methods

## *III.II.I Biomimetic Mg and Mg,$CO_3$-substituted hydroxyapatites*

The biomimetic Mg,$CO_3$-substituted hydroxyapatite used in this work was suitably synthesized by ISTEC-CNR, Faenza, Italy. Sodium hydrogen carbonate ($NaHCO_3$) was used as carbonate source, in order to favor the carbonation in the B-site (phosphate position).

Many works have highlighted that the introduction of carbonate ions in the reaction mixture by bubbling carbon dioxide gas improves the contribute of A-site (hydroxyl) carbonation of synthetic Mg-substituted hydroxyapatite[6-7,16] giving out carbonated apatites characterized by a high A/B carbonation ratio. Mg ions are bivalent as Ca ions, thus the carbonate ion is not "forced" to substitute in the phosphate site in order to preserve the charge balance, as on the contrary occurs for the Na,$CO_3$ co-substituted hydroxyapatite, in which the substitution of bivalent $Ca^{2+}$ with monovalent $Na^{+}$ stimulates the substitution of trivalent anion $PO_4^{3-}$ with the bivalent anion $CO_3^{2-}$.

The use of sodium hydrogen carbonate as carbonate source for the synthesis of Mg,B–$CO^3$ co-substituted hydroxyapatite appears interesting also considering that Na ions are present in the bone mineral, thus the synthetic product can not be chemically disadvantaged, if Na ion partially enters in the apatite structure.

In this work, the inclusion of synthetic hydroxyapatite simultaneously doped with magnesium and carbonate ions (MCHA) was assessed from a mechanical and biological point of view.[2]

The synthesis method used allows to obtain hydroxyapatites with a carbonate substitution ranging from 6 to 8 weight percent (w %), and a distribution between the two sites of about 40-45 w % for site A and consequently 55-60 w % for site B. With the same process it is possible to uniformly dope the carbonate hydroxyapatite with magnesium, resulting in a Mg concentration of about 6-8 % if expressed as a molar ratio with respect to calcium, or, if expressed as weight percentage, a Mg quantity ranging from 1.0 to 2.7 w %. The introduction of Mg causes a partial collapse of the crystalline structure of the hydroxyapatite, but x-ray analysis has shown the persistence of the characteristic bands of this type of structure: the resulting product

still remains hydroxyapatite, even though at the nanostructure level it presents a low level of crystallinity (estimated around 40-60%).[2]

The molar ratio of (Ca−Mg)/P in the resulting compound exceeds 1.7 and is thus above the value of 1.67 of non-substituted hydroxyapatites; in fact, the carbonate substitution has taken place mainly at site B. At any rate, the resulting material is homogenous and for purely descriptive purposes can be represented as an intermediate compound between the following two limit-defining formulas, assuming a constant Mg/Ca ratio:

$$Ca_{6.4}Mg_{0.5}(HPO_4)_{3.8}(CO_3)_{2.1}(OH)_2 \quad (1)$$

$$Ca_{6.4}Mg_{0.55}(PO_4)_{0.5}(HPO_4)_{3.5}(CO_3)_{1.7}(CO_3) \quad (2)$$

where formula 1 would show a compound in which all substitutable sites B have been substituted with carbonate and formula 2 a compound in which all substitutable sites A have been substituted with carbonate. Analogous representations can be made for other compounds with different Mg/Ca ratio.[2]

Basically, the MCHA employed in the present work may be obtained through a synthesis process, the classical neutralization method, described below.[2]

A phosphoric acid solution and a sodium bicarbonate solution are added simultaneously over a period of 3-5 hours to a calcium hydroxide suspension and a magnesium salt (preferably hexahydrated magnesium chloride), while the temperature is maintained around 35-45°C. Once the addition is complete, the mixture is stirred for 1-6 hours and is then left to rest at room temperature for 20-28 hours. The hydroxyapatite is filtered by centrifugation or filtration, washed with water and dried.[2]

## *III.II.II 3D Scaffold Design and Preparation*

3D rapid prototyped composite scaffolds were produced by embedding biomimetic hydroxyapatite into a poly(ε-caprolactone) (PCL) matrix.

Poly(ε-caprolactone) (PCL, $M_w$=65000 g $mol^{-1}$ - Aldrich) pellets were dissolved in tetrahydrofuran (THF) through stirring at room temperature.

MCHA nanoparticles and, subsequently, ethanol were added to the PCL/THF solution during stirring. A PCL/MCHA weight ratio (w/w) 80/20 was used. An ultrasonic bath

(Branson 1510 MT) was also employed to optimize the nanoparticles dispersion in the polymer solution.

3D cylindrical scaffolds characterized by a diameter (D) of 10 mm and a height ($h_0$) of 10.2 mm, were fabricated through 3D Fiber Deposition technique, using a Bioplotter dispensing machine (Envisiontec GmbH, Germany) equipped with a CAD/CAM system (Figure III.II). 3D scaffolds were obtained by alternatively extruding and depositing the polymer fibers with a 0°/90° pattern. The nozzle used to extrude PCL and PCL/MCHA fibers was a stainless steel needle characterized by an inner diameter of 400 μm. Each scaffold was characterized not only by the fiber diameter (depending on the needle diameter and/or the deposition speed), but also by the fiber spacing (strand distance, i.e. center-to-center distance) and layer thickness, which influence the overall pore size. The values of strand distance were set to 640 μm, while for the layer thickness was chosen about 320 μm. A deposition speed of 50-55 mm/min was used.

Single polymeric (PCL) and nanocomposite (PCL/MCHA) fibers and bi-layered scaffolds characterized by a 0°/90° pattern were also manufactured for nanoindentation tests and cell adhesion study, respectively.

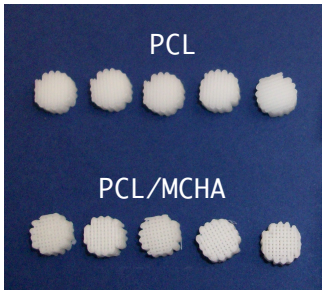


**Figure III.II: Polymeric (PCL) and nanocomposite (PCL/MCHA) cylindrical scaffolds obtained through 3D Fiber Deposition technique.**

## *III.II.III Micro-Computed Tomography*

A micro-computed tomography (Micro-CT) was performed through a SkyScan 1072 (Aartselaar, Belgium) system using a rotational step of 0.9° over an angle of 180°, in order to analyze the internal structure, pore shape and size of the 3D polymeric (PCL) and nanocomposite (PCL/MCHA) scaffolds fabricated via rapid prototyping technique. Cross-sections and 3D model of PCL scaffolds were reconstructed using

Skyscan's software package and Image J software, for image analysis and visualization of the results from Micro-CT system scan. The pore network was visualized and the pore interconnectivity was studied.

## *III.II.IV Nanoindentation tests*

Nanoindentation tests were carried out on polymeric (PCL) and nanocomposite (PCL/MCHA) fibers, obtained through a Bioplotter Dispensing Machine and characterized by a diameter of 340-360 μm.

All the tests were performed in a 1-5 mN load range, using a Nanotest Platform (Micromaterials, U.K.) with a diamond pyramid-shaped Berkovich-type indenter tip. Trapezoidal load functions characterized by a loading-unloading rate of 300 μN/s and a peak-load hold period of 20 s were imposed. Load-depth curves, values of hardness and reduced modulus were evaluated. In particular, hardness and reduced modulus were evaluated using the methods introduced by Oliver and Pharr (1992), as previously described in Chapter II.

## *III.II.V Compression tests*

Compression tests were performed on the 3D polymeric (PCL) and nanocomposite (PCL/MCHA) cylindrical scaffolds, characterized by a diameter (D) of 10 mm and a height ($h_0$) of 10.2 mm. All the tests were carried out at a rate of 1 mm/min up to a strain value of 0.5 mm/mm, using an INSTRON 5566 testing machine. The stress was evaluated as the force $F$ measured by the load cell divided by the total area of the apparent cross-section of the scaffold ($A_0 = \pi D^2/4$):

$$\sigma = \frac{F}{A_0}$$

while the strain $\varepsilon$ was defined as the ratio between the scaffold height variation $\Delta h$ and its initial height $h_0$:

$$\varepsilon = \frac{\Delta h}{h_0}$$

## *III.II.VI Microscopy and Cell Adhesion Study*

Numerous autologous sourcing sites together with the comprehension of the mechanisms that regulate, *in vitro*, expansion and differentiation making it possible to consider Mesenchymal stem cells (hMSCs) as an integral part of tissue engineering.[33-41] Much attention has been focused on the questions related to the true potential of MSCs in terms of plasticity and what marker can be used to identify true MSCs from a cell characterized by a limited plasticity, due to various level of differentiation.[42-51] Therefore, it is necessary to improve the knowledge on how it is possible to control and influence MSCs behavior starting from the awareness of cell-material interaction, such as cell adhesion and spreading, in order to understand what biological stimuli are required in order to obtain different functional cell types, (osteoblasts, chondrocytes, adipocytes and hepatocytes) from an MSC-like population i.e. simply by using supplemented mediums (Figure III.III).[52-55]

To date, it is possible to guide MSC *in vitro* differentiation by means of growth factors and cytokines, but the guidance of cell differentiation driven by specific substrate/scaffold (i.e. cell recognition could be improved by using different material or different composition) represents a more attractive challenge in tissue engineering.

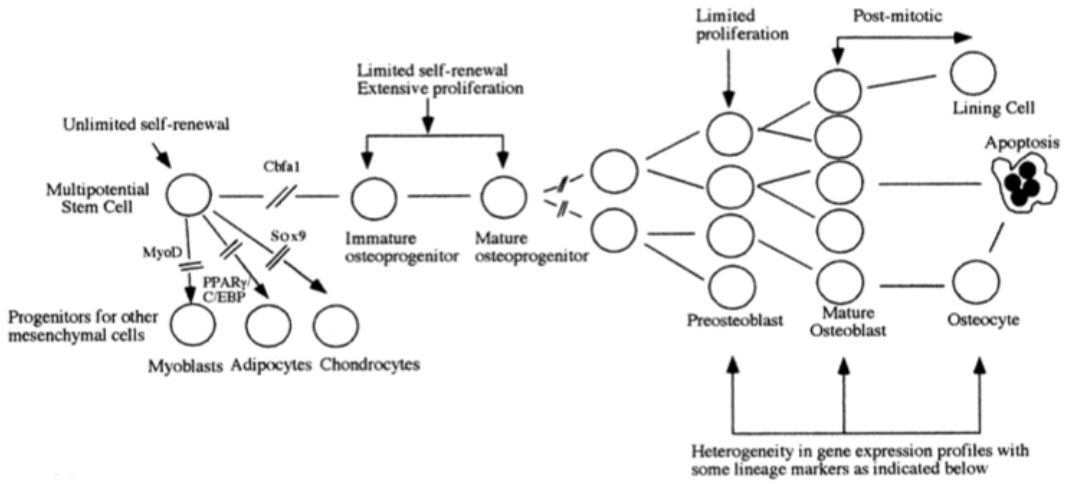


**Figure III.III: Assumed steps in the osteoblast lineage: different stages of proliferation and differentiation are involved.[54,55]**

In this work, human Mesenchimal Stem Cells (hMSCs) were maintained at 37°C and 5% $CO_2$ in Dulbecco's modified Eagle medium (DMEM) supplemented with 10% fetal bovine serum (FBS, BioWhittaker, Walkersville, MD), 2 mM L-glutamine

(Sigma, St. Louis, MO), 1000 U/l penicillin (Sigma, St. Louis, MO) and 100 mg/l streptomycin (Sigma, St. Louis, MO). In particular, PCL, and PCL/MCHA 3D fiber-deposited scaffolds were sterilized with antibiotics and pre-incubated in serum-free medium for 16-18 h. After the incubation, 5 x $10^4$ cells were seeded on all the different kinds of 3D scaffolds and grown in DMEM-w/o FBS to avoid unspecific cell adhesion depending on serum protein adsorption.

Firstly, Scanning Electron Microscopy (SEM) was performed by a Leica 420 microscope in order to evaluate morphological structure and hence the architecture of the scaffolds. 3D fiber-deposited scaffolds were rinsed with PBS and fixed with 2.5% glutaraldehyde (pH=7.4) (Sigma-Aldrich, Italy) for 2h at room temperature, dehydrated in graded ethanol concentrations (from 50% to 100% v/v in ethanol), air-dried, gold sputtered and analyzed by SEM. Different polymeric (PCL) and nanocomposite (PCL/MCHA) scaffolds were studied.

Cell-scaffold constructs, made from 3D fiber-deposited scaffolds seeded with hMSCs, were analyzed through stereomicroscope (*OLYMPUS SZX7*), in order to study cell adhesion on the polymeric and nanocomposite substrate, by staining with *crystal violet* and *toluidine blue*.

In the first case, *crystal violet* staining was performed by using glutaraldehyde for 30 min, at room temperature. The cell-scaffold constructs were successively rinsed three times with PBS buffer and the cells were stained with crystal violet 0.1% (w/v, Sigma Aldrich) for 60 min at room temperature. The dye's solution was then aspirated and the cell-scaffold constructs were washed twice in PBS. The cells adhered to the substrate material was colored in purple.

At 24 h after seeding, cell adhesion and distribution within the PCL based scaffolds was also verified by Toluidine blue staining. Briefly, samples were washed in phosphate buffered solution (PBS), fixed in formalin 4% for 10 min, rinsed in PBS and stained with Toluidine Blue for 5-10 minutes. Samples were then washed in distilled water to remove extra stain, and immediately analyzed by stereomicroscopy at different magnifications. Furthermore, cell-scaffold constructs were also analyzed through Confocal Laser Scanning Microscopy (CLSM). They were fixed with 4% paraformaldeyde for 20 min at room temperature, rinsed twice with PBS buffer and incubated with PBS-BSA 0.5% to block unspecific binding. Actin microfilaments were stained with phalloidin tetramethylrhodamine B isothiocyanate (Sigma-Aldrich). Phalloidin was diluted in PBS-BSA 0.5% and incubated for 30 min at room

temperature. The images were acquired at different times from cell seeding by using a He-Ne excitation laser at the wavelength of 543 nm and a 20x objective.

At 21 days after cell seeding, in order to evaluate if MCHA nanoparticles may act as a bioactive solid signal able to induce osteogenic differentiation of the hMSCs, cell-scaffold constructs were also analyzed through stereomicroscope by *alizarin red* staining, comparing the data obtained with those related to a "2D" control element, characterized by cells in osteogenic medium (OM), (made from 10% FBS; 0.1 μM di dexamethasone; 50 μM ascorbate-2-phosphate; 10 mM β-glycerophosphate; 1% penicillin/streptomycin; 1% L-glutamine). The alizarin red is generally used in biochemical analysis to determine the presence of calcium deposits by osteogenic cell line. As for the experimental methodology, cells were fixed in glutaraldehyde 0.25% for 15 minutes at room temperature; the cell-scaffold constructs were washed several times with PBS and then the cells were stained with Alizarin Red S 2% (Sigma Alrich) for 10 minutes; successively, the cell-scaffold constructs were washed several times with de-ionized water to remove excess of dye and analyzed through a stereomicroscope.

In order to better understand the effect of the inclusion of MCHA in terms of osteogenic differentiation, the potential differentiation of hMSCs was evaluated by the osteoblast-phenotype marker (alkaline phosphatase, *ALP*) measured at 7, 14 and 21 days after cell seeding.

Alkaline Phosphatase represents an osteogenic differentiation marker, as it is normally used to evaluate the scaffold ability to induce osteogenic differentiation. For this reason, ALP/DNA tests were performed in order to evaluate the effect of the inclusion of MCHA nanoparticles on osteogenic differentiation of hMSCs.

Briefly, the samples were analyzed using pNPP Alkaline Phosphatase Assay SensoLyteTM enzymatic kit (Anaspec), that is a colorimetric kit based on the activity of the dephosphorylating enzyme:

$$\text{p-Nitrophenol phosphate} + H_2O \rightarrow \text{pi} + \text{p-nitrophenol}$$

Generally, alkaline phosphatase is associated with a secondary antibody, using paranitrophenol-phosphate (pNPP) as substrate; pNPP, after being dephosphorylated by the alkaline phosphatase, is yellow-colored, making it possible to detect its presence at a wavelength of 405 nm. Thus, by measuring the amount of p-nitrophenol at 405 nm, the alkaline phosphatase activity can be analyzed.

In this work, different kinds of cell-scaffold constructs were freeze thawed three times in 30 min cycles of -70°C and 37°C. p-Nitrophenol phosphate in a diethanol-amino buffer (Merck, UK) was used as a substrate for ALP. The release of the reaction product p-nitrophenol (yellow color) was quantified using a spectrophotometer (Lambda 25, Perkin-Elmer) at a wavelength of 405 nm.

The results were then normalized for total DNA content, using the PicoGreen dsDNA Kit Quant-ITTM Reagent.

## *III.II.VII Gene expression: Real Time quantitative PCR*

The termination of the proliferation process and, subsequently, the formation of a collagenous extracellular matrix (ECM) underlie the differentiation from osteoprogenitors into mature, secretory osteoblasts. In primary osteoblast cultures and non-transformed osteoblast cell lines, the expression of specifical differentiation markers follows a clear temporal sequence (Figure III.IV). Genes associated with cell proliferation, such as H4 histone, C-FOS, and C-MYC, are expressed at early times along with those encoding the proαl(l) and proα2(1) propeptides of type I collagen. Initial collagen matrix accumulation precedes and is essential for sequential expression of the differentiation-related proteins, alkaline phosphatase, the PTH/PTHrP receptor, bone sialoprotein, and osteocalcin.[56-63]

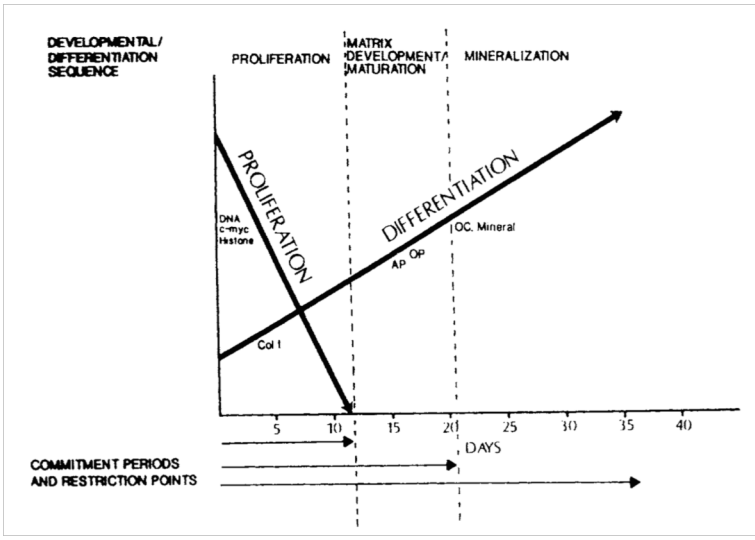


**Figure III.IV: Cell growth versus differentiation-related gene expression for the various early intermediates during the *in vitro* cultivation of calvarial osteoblasts. Arrows indicate proliferation and differentiation trends. H4 histone gene expression is most closely correlated with cell division. Other genes expressed at this time are c-fos and c-jun. Abbreviations: Col1, type I collagen; AP, alkaline phosphatase; Op, osteopontin; and OC, osteocalcin. Although Col I mRNA levels are highest during the proliferation phase, matrix deposition continues to increase throughout the entire culture period.[58]**

Similar pattern of gene expression is also seen *in vivo* and in organ culture; osteoprogenitors adjacent to bone are highly proliferative and express low levels of bone-specific proteins, while secretory osteoblasts on the bone surface stop dividing and produce large amounts of bone-specific ECM.[64,65] Thus, a complete model for transcriptional regulation in osteoblasts must explain the conversion of mesenchymal stem cells to osteoprogenitors as well as the influences of cell proliferation and ECM synthesis on gene expression.

Specific changes in gene expression are attributable at the progression from uncommitted stem cell to osteoprogenitor and finally mature osteoblast and osteocyte. A common believe in development is that specific transcription factors or groups of factors are able to control the process of lineage commitment by selectively activating those genes to be expressed in the differentiated state. Several classes of tissue-specific transcription factors have been described, including the basic helix/loop/helix (bHLH) family involved in myogenic, myeloid, erythroid, and neuronal differentiation,[66] bHLH leucine zipper factors involved in adipocyte and liver differentiation,[67,68] orphan members of the steroid receptor superfamily such as HNF-4 involved in liver differentiation[68] and POU-domain factors involved in pituitary differentiation.[69] Several experimental approaches have been successfully used to identify transcription factors controlling tissue-specific gene expression. It is possible to identify two main approaches: (1) identification of factors able to confer a differentiated phenotype on an undifferentiated cell or tissue, and (2) identification of promoter elements able to confer tissue-specific expression on genes associated with a given phenotype, with subsequent identification and functional testing of nuclear proteins associating with these elements. The classic example of the first type of approach is the discovery of myogenic differentiation protein (MyoD), a muscle-specific bHLH transcription factor. MyoD was isolated from a cDNA library enriched for transcripts present in a myogenic clone of C3HlOTI/2 cells that were not present in wild-type undifferentiated cells. Transfection of MyoD into wild-type C3H1OT1/2 cells induced myotube formation and muscle-specific gene expression.[70] MyoD was subsequently shown to bind to and activate skeletal muscle-related genes through a specific DNA element called an E-box and having the general sequence Cytosine-Adenine-n-n-Thymine-Guanine (CAnnTG). Four other myogenic bHLH factors (myogenin, myf-5, MRF-4, and myf-6) were subsequently cloned and shown to be involved in various steps in myoblast/myotube formation.[71] Although there is

considerable redundancy between members of the MyoD family, gene knockout studies with one family member, myogenin, indicate that this factor is essential for the formation of skeletal muscle.[66] Similarly, neuroD, a second type of bHLH protein, can convert presumptive epidermal cells into neural cells when its mRNA is injected into Xenopus embryos.[72] An example of the second approach is the isolation of the hepatocyte-specific factor, HNF-1. This transcription factor was identified in hepatocyte nuclear extracts by its ability to bind to an oligonucleotide containing a sequence in the ornithine transcarbamylase gene promoter, essential for liver-specific expression.[68]

Although several studies on osteoblast gene regulation have used both of the experimental approaches above described, authors have achieved the greatest success in this area by focusing their research on specific gene promoters and associated nuclear factors. The osteocalcin gene and genes encoding the proαI(I) and proα2(I) chains of type I collagen have intensively been studied. Recently, several laboratories have also initiated studies on the bone sialoprotein gene. The type I collagen genes, subject of many and complex controls in a number of tissues in addition to bone, have been recently reviewed.[73,74]

Runx2 is a bone-related transcriptional factor, homologous to the Drosophila protein, Runt.[75-77] This protein is essential for the differentiation of osteoblasts from mesenchymal precursors and bone formation. It has been demonstrates that Runx2 can directly stimulate transcription of osteoblast-related genes such as those encoding osteocalcin (OC), type I collagen, osteopontin (OP) and collagenase 3 by binding to specific enhancer regions containing the core sequence PuCCPuCA (where Pu is for purine),[75-80] although the molecular mechanism of Runx2 action is already unknown. Runx2 is expressed exclusively in mineralized tissues and their precursors, but, in many cases, there is a poor correlation between actual Runx2 mRNA or protein levels and the expression of osteoblast-related genes. Thus, Runx2 expression precedes osteoblast differentiation and OC expression by several days.[75-77] Also, in several osteoblast cell culture systems, Runx2 protein levels are not very well correlated with expression of its targeted genes.

Thus, as osteoblasts must establish a type I collagen-containing ECM before they can differentiate and express osteoblast-related genes such as those encoding OC, bone sialoprotein, alkaline phosphatase and the parathyroid hormone/parathyroid hormone-

related protein receptor and, ultimately, mineralize[55], the ECM signals are needed to the differentiating preosteoblast by binding to b1 subunit-containing integrins (a2b1 and, possibly, a1b1). [78,82-84] Disruption of integrin signaling using either blocking antibodies or peptides that mimic the cell-binding domain of collagen completely blocks ECM-dependent differentiation. This observation is highly significant for the comprehension of osteoblast metabolism since, through integrins, cells can sense their ECM environment and respond to changes in mechanical loading.[78,85]

Moreover, it is well established that mechanical loading plays an important role in the regulation of bone homeostasis and skeletal morphology during development and in postnatal life where it increases bone density and strength. In contrast, skeletal unloading in humans and rats, as seen during space flight, is associated with bone loss and compromised bone mechanical properties. Mechanical stimulation has also been examined in a variety of cells *in vitro* including epithelial cells, fibroblast, chondrocytes, and osteoblasts.[78,86] Mechanically strained osteoblasts express increased levels of osteopontin (OP), osteocalcin (OC), and collagen I/ III mRNA.[78,87-88]

Although the importance of mechanical loading in the development and maintenance of bone integrity is undisputed, the mechanisms underlying mechano-transduction through which osteoblasts sense and convert mechanical stimuli into cellular responses are largely unknown. In particular, the MAP kinase pathway is one of the principle signal transduction cascades to be associated with mechano-transduction. Integrins, which connect the cytoskeleton to the extracellular matrix and mediate a variety of signaling cascades, may transduce mechanical stimuli into biochemical signals. Two recent studies established an important link between Runx2 and mechano-transduction. Ziros and coworkers[89] have highlighted that Runx2 may act as a target for mechanical signals in human periodontal ligament (hPDL) cells (i.e., osteoblast-like cells which can differentiate toward osteoblasts in response to a variety of extracellular stimuli.).[78,89] Specifically, low level continuous mechanical stretching of hPDL cells dramatically increased binding of Runx2 to OSE2 DNA in gel retardation mobility shift assays, although a slight increase in Runx2 mRNA or protein was also observed. This stimulation was detected after as little as 30 min of stretching, peaked after 6 h, and lasted for at least 12 h. Extracellular Regulated Kinase 1 and 2 (ERK1/2) phosphorylation was activated in a time-dependent manner in mechanically stretched hPDL cells and was well correlated with the increase in

Runx2 binding activity. Furthermore, the stretch-induced increase in Runx2 DNA binding activity was completely abolished by U0126, a specific inhibitor of ERK1/2 activation. Of particular interest, stretch-activated ERK physically interacted with Runx2 and could phosphorylate this transcription factor *in vitro*. In separate studies, Wang et al. provided evidence that both ERK activation and Runx2 phosphorylation are required for mechanical signaling in human and rat bone marrow stromal cells.[78,90] They showed that extra-corporeal shock wave (ESW), an alternative non-invasive method for the promotion of bone growth and tendon repair, promoted stromal cell proliferation and differentiation to osteoblasts. Specifically, optimal ESW treatment of bone marrow stromal cells at 0.16 $mJ/nm^2$ for 500 impulses increased [3H]-thymidine incorporation into DNA, alkaline phosphatase activity, OC gene expression, and bone nodule formation. Of particular interest, ESW dramatically stimulated ERK-dependent Runx2 phosphorylation although it did not change the Runx2 protein levels. Thus, mechanical force may regulate osteoblast proliferation and differentiation as well as bone formation through MAPK-dependent Runx2 phosphorylation.

In this work, cells from a human cell line (MG63) were cultured in Coon's F12 modified medium supplemented with 10% fetal calf serum (FCS), 2 mM glutamine, 100 IU/ml penicillin and 100mg/ml streptomycin. The culture medium was changed every 3 days. When the cells became confluent, they were detached with 0.05% trypsin-0.01% EDTA and re-plated until the next confluence. All cultures were performed within 37°C-5% $CO_2$ humidified incubators.

Cells from a human cell line (MG63) were selected in order to avoid a dedifferentiation or a transdifferentiation. Transdifferentiation is a process whereby a cell type committed to and progressing along a specific developmental lineage switches into another cell type of a different lineage through genetic "reprogramming". Indeed, it has already been demonstrated that MSCs exposed to osteogenesis-inducing factors can maintain their potential of differentiation into adipocytes and chondrocytes. Osteogenic differentiation of MSCs is characterized by three distinct phases: cell proliferation, cessation of proliferation and secretion of extracellular matrix and finally mineralization of extracellular matrix, resulting in mature osteoblasts. It has been widely accepted that as osteogenic differentiation progresses, the multiple differentiation potentials of mesenchymal cells gradually become more restricted, such that terminally committed osteoblasts are unable to

differentiate into other cell types. However, Lin Song and Rocky S. Tuan[91] showed that MSCs cultured under osteogenic conditions for 10, 20, or 30 days maintained their ability to differentiate into adipocytes and chondrocytes. Even the fully differentiated osteoblasts (after 30 day induction), identified by expression of alkaline phosphatase, bone sialoprotein, and osteocalcin, histochemically detectable alkaline phosphatase activity and the elaboration of calcified extracellular matrix, were able to change their differentiation program and became lipid-producing adipocytes and chondrocytes that produced sulfated proteoglycan, collagen type II, and link protein.
An interesting phenomenon during the transdifferentiation process was the extensive cell proliferation that preceded the phenotypic switch. When MSCs were cultured in osteogenic medium for 30 days, adherent cells formed large osteoblastic nodules (Figure III.V A, a). When the osteogenesis-inducing medium was replaced with control medium, spindle-shaped fibroblast-like cells started to migrate out of the calcified matrix nodule (Figure III.V A, b) and were morphologically similar to the original MSCs.

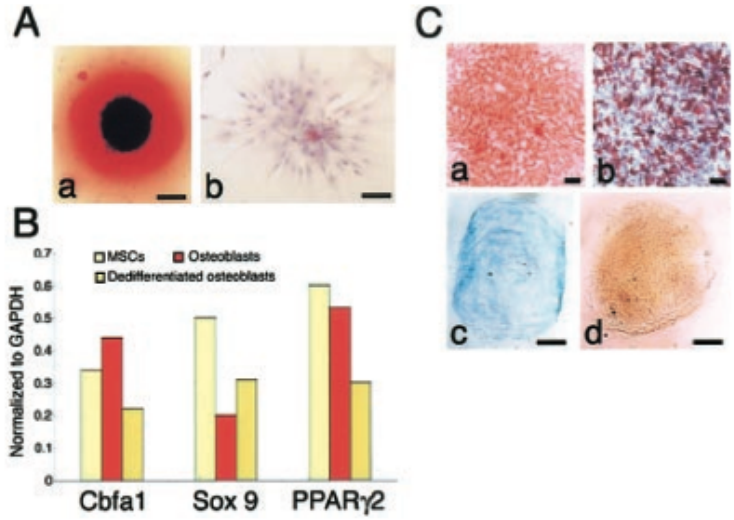


**Figure III.V: Osteoblasts derived from osteogenic differentiation of hMSCs were capable of dedifferentiation and retention of multidifferentiation potential. A) A fully differentiated osteoblastic nodule in osteogenic culture of hMSCs (30 days) stained with alizarin red (a). Fibroblastic cells derived from the osteoblastic nodule migrated out and proliferated (b). B) Expression levels of lineage-specific transcription factors (Cbfa1, Sox9, and PPARγ2) during osteogenesis and osteoblast dedifferentiation. C) Cells derived from the osteoblastic nodule differentiated into 3 mesenchymal lineages: osteoblasts (a, alizarin red stain), adipocytes (b, Oil red O stain), and chondrocytes (c, Alcian blue stain; d, immunohistochemical staining of collagen type II). Scale bar, 50 μm. [91]**

Since cell division is required for demethylation, a critical step for genome reprogramming, perhaps without the pressure of inducing factors, fully differentiated

MSC-derived cells could resume cell proliferation, modify their gene expression profile, and return to a more primitive stem cell-like stage. The phenotypic changes were observed together with a fluctuation in the expression of lineage-specific transcription factors: core binding factor A1 (Cbfa1) for osteogenesis, Sry-related HMG box 9 (Sox9) for chondrogenesis, and Peroxisome proliferator-activated receptor γ 2 (PPARγ2) for adipogenesis (Figure III.V B). As expected, expression of Cbfa1 was up-regulated during osteogenesis, whereas both Sox9 and PPARγ2 were down-regulated compared with undifferentiated MSCs. On the other hand, expression levels of all three transcription factors decreased during osteoblast dedifferentiation, which suggested that cells might return to an uncommitted developmental stage from a fully determined cell type. The dedifferentiated cells derived from the osteoblasts not only exhibited similar morphology as MSCs, but also exhibited MSC-like multidifferentiation potentials. As shown in Figures III.V C and III.VI, these fibroblast-like cells formed mature osteoblasts (Figure III.V C a), adipocytes (Figure III.V C b), and chondrocytes (Figure III.V C c, d).

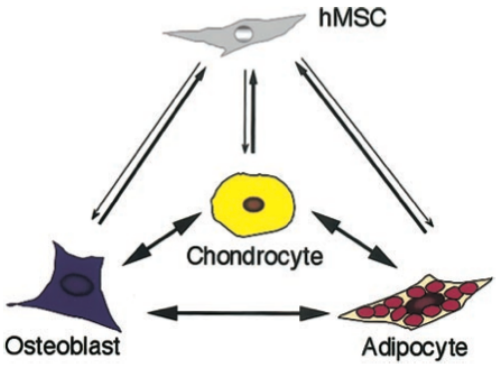


**Figure III.VI: A transdifferentiation model of MSCs. Osteoblasts, adipocytes, and chondrocytes differentiated from MSCs were able to transdifferentiate into other mesenchymal cell types. Fully differentiated cells were also capable of dedifferentiation into a primitive stem-like cell type and retention of multiple differentiation potential.[91]**

Therefore, in order to avoid problems related to a dedifferentiation or a transdifferentiation of hMSCs from osteoblast precursor to other mesenchymal cell types, MG63 cell line was selected. MG63 cell line derived from an osteosarcoma and they are better known as osteoblast-like cells; so, we assume MG63 as hMSCs differentiated in osteoblast precursor, the aim being to acquire data related to typical gene expression of collagenous ECM secretion: Runx2, Collagen type I (Coll I) and osteopontin (OP).

In this context, polymeric (PCL) and nanocomposite (PCL/MCHA) scaffolds were homogeneously loaded with $10^4$ cells/ml. After 1 hour, additional complete medium (6 ml) was added to cover the overall 3D scaffold. Cell-scaffold constructs were all maintained in static culture for 24 h, to allow a complete cell adhesion. Successively, while some cell-scaffold constructs were maintained in static conditions, other ones were moved within a bioreactor system previously developed,[92] and perfused in alternate directions at a flow rate of 1.2 ml/min through the pores of scaffolds (appendix I contains a part of the Wendt's work (2003)[93] related to the specific bioreactor used in this work. So, for detail, see following appendix I, Wendt 2003 and Scaglione 2006).[92,93]

MG63 cells were cultured on polymeric (PCL) and nanocomposite (PCL/MCHA) scaffolds for two weeks under osteogenic conditions, consisting of control medium supplemented with 10 nM Dexametasone, 0.25 mM L-ascorbic acid-2-phosphate and 10 mM b-glycerophosphate.[94] Cultures were then harvested at timed intervals and processed for biochemical and mRNA analysis. In particular, total messenger RNA was extracted by the cells cultured within 3D PCL based scaffolds, either under static or dynamic stimulation, by using the PerfectPure RNA Cultured Cell Kit (5-Prime GmbH, Hamburg, Germany) according to the manufacturer's instructions. mRNA was also extracted by cells before their biomechanical stimulation within the bioreactor system.

Briefly, scaffolds were incubated for 10-15 min with the lysis buffer, on ice, to allow a complete solution infiltration within the 3D structure. The SuperScript III Reverse Trascriptase (Invitrogen) was used to perform standard RT-PCR reactions. Primer sets for each gene of interest were derived from published sequences. The expression level of genes encoding the most typical osteoblast-related membrane and extracellular matrix molecules (i.e., Coll I, OP) was evaluated. The transcriptional factor of the osteogenic lineage (i.e. RUNX-2) was also evaluated. The Gly-Ala-Pro-Asp-His (GAPDH) rRNA was selected as a reference gene.

Samples of cDNAs were amplified with the RealMasterMix SYBR ROX 2,5X (5'-Prime) in an Eppendorf Mastercycler Realplex apparatus. Delta Ct method was used. For each gene, different RNA concentrations were used, and the related standard curves provided. Real time PCR runs were performed in quadruplicate for each sample and the specificity of the reaction products was counterchecked by the analysis of the melting curve.

In the present study, RT-PCR analysis was performed on cell-scaffold constructs under static or dynamic stimulation by dr. S. Scaglione from Institute of Electronics, Computer and Telecommunication Engineering (IEIIT) of the National Research Council (CNR) – Genoa (Italy), and prof. R. Quarto from Department of Sperimental Medicine (DIMES), University of Genoa (Italy).

# *Appendix I*

For the direct perfusion of a cell suspension through the pores of 3D scaffolds, Wendt et al., 2003, designed and fabricated a novel bioreactor. As shown in Figure A.I, scaffolds were placed in polysulfone/Teflon chambers (one scaffold per chamber) that were positioned at the bottoms of two glass columns and connected through a U-shaped glass tube at their base. Flow of the cell suspension was induced with the use of a vacuum pump and the flow rate regulated with a flow meter. The direction of flow was reversed when the fluid level in one column reached an optical sensor placed near the top of each glass column. The sensor detected the cell suspension, actuating a pair of solenoid valves, switching the vacuum to the opposite column, and therefore reversing the direction of fluid flow. Because scaffolds were press-fit into the chamber, the cell suspension could not deviate around the scaffold and was therefore forced to flow through its pores. The bioreactor was oriented vertically to avoid cells from settling onto the glass columns as would occur if in horizontal oriented.

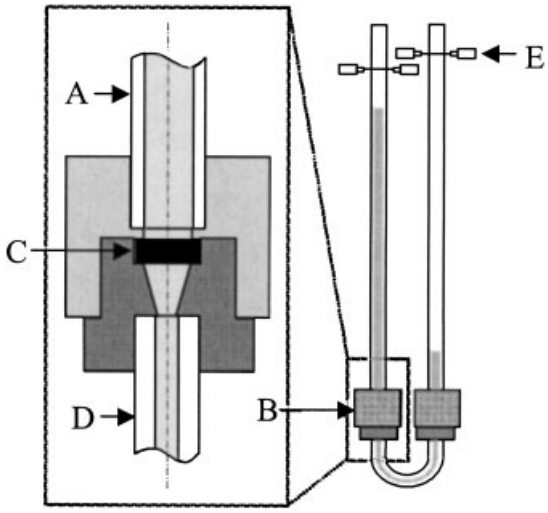


**Figure A.I: Perfusion seeding bioreactor. The cell suspension oscillates between the two glass columns (A), flowing through the sample chamber (B), scaffold (C), and U-tube (D). The direction of flow reverses when the cell suspension reaches the level of the sensors (E).**

Briefly, polymeric (PCL) or composite (PCL/MCHA) scaffolds were press-fit into the chambers ensuring fluid flow through the scaffold. $10^7$ cells in 4 ml medium were added to each pair of columns and perfused in alternate directions at a flow rate of 1.2 ml/min through the pores of each scaffold.

# III.III Results and discussion

## *III.III.I Micro-Computed Tomography*

Micro-computed tomography (Micro-CT) is an advanced and nondestructive method that allows to analyze the morphological features and architecture of the scaffolds. In this context, Micro-CT analyses were performed on cylindrical PCL and PCL/MCHA scaffolds, characterized by a diameter (D) of 10 mm and height (H) of 10.2 mm, using a SkyScan microtomography 1072 (Aartselaar, Belgium).

Micro-CT analyses allow to analyze the internal structure of porous scaffolds from a series of layered two-dimensional images, or cross-sections, (Figure III.VII), and successively to create 3D models of the entire structure, using appropriate softwares (ANT, SkyScan 1072, Belgium) (Figure III.VIII).

Micro-CT analyses have allowed to confirm that 3D Fiber Deposition technique bears the realization of 3D porous structures, characterized by precise and controlled pore shape and size, showing an average fiber diameter of 320-340 μm and a fiber spacing of about 640 μm, as determined during parameter setting. Scaffold interconnectivity, which is normally defined as 100% x volume of interconnected pores/volume sum of interconnected and closed pores, has been also evaluated and found to be equal to 100%.[79]

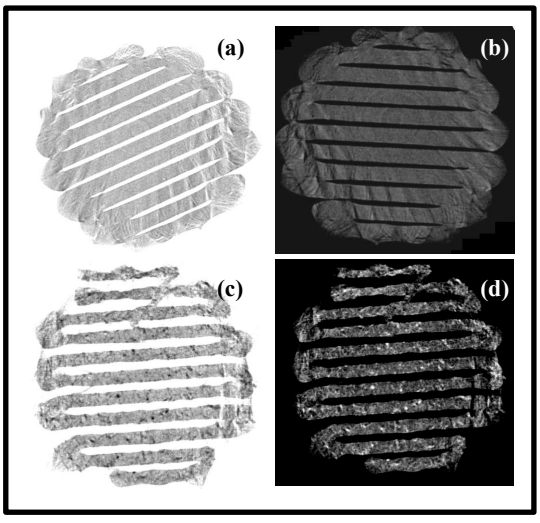


**Figure III.VII: Cross-section of PCL (a, b) and PCL/MCHA (c, d) cylindrical scaffold characterized by a 0°/ 90° lay-down pattern.**

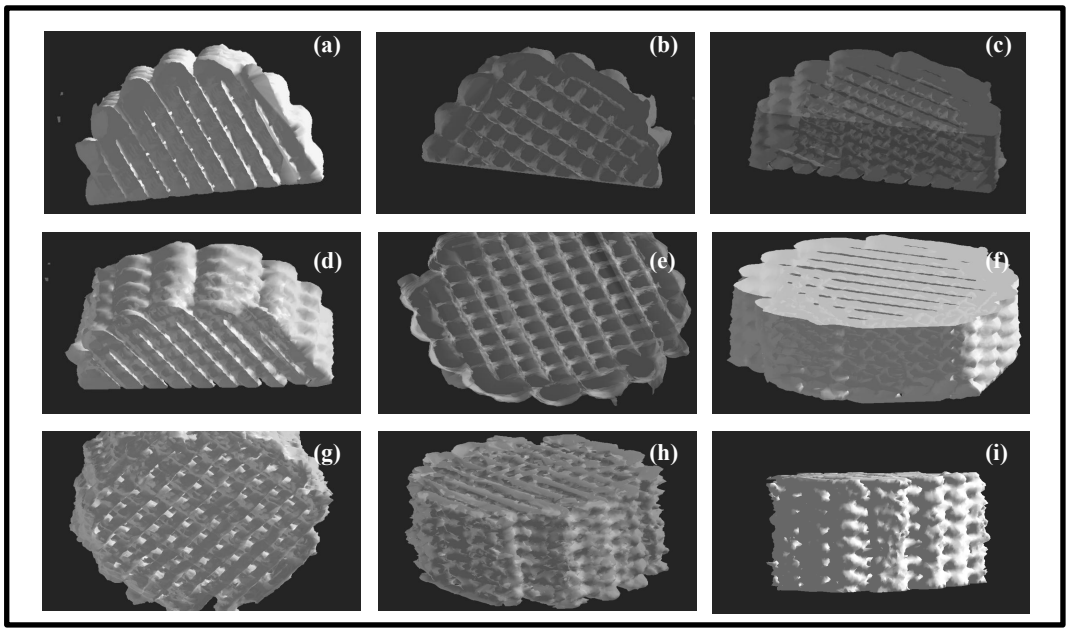


**Figure III.VIII: 3D reconstructions of PCL (a-f) and PCL/MCHA (g-i) cylindrical scaffold obtained from Micro-CT analysis.**

## *III.III.II Nanoindentation tests*

As already highlighted in the Chapter II, advanced materials and biological tissues exhibit hierarchical structures with peculiar micro- and nano-features. In this context, nanoindentation results a powerful tool to analyze tissues and biomaterials measuring local material properties.[5,85-89]

Accordingly, nanoindentation tests were carried out in order to highlight the effect of the inclusion of MCHA nanoparticles on the topography and surface properties of the neat PCL fiber trying to correlate these features with their mechanical and biological performances.

In particular, results from nanoindentation measurements on PCL and PCL/MCHA fibers have highlighted not substantial differences in terms of load-depth curves. However, in the case of PCL fibers, both hardness (H) and reduced modulus ($E_r$) generally decrease as load increases from 1 up to 4 mN whilst PCL/MCHA fibers have shown values of the above mentioned parameters that increase by varying the applied load from 1 to 3 mN (Figure III.IX).

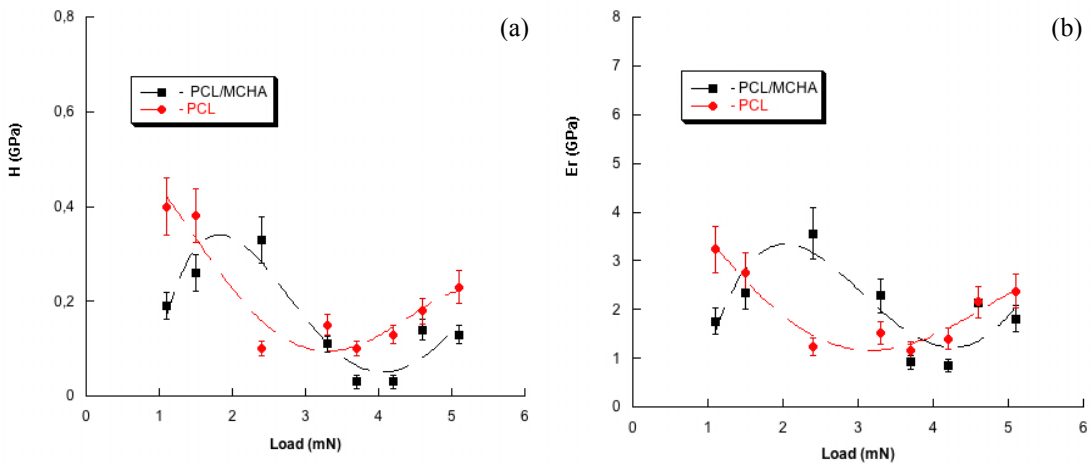


**Figure III.IX: Results obtained from nanoindentation tests performed on PCL and PCL/MCHA fibers – hardness (a) and reduced modulus (b) as function of the applied load (1-5 mN). Data are graphically reported as mean value, and bars represent the standard deviation. The dashed lines are just a guide for the eye.**

## *III.III.III Compression tests*

Compression tests have evidenced that the mechanical behavior of the 3D PCL/MCHA nanocomposite scaffolds is qualitatively similar to that of the PCL structures. With regard to the stress-strain curve, a linear region is evident at low values of strain, suggesting an initial stiff mechanical response. This zone is followed by a region with lower stiffness, and, finally, it can be noticed another stiff portion of the stress-strain curve (Figure III.X).

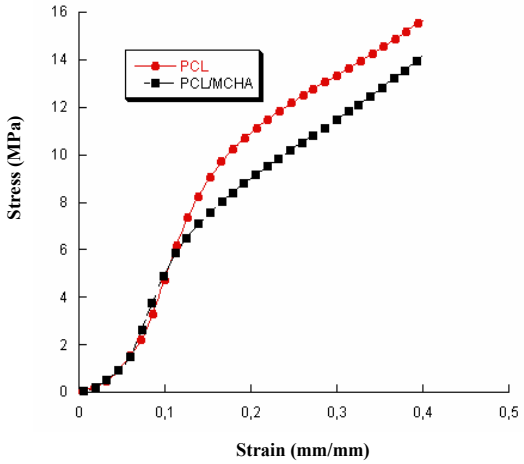


**Figure III.X: Effect of the inclusion of MCHA nanoparticles on the mechanical properties of 3D rapid prototyped scaffolds. Typical stress-strain curves for PCL and PCL/MCHA scaffolds characterized by a 0°/90° lay-down pattern.**

Values of compressive modulus and maximum stress (at 0.5 mm/mm) have been reported in the following table III.I.

| Scaffold | Modulus E (MPa) | Maximum Stress at 0.5 mm/mm σ (MPa) |
|---|---|---|
| PCL | 65.3 ± 4.9 | 16.2 ± 1.3 |
| PCL/MCHA | 79.5 ± 6.1 | 13.9 ± 1.1 |

**Tabella III.I: Effect of the inclusion of MCHA nanoparticles on the mechanical properties of 3D rapid prototyped scaffolds. Compressive modulus and maximum stress reported as mean value ± standard deviation, for PCL and PCL/MCHA scaffolds.**

Figure III.X and Table III.I clearly suggest that the presence of MCHA nanoparticles improves the compressive modulus, as shown by the slope of the initial linear region of the stress-strain curve, however slightly reducing the stress value at higher strains.

## *III.III.IV Microscopy and Cell Adhesion Study*

All the steps carried out till this point can be briefly summarized as follows: a) design and fabrication of morphologically-controlled scaffolds through 3D Fiber Deposition technique; b) compression and nanoindentation tests performed to assess the effect of the nanoparticles inclusion on the surface and bulk PCL properties, respectively.
However, even though the above mentioned steps are crucial, the knowledge of cell-material interactions results to be a key element in designing advanced multifunctional scaffolds for hard tissue engineering with suitable morphology and properties, that are able to guide cell activity. For this reason, as a final step of this research, in order to analyze the effect of the inclusion of MCHA nanoparticles from a biological point of view, the interaction with human Mesenchymal Stem Cells (hMSCs) was studied through stereomicroscope and Confocal Laser Scanning Microscopy (CLSM).
Firstly, Scanning Electron Microscopy (SEM) analyses were performed on polymeric (PCL) and nanocomposite (PCL/MCHA) scaffolds in order to analyze morphological structure and to assess the presence and hence the distribution of MCHA nanoparticles within the polymeric matrix.

The Scanning Electron Microscopy performed on polymeric (PCL) and nanocomposite (PCL/MCHA) cylindrical scaffolds has allowed to highlight the well organized porous structures (i.e., architecture, fiber spacing, effective fiber diameter) (Figure III.XI).

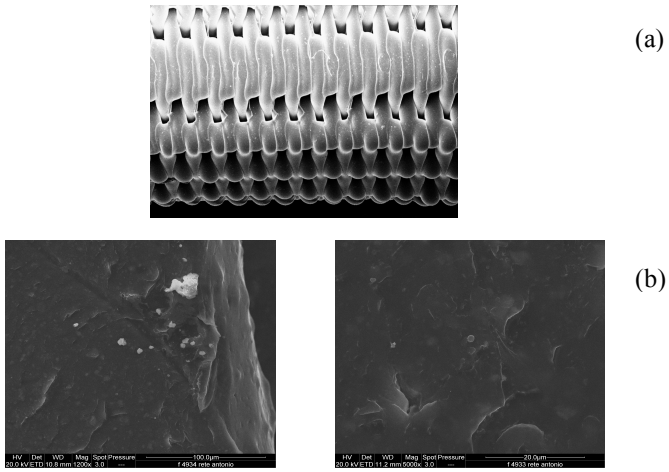

(a)

(b)

**Figure III.XI: Results from SEM analyses - (a) lateral view of a cylindrical PCL scaffold obtained through 3D Fiber Deposition technique and characterized by a 0°/90° lay-down pattern; (b) two different images of nanocomposite PCL/MCHA fiber.**

Images obtained through Scanning Electron Microscopy (SEM) have shown that 3D Fiber Deposition technique allows the realization of morphologically-controlled structures characterized by a fully pore interconnection (100%), a fiber diameter of about 320 μm and a fiber spacing of 640 μm, in agreement with the setting values.

Moreover, SEM analyses performed on nanocomposite scaffolds (PCL/MCHA) have highlighted the presence of MCHA nanoparticles also on the fiber surface (Figure III.XI b).

In order to analyze the effect of the inclusion of MCHA nanoparticles from a biological point of view, the interaction with human Mesenchymal Stem Cells (hMSCs) through crystal violet staining was studied (Figure III.XII and III.XIII), showing that hMSCs are able to recognize and consequently to adhere and proliferate on both polymeric and nanocomposite scaffolds. Moreover, it is clearly evident that hMSCs better adhere on the fiber and within the interstices of the 3D morphologically-controlled nanocomposite scaffolds (Figure III.XIII). This is probably due to the presence of MCHA nanoparticles, which may act as a "bioactive solid signal", and/or to a higher value of the surface roughness if compared to the neat PCL scaffolds.

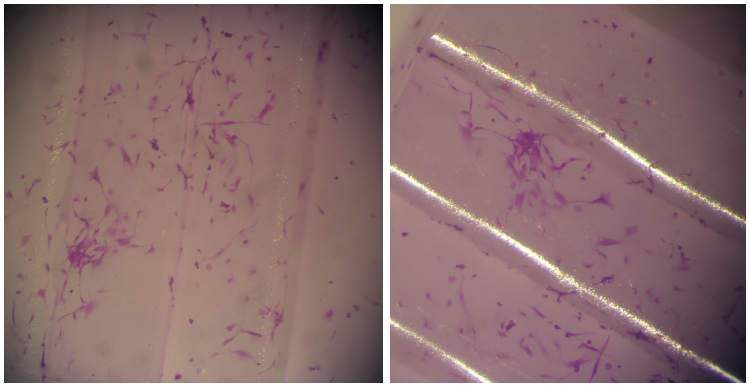

**Figure III.XII: Crystal violet staining performed on cell-scaffold constructs. 3D fiber-deposited PCL scaffolds seeded with human Mesenchymal Stem Cells.**

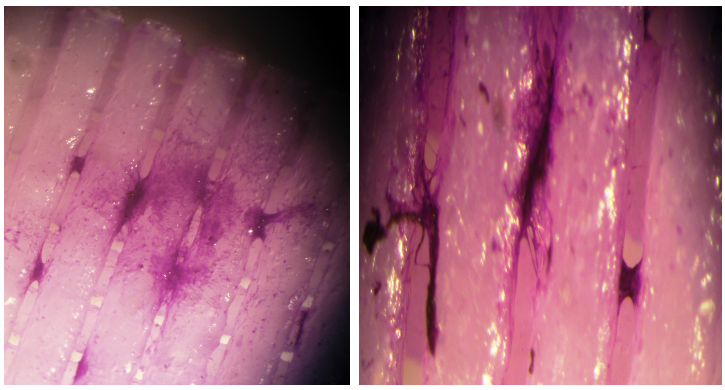

**Figure III.XIII: Crystal violet staining performed on cell-scaffold constructs. 3D fiber-deposited PCL/MCHA scaffolds seeded with human Mesenchymal Stem Cells.**

Cell adhesion was studied through Toluidine Blue staining under stereomicroscopy, at 24h after cell seeding. Cells were able to adhere onto both polymeric (PCL) and nanocomposite (PCL/MCHA) scaffolds (Figure III.XIV).

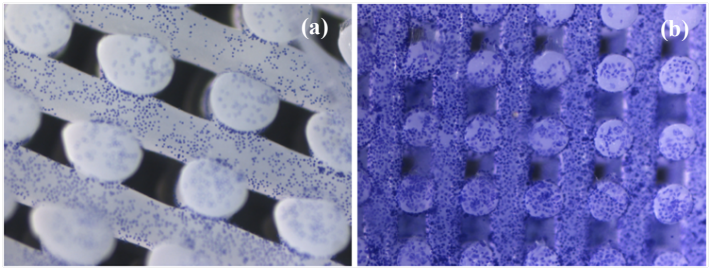


**Figure III.XIV: Cell adhesion onto different scaffolds was observed through Toluidine Blue staining under stereomicroscopy. Cells were able to adhere onto both PCL (a) and PCL/MCHA (b) scaffolds. hMSCs were displayed well attached and spread onto the PCL/MCHA surface (b). Images supplied by dr. S. Scaglione and prof R. Quarto.**

It is worth noting that hMSCs better adhere on the fiber and within the interstices of the 3D morphologically-controlled nanocomposite scaffolds; at high magnification,

cells seem to be well attached and spread onto the PCL/MCHA surface (Figure III.XIV b).

Finally, cell-scaffold constructs were also analyzed via Confocal Laser Scanning Microscopy (CLSM) through phalloidin staining, in order to observe actin filaments orientation and, hence, cytoskeleton morphology.

The following figure III.XV reports the results in terms of cell adhesion and spreading obtained from CLSM analyses. These analyses have highlighted that hMSCs well adhere and spread on both polymeric and nanocomposite scaffolds. However, if compared to the case of neat PCL scaffolds (Figure III. XV a and b), a higher cell number and a better cell spreading on PCL/MCHA scaffolds are well evident (Figure III.XV c and d).

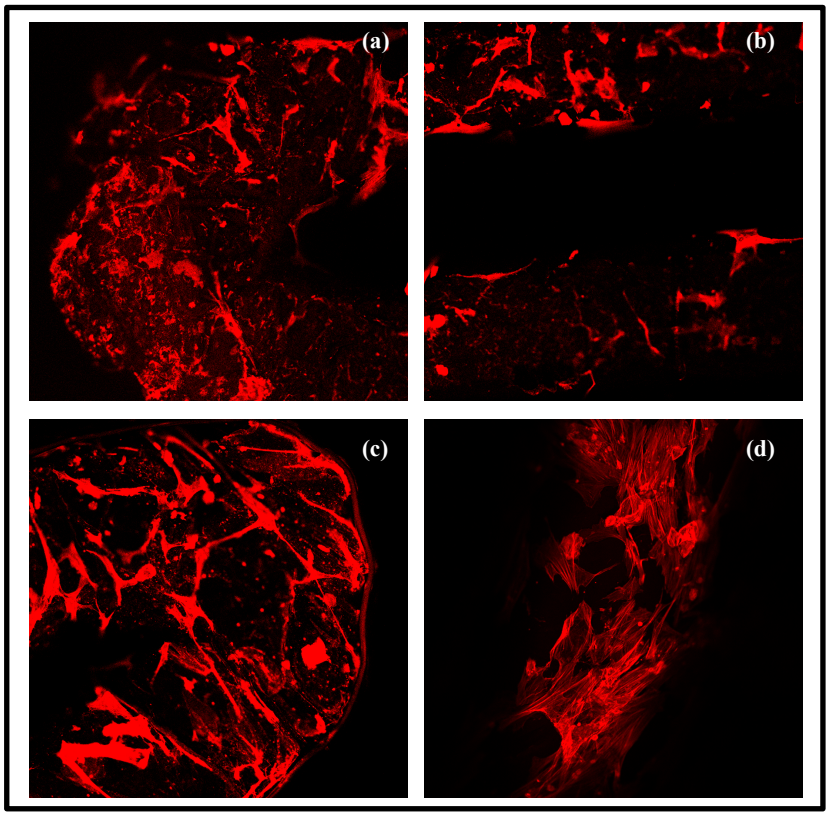


**Figure III.XV: Confocal laser scanning microscope images of phalloidin staining of actin filaments. Images related to cell-scaffold constructs: hMSCs seeded on 3D fiber-deposited PCL scaffolds (a and b) and PCL/MCHA scaffolds (c and d).**

In order to evaluate if MCHA nanoparticles act as a solid bioactive signal and if PCL/MCHA nanocomposite is able to induce osteogenic differentiation, at 21 days after cell seeding, Alizarin red staining was also performed, and results were compared to those obtained from hMSCs seeded on a bidimensional support.

Figures III.XVI and III.XVII show the results obtained by means of Alizarin red staining, in which red-colored calcium deposits are evident.

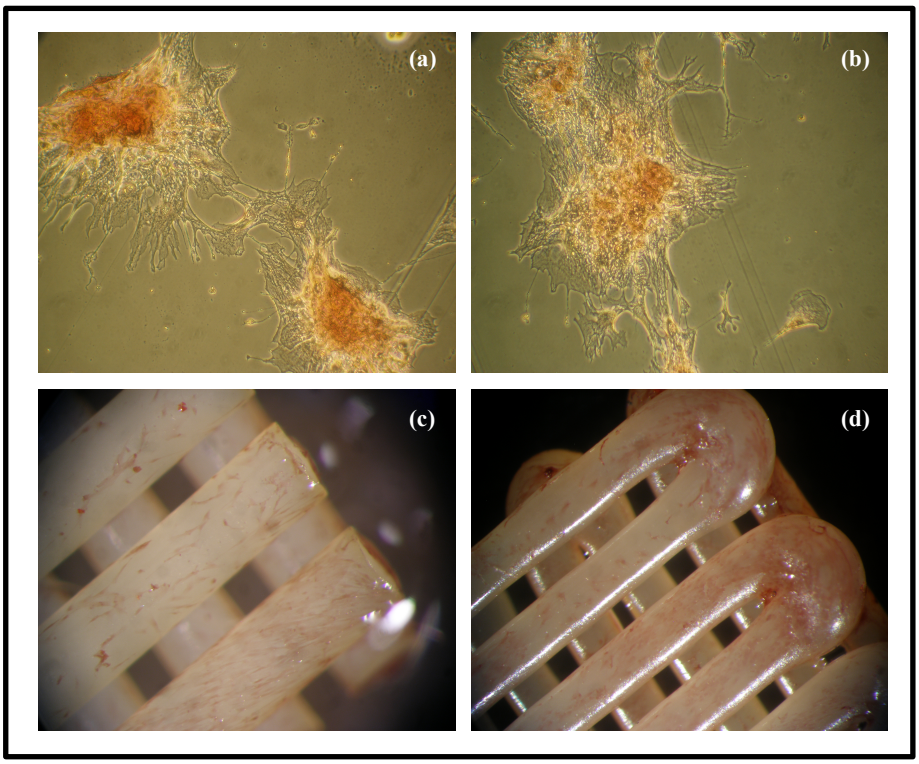


**Figure III.XVI: Alizarin Red staining at 21 days after cell seeding – hMSCs seeded on 2D support as control(a and b); 3D fiber-deposited PCL scaffold seeded with hMSCs (c and d).**

Alizarin Red staining was initially performed on polymeric (PCL) and nanocomposite (PCL/MCHA) scaffolds, before cell seeding, in order to highlight the presence of calcium deposits also on the surface of the composite scaffolds, as clearly evidenced in Figure III.XVII (b). Positive red staining was observed in samples with MCHA crystals, while pure PCL scaffolds were negative to the staining.

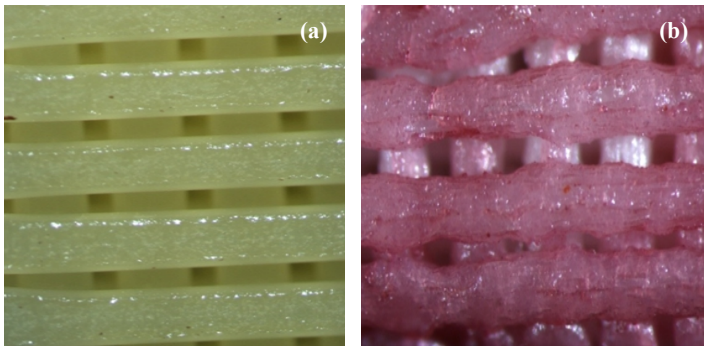


**Figure III.XVII: Alizarin Red staining performed on PCL and PCL-MCHA scaffolds (a and b, respectively). Positive red stain was observed in samples enriched with a HA crystals, while pure PCL scaffolds were negative to the staining. Images supplied by dr S. Scaglione and prof. R. Quarto.**

Confirming the above results from crystal violet staining, we can just suppose that composite scaffolds, because of the presence of MCHA nanoparticles on the fiber surface, that may act as a solid bioactive signal, can better induce osteogenic differentiation of the hMSCs compared with neat PCL scaffolds. Anyway it is not possible to precisely distinguish the cells from the calcium deposits that are typical of the MCHA. Future works will be carried out in order to overcome this limitation, taking into account that a further investigation was also performed through a quantitative analysis, ALP/DNA, shown hereinafter (Table III.III). ALP activity was evaluated at 7, 14 and 21 days after cell seeding. Results are reported in table III.III, in terms of mean values ± standard deviation and normalized to the total DNA content. As reported in table III.III, cell-scaffold constructs made from PCL/MCHA scaffolds and hMSCs showed ALP activity values higher and even twice as those obtained for cell-scaffold constructs made from PCL scaffolds and hMSCs, both at 14 and 21 days after cell seeding. Both kinds of scaffolds have evidenced a peak value at 14 days after cell seeding.

The shape acquired by the cell adhered to the substrate influence cell proliferation and differentiation: for tis reason, the results obtained from the ALP/DNA assay are consistent with the morphological differences observed on different substrates.

| | **ALP Activity (%) [ng ALP/ng DNA]** | | |
|---|---|---|---|
| | **7 days** | **14 days** | **21 days** |
| **PCL-hMSCs** | --- | 64.0 | 33.0 |
| **PCL/MCHA-hMSCs** | --- | 110.0 | 66.0 |

**Table III.III: Effect of the inclusion of MCHA nanoparticles on the biological performances of cell-scaffold constructs. Osteogenic differentiation of hMSCs: ALP/DNA. Results in ng/ng (%) are reported as mean value ± standard deviation, for PCL and PCL/MCHA cell-scaffolds constructs.**

## *III.III.V Gene expression: Real Time quantitative PCR*

In order to determine if the expression of the investigated genes was regulated by the chemical composition of the scaffolds (PCL and PCL/MCHA) either under static culture or under perfusion, mRNA levels were measured, in OM, after 14 days culture.

Both Runx-2 and Col-I did not reveal significant variations among different scaffold, while OP gene levels were significantly more expressed in PCL/MCHA scaffolds cultured under perfusion if compared to PCL scaffolds cultured under the same conditions, and to the statically cultured scaffolds (Figure III.XVIII).

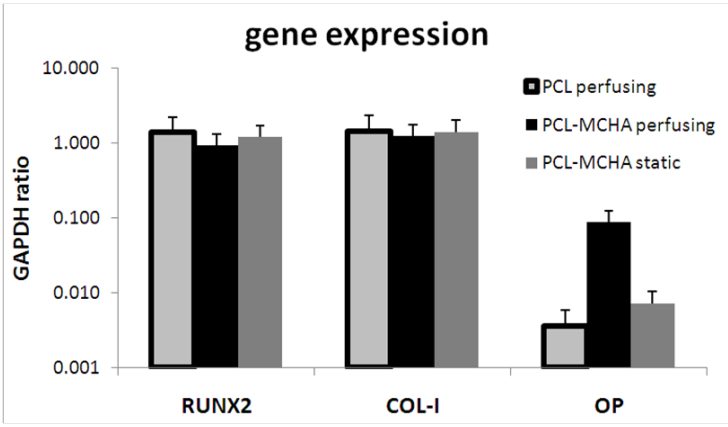


**Figure III.XVIII: Quantitative real time RT-PCR analysis was assessed for expression of transcriptional factor related to the osteogenic lineage (RUNX-2) and osteoblast-related genes (Col-I and OP) in human cells cultured either on PCL or PCL-MCHA scaffolds under perfusion. As control, PCL-MCHA cultured in static condition was used. Expression levels of each gene are reported as ratio to average levels of GAPDH reference gene.**

## *III.III.VI Design and preparation of customized PCL/MCHA scaffolds for mandibular simphysis and ramus tissue engineering*

Nanocomposite scaffolds (PCL/MCHA) for human mandibular symphysis and ramus tissue engineering were designed and manufactured by integrating different techniques such as 3D scanning, 3D modeling and rapid prototyping, with those related to the preparation of PCL/MCHA nanocomposite material for scaffolds processing. A scheme of the production process of those scaffolds may be summarized in the following Figure III.XIX.

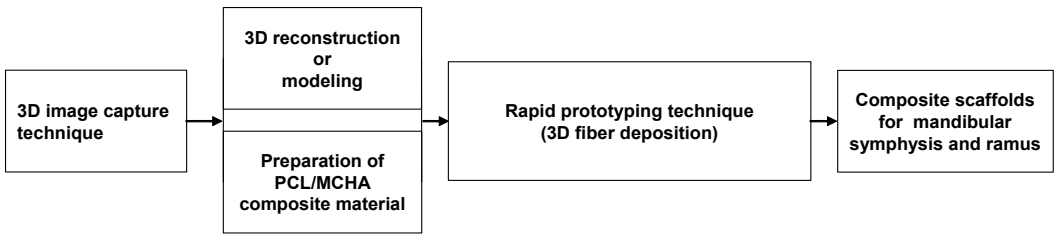


**Figure III.XIX: Production process of the proposed scaffolds.**

### *3D image capture technique and 3D modeling*

3D scanning was performed through a Cyberware Mini Shop Model scanner, in order to capture the image and, hence, shape and size of a natural human mandible.

The point clouds produced by 3D scanners are usually not used directly, and most applications instead use polygonal 3D models, NURBS surface models, or editable feature-based CAD models. The process of converting a point cloud into a usable 3D model is called "reconstruction" or "modeling". Consequently, the 3D model of human mandible was then reconstructed using Rapidform software (2007) (Figure III.XX), thus creating the NURBS that describe the complex geometry of the mandible.

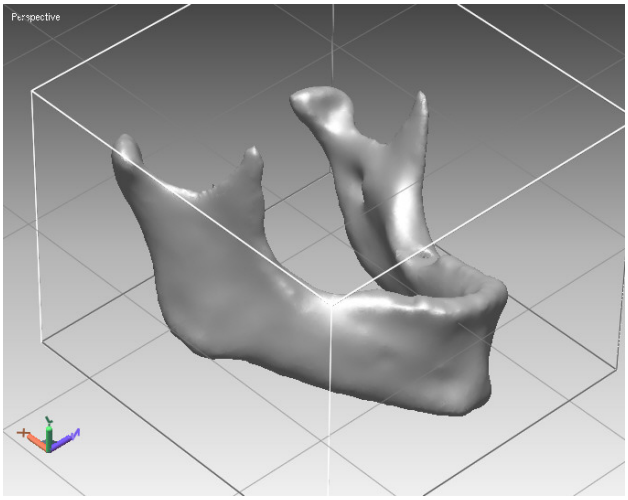


**Figure III.XX: 3D reconstruction of human mandible.**

To manufacture scaffolds for mandibular symphysis and ramus tissue engineering through rapid prototyping technique, the design was then exported as an STL file using Materialise Magics (v. 9.5) (Figures III.XXI, III.XXII and III.XXIII) which offers advanced and highly automated tools for STL manipulation. Using this software, it is possible to interact directly on defective triangles and thus very quickly resolve any errors. Accordingly, this software was tuned to the needs and characteristics of the rapid prototyping process considered.

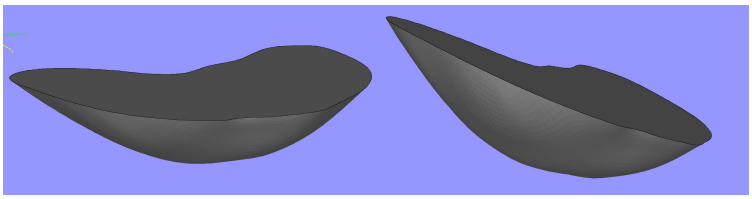

**Figure III.XXI: 3D reconstruction of mandibular symphysis.**

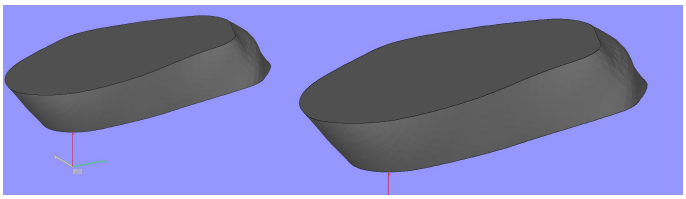

**Figure III.XXII: 3D reconstruction of a mandibular ramus portion.**

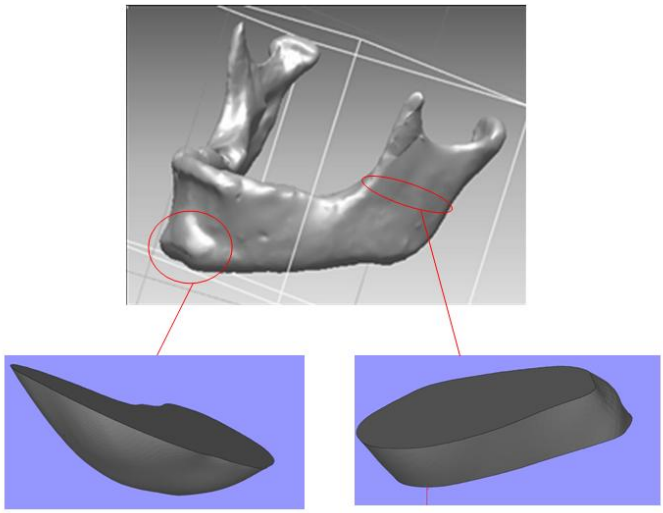

**Figure III.XXIII: 3D reconstruction through Rapidform and Materialise Magics: human mandible, symphysis and ramus portion.**

### *Preparation of PCL/MCHA nanocomposite material and 3D fiber-deposited scaffold*

PCL/MCHA nanocomposite pellets and 3D fiber-deposited scaffolds were manufactured according to specific procedure already described in the paragraph III.II.II. In particular, models of mandibular symphysis and ramus portion were loaded on the Bioplotter CAD/CAM system. Hence, they were plotted layer-by-layer, extruding and depositing PCL/MCHA fibers according to a 0/90° lay-down pattern.

Images of customized PCL/MCHA nanocomposite scaffolds for mandibular symphysis and ramus portion tissue engineering are reported in the following Figure III.XXIV.

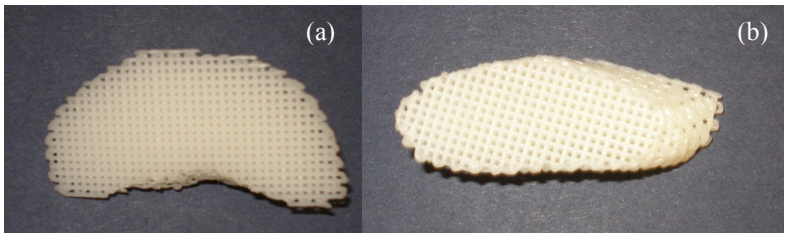


**Figure III.XXIV: Customized PCL/MCHA nanocomposite scaffolds for mandibular symphysis (a) and ramus portion (b) tissue engineering.**

## III.IV Conclusions and future trends

In the field of hard tissue engineering, the possibility to make appropriate modifications into hydroxyapatite reticular structure for guiding specific cell responses together with the ability to tailor the morphology, hence the mechanical and transport properties of composite scaffolds through a suitable topological optimization process should represent a great challenge.

As a first step, the design of 3D rapid prototyped PCL/Mg,$CO_3$-substituted hydroxyapatite (MCHA) nanocomposite scaffolds for bone tissue engineering has been described. Successively, the effect of the inclusion of MCHA nanoparticles have been properly assessed through experimental tests. In particular, a nanoparticle amount of 20% by weight embedded into the polymeric matrix seems to enhance both stiffness and biological performances.

An approach toward the design and development of customized PCL/MCHA nanocomposite scaffolds for human mandibular symphysis and ramus tissue engineering have been also proposed by integrating different techniques such as 3D scanning, 3D modeling and 3D Fiber Deposition technique, with those related to the preparation of PCL/MCHA nanocomposite material for scaffolds processing. Furthermore, the possibility to create 3D heterogeneous bilayered scaffolds (PCL and PCL/MCHA), composed of two distinct but integrated layers for the cartilage and bone regions should be also taken into account for the regeneration of osteochondral defects.

In recent studies[95-96], it has been studied the possibility to obtain iron-doped hydroxyapatite, as an intrinsically magnetic compound which can be embedded into a polymer matrix[97-99] in order to make new conceptually type of magnetic scaffolds for tissue regeneration and orthopaedic surgery. The magnetic moment of the scaffolds

introduces the fascinating possibility to continuously control and reload them with scaffold precursors and active factors (e.g. Vascular Endothelial Growth Factor, VEGF). Such magnetic scaffolds can be imagined as fixed "stations" that offer a long-living assistance to the tissue engineering via a controlled *in vivo* supply of bio-agents functionalized to magnetic nanoparticles injected in the proximity of the scaffold. This innovative approach offers the unique possibility to adjust the scaffold activity to the personal needs of each patient. It would be possible to precisely control the growth factors delivery time and site, therefore allowing the proper regeneration of damaged tissues and the prevention of their degeneration.

Conceptually innovative solution for designing magnetic scaffolds for tissue engineering was recently proposed,[100] the aim being to design magnetic scaffolds through the dip coating technique that are able to attract and take up *in vivo* growth factors, stem cells, or other bioagents bound to magnetic particles. Accordingly, the design and preparation of 3D fiber-deposited magnetic PCL/iron oxide ($Fe_3O_4$) scaffolds have been proposed, also studying the effect of $Fe_3O_4$ nanoparticles on the biological, mechanical, and magnetic performances.[99]

Preliminary Confocal Laser Scanning Microscopy was carried out on the PCL/$Fe_3O_4$ nanocomposite fibers, in order to study human mesenchymal stem cell adhesion and spreading, at 72 h after cell seeding. A PCL/$Fe_3O_4$ nanoparticles weight ratio (w/w) of 90/10 was used. To visualize the cells adhered on the nanocomposite fibers, the phalloidin-labeled actin filament fluorescence intensity was measured with several steps along the length of the fibers by means of a confocal laser scanning microscope (Zeiss LSM 510/Confocor 2, Oberkochen, Germany).

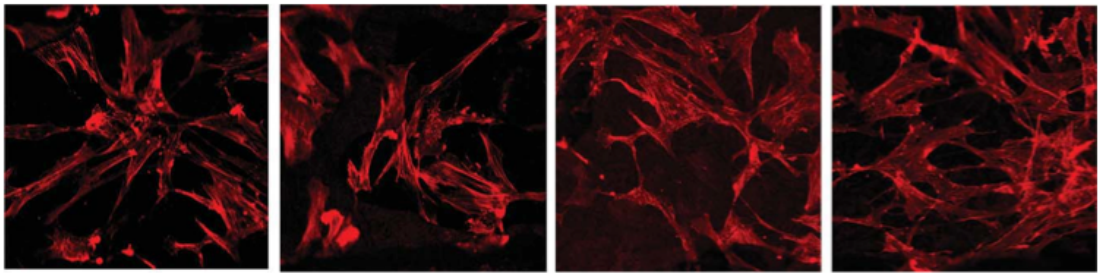

**Figure III.XXV: Images obtained from confocal analysis with several steps along the length of the nanocomposite fibers, highlighting the phalloidin-labeled actin filaments.[99]**

This qualitative analysis evidenced that hMSCs better adhered on PCL/$Fe_3O_4$ scaffolds compared to cells seeded on neat PCL structures, as confirmed by previously reported analyses. An increase in the adhered number and a marked spreading of hMSCs was also well shown in the case of composite structures (Figure III.XXV). Future works will focus on the possibility to employ iron-doped hydroxyapatite in designing 3D rapid prototyped composite scaffolds, the rationale being to study the effect on cell behavior due to the synergic contribution of the surface topography of the composite fibers and the chemistry of the iron-doped hydroxyapatite nanoparticles and those due to an applied magnetic field.

# References


1. E. Landi, A. Tampieri, M. Mattioli-Belmonte, G. Celotti, M. Sandri, A. Gigante, P. Fava, G. Biagini. *Biomimetic Mg- and Mg,$CO_3$-substituted hydroxyapatites: synthesis characterization and in vitro behavior*. Journal of the European Ceramic Society 2006; 26: 2593–2601.
2. N. Roveri. *Biomimetic compounds containing hydroxyapatite substituted with magnesium and carbonate, and processes used to obtain them.* American Patent N°: US2007/0172433 A1, United States.
3. E. Landi, G. Celotti, G. Logroscino, A. Tampieri. *Carbonated Hydroxyapatite as Bone Substitute*. Journal of the European Ceramic Society 2003; 23: 2931-2937.
4. S.A. Redey, S. Razzouk, C. Rey, D. Bemache-Assollant, G. Leroy, M. Nardin, G. Cournot. *Osteoclast adhesion and activity on synthetic hydroxyapatite, carbonated hydroxyapatite and natural calcium carbonate: relationship to surface energies.* Journal of Biomedical Material Research 1999; 45: 140-147.
5. S.A. Redey, M. Nardin, D. Bemache-Assollant, C. Rey, P. Delannoy, L. Sedel, P.J. Marie. *Behaviour of human osteoblastic cells on stoichiometric hydroxyapatite and type A carbonate apatite: role of surface energy.* Journal of Biomedical Material Research 2000; 50: 353-364.
6. I.R. Gibson, W. Bonfield. *Preparation and Characterization of Magnesium/Carbonate co-substituted Hydroxyapatites*. Journal of Material Science: Materials in Medicine 2002; 13: 685-693.
7. I. R. Gibson, W. Bonfield. *Novel synthesis and characterization of an AB-type carbonate-substituted hydroxyapatite*. Journal of Biomedical Material Research 2002; 59: 697-708.
8. A. Bigi, G. Falini, E. Foresti, M. Gazzano, A. Ripamonti, N. Roveri. *Magnesium influence on hydroxyapatite crystallization.* Journal of Inorganic Biochemistry 1993; 49: 69-78.
9. S. Baravelli, A. Bigi, A. Ripamonti, N. Roveri, E. Foresti. *Thermal behavior of bone and synthetic hydroxyapatites submitted to magnesium interaction in aqueous medium.* Journal of Inorganic Biochemistry 1984; 20: 1-12.
10. A. Bigi, A. Ripamonti, M.H.J. Koch, G. Cojazzi, G. Pizzuto, N. Roveri.

*Structural analysis of turkey tendon collagen upon removal of the inorganic phase* International Journal of Biological Macromolecules 1991; 13: 110-114.

11. A. Bigi, E. Foresti, R. Gregoriani, A. Ripamonti, N. Roveri, J.S. Sha. *The Role of Magnesium on the Structure of Biological Apatites*. Calcified Tissue International 1992; 50: 439-444.
12. A. Bigi, G. Falini, E. Foresti, M. Gazzano, A. Ripamonti, N. Roveri. *Rietveld structure refinements of calcium hydroxylapatite containing magnesium*. Acta Crystallographica Section B 1996; 52: 87-92.
13. A. Tampieri, G. Celotti, E. Landi, M. Sandri, N. Roveri, G. Falini. *Biologically inspired synthesis of bone-like composite: Self-assembled collagen fibers/hydroxyapatite nanocrystals*. Journal of Biomedical Material Research, Part A. 2003; 67: 618-625.
14. E. Landi, G. Logroscino, L. Proietti, A. Tampieri, M. Sandri, S. Sprio. *Biomimetic Mg-substituted hydroxyapatite: from synthesis to in vivo behavior*. Journal of Material Science: Materials in Medicine 2008; 19: 239–247.
15. E. Landi, A. Tampieri, G. Celotti, S. Sprio. *Densification behaviour and mechanisms of synthetic hydroxyapatites*. Journal of the European Ceramic Society 2000; 20: 2377-2387.
16. E. Landi, A. Tampieri, G. Celotti, L. Vichi, M. Sandri. *Influence of synthesis and sintering parameters on the characteristics of carbonate apatite*. Biomaterials 2004; 25: 1763–1770.
17. K.S. TenHuisen, P.W. Brown. *Effects of magnesium on the formation of calcium deficient hydroxyapatite from $CaHPO_4{\cdot}2H_2O$ and $Ca_4(PO_4)_2O$*. Journal of Biomedical Material Research 1997; 36: 306–314.
18. R.N. Correia, M.C.F. Magalhaes, P.A.A.P. Marques, A.M.R. Senos. *Wet synthesis and characterization of modified hydroxyapatite powders*. Journal of Material Science: Materials in Medicine 1996; **7**: 501–505.
19. M.A. Fanovich, M-S. Castro, J.M. Porto Lopez. *Analysis of the microstructural evolution in hydroxyapatite ceramics by electrical characterisation*. Ceramic International 1999; 25: 517–522.
20. A. Bigi, F. Marchetti, A. Ripamonti, N. Roveri. *Magnesium and strontium interaction with carbonate-containing hydroxyapatite in aqueous medium.* Journal of Inorganic Biochemistry 1981; 15: 317–327.

21. H.S. Ryu, K.S. Hong, J.K. Lee, D.J. Kim, J.H. Lee, B.S. Chang, D.H. Lee, C.K. Lee, S.S. Chung. *Magnesia-doped HA/beta-TCP ceramics and evaluation of their biocompatibility*. Biomaterials 2004; 25: 393–401.
22. S.R. Kim, J.H. Lee, Y.T. Kim, D.H. Riu, S.J. Jung, Y.J. Lee, S.C. Chung, Y.H. Kim. *Synthesis of Si, Mg substituted hydroxyapatites and their sintering behaviours.* Biomaterials 2003; 24: 1389–1398.
23. I.V. Fadeev, L.I. Shvorneva, S.M. Barinov, V.P. Orlovskii. *Synthesis and structure of magnesium-substituted hydroxyapatite.* Inorganic Material 2003; 39: 947–950.
24. D. M. Ebenstein, L. A. Pruitt. *Nanoindentation of biological materials*. Nano Today 2006; 1: 26-33.
25. R.Z. LeGeros. *Properties of osteoconductive biomaterials: calcium phosphates*. Clinical Orthopaedics and Related Research 2002; 395: 81-98.
26. A.G. Mikos, G. Sarakinos, S.M. Leite, J.P. Vacanti, R. Langer. *Laminated three-dimensional biodegradable foams for use in tissue engineering*. Biomaterials 1993; 14: 323-330.
27. L.E. Freed, G. Vunjak-Novakovic, R.J. Biron, D.B. Eagles, D.C. Lesnoy, S.K. Barlow, R. Langer. *Biodegradable polymer scaffolds for tissue engineering*. Biotechnology 1994; 12: 689-693.
28. W.C. Oliver, G.M. Pharr. *An improved technique for determining hardness and elastic modulus using load and displacement sensing indentation experiments*. Journal of Material Research 1992; 7: 1564-1583.
29. W.C. Oliver, G.M. Pharr. *Measurement of hardness and elastic modulus by instrumented indentation: Advances in understanding and refinements to methodology.* Journal of Material Research 2004; 19: 3-20.
30. B.J. Briscoe, L. Fiori, E. Pelillo. *Nano-indentation of polymeric surfaces.* Journal of Physics D, Applied Physics 1998; 31: 2395-2405.
31. Y. Hu, L. Shen, H. Yang, M. Wang, T. Liu, T. Liang, J. Zhang. *Nanoindentation Studies on Nylon 11/Clay Nanocomposites.* Polymer Testing 2006; 25: 492-497.
32. C. Klapperich, K. Komvopoulos, L. Pruitt. *Nanomechanical Properties of Polymers Determined From Nanoindentation Experiments.* Journal of Tribology – Trans. ASME 2001; 123: 624-631.

33. J.M. Curran, R. Chen, J.A. Hunt. *The guidance of human mesenchymal stem cell differentiation in vitro by controlled modifications to the cell substrate*. Biomaterials 2006; 27: 4783–4793.
34. J.Q. Zhang, P. Shan, Y. Ma, P. Jiang, J. Chen, Y. Wen, Y. Zhou, H.Qian, X. Pei. *Differentiation potential of bone marrow mesenchymal stem cells into retina in normal and laser-injured rat eye.* Science in China. Series C: Life Science/Chinese Academy of Sciences 2004; 47: 241–50.
35. L.B. Chen, X.B. Jiang, L. Yang. *Differentiation of rat marrow mesenchymal stem cells into pancreatic islet beta-cells.* World Journal of Gastroenterology 2004; 10: 3016–20.
36. S.L. Beeres, D.E. Atsma, A. van der Laarse, D.A. Pijnappels, J. van Tuyn, W.E. Fibbe, A.A. de Vries, D.L. Ypey, E.E. van der Wall, M.J. Schalij. *Human adult bone marrow mesenchymal stem cells repair experimental conduction block in rat cardiomyocyte cultures*. Journal of the American College of Cardiology 2005; 46: 1943–1952.
37. R. Cancedda, G. Bianchi, A. Derubeis, R. Quarto. *Cell therapy for bone disease: a review of current status.* Stem Cells 2003; 21: 610–619.
38. A.R. Derubeis, R. Cancedda. *Bone marrow stromal cells (BMSCs) in bone engineering: limitations and recent advances*. Annals of Biomedical Engineering 2004; 32: 160–165.
39. M. Mastrogiacomo, A. Muraglia, V. Komlev, F. Peyrin, F. Rustichelli, A. Crovace, R. Cancedda. *Tissue engineering of bone: search for a better scaffold*. Orthodontic and Craniofacial Research 2005; 8: 277–284.
40. P. Giannoni, A. Pagano, E. Maggi, R. Arbico, N. Randazzo, M. Grandizio, R. Cancedda, B. Dozin. *Autologous chondrocyte implantation (ACI) for aged patients: development of the proper cell expansion conditions for possible therapeutic applications*. Osteoarthritis and Cartilage 2005; 13: 589–600.
41. M. Malpeli, N. Randazzo, R. Cancedda, B. Dozin. *Serum-free growth medium sustains commitment of human articular chondrocyte through maintenance of Sox9 expression.* Tissue Engineering 2004; 10: 145–155.
42. R. Cancedda, B. Dozin, P. Giannoni, R. Quarto. *Tissue engineering and cell therapy of cartilage and bone*. Matrix Biology 2003; 22: 81–91.

43. J.M. Curran, R. Chen, J.A. Hunt. *Controlling the phenotype and function of mesenchymal stem cells in vitro by adhesion to silane-modified clean glass surfaces*. Biomaterials 2005; 26: 7057–7067.
44. P.S. In 't Anker, S.A. Scherjon, C. Kleijburg-van der Keur, G.M. de Groot-Swings, F.H. Claas, W.E. Fibbe WE, H.H. Kanhai. *Isolation of mesenchymal stem cells of fetal or maternal origin from human placenta.* Stem Cells 2004; 22: 1338–1345.
45. Y. Jiang Y, B.N. Jahagirdar, R.L. Reinhardt, R.E. Schwartz, C.D. Keene, X.R. Ortiz-Gonzalez, M. Reyes, T. Lenvik, T. Lund, M. Blackstad, J. Du, S. Aldrich, A. Lisberg, W.C. Low, D.A. Largaespada, C.M. Verfaillie. *Pluripotency of mesenchymal stem cells derived from adult marrow*. Nature 2002; 418: 41–49.
46. H. Mikkers, J. Frisen. *Deconstructing stemness*. The EMBO Journal 2005; 24: 2715–2719.
47. S. Sethe, A. Scutt, A. Stolzing. *Aging of mesenchymal stem cells*. Ageing Research Review 2005; 5: 91-116.
48. F.Z. Lu, M. Fujino, Y. Kitazawa, T. Uyama, Y. Hara, N. Funeshima, J.Y. Jiang, A. Umezawa, X.K. Li. *Characterization and gene transfer in mesenchymal stem cells derived from human umbilical-cord blood*. The Journal of Laboratory and Clinical Medicine 2005; 146: 271–278.
49. F.H. McLaren, C.N. Svendsen, P. Van der Meide, E. Joly. *Analysis of neural stem cells by flow cytometry: cellular differentiation modifies patterns of MHC expression*. Journal of Neuroimmunology 2001; 112: 35–46.
50. M. Reyes, T. Lund, T. Lenvik, D. Aguiar, L. Koodie, C.M. Verfaillie. *Purification and ex vivo expansion of postnatal human marrow mesodermal progenitor cells*. Blood 2001; 98: 2615–2625.
51. H.E. Young, T.A. Steele, R.A. Bray, J. Hudson, J.A. Floyd, K. Hawkins, K. Thomas, T. Austin, C. Edwards, J. Cuzzourt, M. Duenzì, P.A. Lucas, A.C. Jr. Black. *Human reserve pluripotent mesenchymal stem cells are present in the connective tissues of skeletal muscle and dermis derived from fetal, adult, and geriatric donors.* The Anatomical Record 2001; 264: 51–62.
52. F. Barry, R.E. Boynton, B. Liu, J.M. Murphy. *Chondrogenic differentiation of mesenchymal stem cells from bone marrow: differentiation-dependent gene*

*expression of matrix components.* Experimental Cell Research 2001; 268: 189–200.

53. J.J. Minguell, A. Erices. *Conget mesenchymal stem cells*. Experimental Biology and Medicine (Maywood) 2001; 226: 507–520.
54. J.E. Aubin. *Regulation of osteoblast formation and function*. Reviews in Endocrine and Metabolic Disorders 2001; 2: 81-94.
55. R.T. Franceschi. *The developmental control of osteoblast-specific gene expression: role of specific transcription factors and the extracellular matrix environment.* Critical Review in Oral Biology and Medicine 1999; 10: 40-57.
56. L.C. Gerstenfeld, S.D. Chipman, J. Glowacki, J.B. Lian. *Expression of differentiated function by mineralizing cultures of chicken osteoblasts.* Developmental Biology 1987; 122: 49-60.
57. L.C. Gerstenfeld, D. Zurakowski, I.L. Schaffer, D.P. Nichols, C.D. Toma, M. Broess, S.P. Bruder, A.I. Caplan. *Variable hormone responsiveness of osteoblast populations isolated at different stages of embryogenesis and its relationship to the osteogenic lineage*. Endocrinology 1996; 137: 3957- 3968.
58. T.A. Owen, M. Aronow, V. Shalhoub, L.M. Barone, L. Wilming, M.S. Tassinari, M.B. Kennedy, S. Pockwinse, J.B. Lian, G.S. Stein. *Progressive development of the rat osteoblast phenotype in vitro: reciprocal relationships in expression of genes associated with osteoblast proliferation and differentiation during formation of the bone extracellular matrix.* Journal of Cellular Physiology 1990; 143: 420-430.
59. R.T. Franceschi, B.S. lyer. *Relationship between collagen synthesis and expression of the osteoblast phenotype in MC3T3-EI cells.* Journal of Bone and Mineral Research 1992; 7: 235-246.
60. Franceschi RT, Romano PR, Park KY (1988). Regulation of type I collagen synthesis by 1,25-dihydroxyvitamin D3 in human osteosarcoma cells. I Biol Chem 263: 18938-18945.
61. R.T. Franceschi, B.S. Iyer, Y. Cui. *Effects of ascorbic acid on collagen matrix formation and osteoblast differentiation in murine MC3T3-E1 cells*. Journal of Bone Mineral Research 1994; 9: 843-854.
62. K. Ibaraki, J.D. Termine, S.W. Whitson, M.F. Young. *Bone matrix mRNA expression in differentiating fetal bovine osteoblasts.* Journal of Bone Mineral Research 1992; 7: 743-754.

63. L.K. McCauley, A. Koh, C.A. Beecher, Y. Cui, T.I. Rosol, R.T. Franceschi. *PTH/PTHrP receptor is temporally regulated during osteoblast differentiation and is associated with collagen synthesis*. Journal of Cellular Biochemistry 1996; 61: 638-647.
64. P.G. Strauss, E. Closs, J. Schmidt, V. Erfle. *Gene expression during osteogenic differentiation in mandibular condyles in vitro*. Journal of Cellular Biology 1990; 110: 1369-1378.
65. L.I. Suva, I.G. Seedor, N. Endo, H.A. Quartuccio, D.D. Thompson, I. Bab I, G.A. Rodanet *Pattern of gene expression following rat tibial marrow ablation*. Journal of Bone Mineral Research 1993; 8: 379-388.
66. E.N. Olson, W.H. Klein. *bHLH factors in muscle development: dead lines and commitments, what to leave in and what to leave out*. Genes and Development 1994; 8: 1-8.
67. P. Tontonoz P, I.B. Kim, R.A. Graves, B.M. Spiegelman. *ADDI: a novel helix-loop-helix transcription factor associated with adipocyte determination and differentiation*. Molecular and Cellular Biology 1993; 13: 4753-4759.
68. A. Nishiyori, H. Tashiro, A. Kimura, K. Akagi, K. Yamamura, M. Mori, M. Takiguchi. *Determination of tissue specificity of the enhancer by combinatorial operation of tissue-enriched transcription factors. Both HNF-4 and C/EBP beta are required for liver-specific activity of the ornithine transcarbamylase enhancer*. Journal of Biological Chemistry 1994; 269: 1323-1331.
69. H.A. Ingraham, V.R. Albert, R.P. Chen, E.B. Crenshaw, H.P. Elsholtz, X. He, M.S. Kapiloff, H.J. Mangalam, L.W. Swanson, M.N. Treacy, M.G. Rosenfeld. *A family of POU-domain and Pit-I tissue-specific transcription factors in pituitary and neuroendocrine development*. Annual Review of Physiology 1990; 52:773-791.
70. H. Weintraub, R. Davis, S. Tapscott, M. Thayer, M. Krause, R. Benezra, T.K. Blackwell, D. Turner, R. Rupp, S. Hollenberg. *The myoD gene family: nodal point during specification of the muscle cell lineage*. Science 1991; 251: 761-766.
71. A. Oldberg, A. Franzen, D. Heinegard. *Cloning and sequence analysis of rat bone sialoprotein (osteopontin) cDNA reveals an Arg-Gly-Asp cell-binding*

*sequence*. Proceedings of the National Academy of Science of the USA 1986; 83: 8819-8823.

72. J.E. Lee, S.M. Hollenberg, L. Snider, D.L. Turner, N. Lipnick, H. Weintraub. *Conversion of Xenopus ectoderm into neurons by NeuroD, a basic helix-loop-helix protein*. Science 1995; 268: 836-844.
73. P. Bornstein. *Regulation of expression of the alpha1 (I) collagen gene: a critical appraisal of the role of the first intron isee comments*. Journal of Matrix Biology 1996; 15: 3-10.
74. M. Dodig, M.S. Kronenberg, A. Bedalov, B.E. Kream, G. Gronowicz, S.H. Clark, K. Mack, Y.H. Liu, R. Maxon, Z.Z. Pan, W.B. Upholt, D.W. Rowe. *Identification of a TAAT-containing motif required for high level expression of the COLlAl promoter in differentiated osteoblasts of transgenic mice*. J Biol Chem 1996; 271: 16422-16429.
75. P. Ducy, G. Karsenty. Two distinct osteoblast-specific cis-acting elements control expression of a mouse osteocalcin gene. Molecular and Cellular Biology 1995; 15: 1858-1869.
76. P. Ducy, C. Desbois, B. Boyce, G. Pinero, B. Story, C. Dunstan, E. Smith, J. Bonadio, S. Goldstein, C. Gundberg, A. Bradley, G. Karsenty. *Increased bone formation in osteocalcin-deficient mice*. Nature 1996; 382: 448-452.
77. P. Ducy, R. Zhang, V. Geoffroy, A.L. Ridall, G. Karsenty. *Osf2/Cbfa 1: a transcriptional activator of osteoblast differentiation.* Cell 1997; 89: 747-754.
78. R.T. Franceschi, G. Xiao. *Regulation of the Osteoblast-Specific Transcription Factor, Runx2: Responsiveness to Multiple Signal Transduction Pathways*. Journal of Cellular Biochemistry 2003; 88: 446–454.
79. N. Selvamurugan, W.Y. Chou, A.T. Pearman, M.R. Pulumati, N.C. Partridge. *Parathyroid hormone regulates the rat collagenase-3 promoter in osteoblastic cells through the cooperative interaction of the activator protein-1 site and the runt domain binding sequence*. Journal of Biological Chemistry 1998; 273: 10647 – 10657.
80. N. Selvamurugan, M.R. Pulumati, D.R. Tyson, N.C. Partridge. *Parathyroid hormone regulation of the rat collage- nase-3 promoter by protein kinase A-dependent transactivation of core binding factor alpha1*. Journal of Biological Chemistry 2000; 275: 5037 – 5042.

81. B. Kern, J. Shen, M. Starbuck, G. Karsenty. *Cbfa1 contributes to the osteoblast-specific expression of Type I collagen genes*. Journal of Biological Chemistry 2001; 276: 7101-7107.
82. Y. Takeuchi, M. Suzawa, T. Kikuchi, E. Nishida, T. Fujita, T. Matsumoto. *Differentiation and transforming growth factor-beta receptor down-regulation by collagen-alpha2beta1 integrin interaction is mediated by focal adhesion kinase and its downstream signals in murine osteoblastic cells.* Journal of Biological Chemistry 1997; 272: 29309–29316.
83. G. Xiao, D. Wang, M.D. Benson, G. Karsenty, R.T. Franceschi. 1998. *Role of the alpha2-integrin in osteoblast-specific gene expression and activation of the Osf2 transcription factor*. Journal of Biological Chemistry 1998; 273: 32988–32994.
84. D. Zimmerman, F. Jin, P. Leboy, S. Hardy, C. Damsky. *Impaired bone formation in transgenic mice resulting from altered integrin function in osteoblasts.* Developmental Biology 2000; 220: 2 – 15.
85. E.H. Danen, R.M. Lafrenie, S. Miyamoto, K.M. Yamada. 1998. *Integrin signaling: Cytoskeletal complexes, MAP kinase activation, and regulation of gene expression*. Cell Adhesion & Communication 1998; 6: 217–224.
86. A.J. Banes, M. Tsuzaki, J. Yamamoto, T. Fischer, B. Brigman, T. Brown, L. Miller. *Mechanoreception at the cellular level: The detection, interpretation, and diversity of responses to mechanical signals*. Biochemistry and Cell Biology 1995; 73: 349 – 365.
87. L.V. Harter, K.A. Hruska, R.L. Duncan. *Human osteoblast-like cells respond to mechanical strain with increased bone matrix protein production independent of hormonal regulation.* Endocrinology 1995; 136: 528–535.
88. R.S. Carvalho, J.L. Schaffer, L.C. Gerstenfeld. *Osteoblasts induce osteopontin expression in response to attachment on fibronectin: Demonstration of a common role for integrin receptors in the signal transduction processes of cell attachment and mechanical stimulation.* Journal of Cellular Biochemistry 1998; 70: 376–390.
89. P.G. Ziros, A.P. Gil, T. Georgakopoulos, I. Habeos, D. Kletsas, E.K. Basdra, A.G. Papavassiliou. *The bone-specific transcriptional regulator Cbfa1 is a target of mechanical signals in osteoblastic cells*. Journal of Biological Chemistry 2002; 277: 23934– 23941.

90. F.S. Wang, C.J. Wang, S.M. Sheen-Chen, Y.R. Kuo, R.F. Chen, K.D. Yang. *Superoxide mediates shock wave induction of ERK-dependent osteogenic transcription factor (CBFA1) and mesenchymal cell differentiation toward osteoprogenitors*. J Biol Chem 2002; 277: 10931–10937.
91. L. Song, R.S. Tuan. *Transdifferentiation Potential Of Human Mesenchymal Stem Cells Derived From Bone Marrow*. The FASEB Journal 2004; 18: 980-982.
92. S. Scaglione, A. Braccini, D. Wendt, C. Jaquiery, F. Beltrame, R. Quarto, I. Martin. *Engineering of Osteoinductive Grafts by Isolation and Expansion of Ovine Bone Marrow Stromal Cells Directly on 3D Ceramic Scaffolds.* Biotechnology And Bioengineering 2006; 93: 181-187.
93. D. Wendt, A. Marsano, M. Jakob, M. Heberer, I. Martin. *Oscillating Perfusion of Cell Suspensions Through Three-Dimensional Scaffolds Enhances Cell Seeding Efficiency and Uniformity.* Biotechnology And Bioengineering 2003; 84: 205-214.
94. C. Maniatopulos, J. Sodek, A.H. Melcher. *Bone formation in vitro by stromal cells obtained from bone marrow of young adult rats.* Cell and Tissue Research 1988; 254: 317-330.
95. G. Salviulo, M. Bettinelli, U. Russo, A. Speghini, L. Nodari. *Synthesis and structural characterization of Fe3+-doped calcium hydroxyapatites: role of precursors and synthesis method.* Journal of Material Science 2011; 46: 910–922.
96. A. Tampieri, E. Landi, M. Sandri, D. Pressato, J. Rivas Rey, M. Banobre López, M. Marcacci. Intrinsically Magnetic Hydroxiapatite. Patent N° MI2010A001420
97. A. Tampieri, E. Landi, F. Valentini, M. Sandri, T. D'Alessandro, V. Dediu, M. Marcacci. *A conceptually new type of bio-hybrid scaffold for bone regeneration*. Nanotechnology 2011; 22: 1-8.
98. M. Bañobre-Lòpez, Y. Piñeiro-Redondo, R. De Santis, A. Gloria, L. Ambrosio, A. Tampieri, V. Dediu, J. Rivas. *Poly(caprolactone) based magnetic scaffolds for bone tissue engineering.* Journal Of Applied Physics 2011; 109: 07B313, 1-3.
99. R. De Santis, A. Gloria, T. Russo, U. D'Amora, S. Zeppetelli, C. Dionigi, A. Sytcheva, T. Herrmannsdörfer, V. Dediu, L. Ambrosio. *A Basic Approach*

*Toward the Development of Nanocomposite Magnetic Scaffolds for Advanced Bone Tissue Engineering*. Journal of Applied Polymer Science 2011; 122: 3599–3605.

100. N. Bock; A. Riminucci; C. Dionigi; A. Russo; A. Tampieri; E. Landi; V.A. Goranov; M. Marcacci; V. Dediu. *A novel route in bone tissue engineering: Magnetic biomimetic scaffolds*. Acta Biomaterialia 2010; 6: 786.

*La città in cui tende il mio viaggio è discontinua nello spazio e nel tempo. Non credere che si possa smettere di cercarla.*

***Italo Calvino**, Le città invisibili*